NASA Technical Paper 1672

Noise Reduction in a Mach 5 Wind Tunnel With a Rectangular Rod-Wall Sound Shield

Theodore R. Creel, Jr., J. Wayne Keyes,
and Ivan E. Beckwith

JUNE 1980

NASA

NASA Technical Paper 1672

Noise Reduction in a Mach 5 Wind Tunnel With a Rectangular Rod-Wall Sound Shield

Theodore R. Creel, Jr., J. Wayne Keyes,
and Ivan E. Beckwith
Langley Research Center
Hampton, Virginia

National Aeronautics
and Space Administration

**Scientific and Technical
Information Office**

1980

SUMMARY

A rod-wall sound shield was tested in the Mach 5 pilot quiet tunnel at the Langley Research Center over a range of Reynolds numbers of 0.5×10^7 to 8.0×10^7 per meter. The model consisted of a rectangular array of longitudinal rods with boundary-layer suction through gaps between the rods. Rod surface pressures, mean free-stream pitot pressures, and fluctuating pitot pressures were measured in the rod-wall sound shield. Transition in the rod boundary layers was determined by axial surveys with surface pitot tubes along the windward ray of the rods. Hot-wire measurements were also made but only at a Reynolds number of 1.5×10^7 per meter. The fluctuating pitot pressure and hot-wire data were obtained in the free stream within the shielded region. These measurements indicated that for a unit Reynolds number of about 1.5×10^7, the rms pressure fluctuations, or noise, in the shielded region were reduced from about 1.5 percent of the mean pressure (the average level present without the shield) to about 0.6 percent. This reduction occurs only when the flow is mostly laminar on the rods. However, the actual nozzle "input" noise as measured upstream on the nozzle centerline before reflection at the shield walls was apparently attenuated only slightly even when the rod boundary layers were laminar. At a lower Reynolds number of about 7.0×10^6 per meter, the nozzle input noise peaks at about 3 percent, and for this condition the noise levels in the shield were attenuated to about 1.5 percent, which is too high for application to a quiet tunnel. At Reynolds numbers above 2.0×10^7 per meter, the measured noise levels were generally higher than nozzle input noise levels, probably due to transition in the rod boundary layers. The small attenuation of the nozzle input noise at intermediate Reynolds numbers when the rod boundary layers at the acoustic origins are laminar is apparently due to the high frequencies of the input noise.

INTRODUCTION

Noise radiated from turbulent boundary layers on the walls of supersonic and hypersonic wind tunnels dominates transition on simple test models (refs. 1 to 3). Thus, the basic problem to solve in the design of a low-noise supersonic wind tunnel is how to reduce the noise radiated into the test section from the nozzle-wall turbulent boundary layers. One method of reducing the directly radiated noise is by using a shield. If a test region is shielded from this noise, the local-stream noise levels can be reduced provided the noise reflected or generated at the shield walls is minimized. Several shields have been tested (ref. 4 to 7), with the first shield being a flat panel with longitudinal rods. This panel was tested at Mach 6 (refs. 4 to 6) at 10° angle of attack to provide induced suction through gaps between the rods to maintain laminar boundary layers on the rods. The results for this flat panel indicate that noise levels in the shielded region were reduced significantly up to Reynolds numbers of about 8 million based on the length of a hypothetical quiet test region (ref. 7).

With the successful testing of the flat rod-wall panel, an axisymmetric sound shield using the rod-wall technique with boundary-layer suction was designed and tested. The flow field in this model was highly nonuniform due to strong focusing of the leading-edge shock on the centerline (ref. 7). Based on these results, another model was designed with a rectangular rod-wall configuration and an "open" leading-edge design. The rectangular design eliminated the centerline focusing problem. However, test data on this model indicated noise levels higher than expected (ref. 7). These large noise levels were thought to be caused by the open leading-edge design which resulted in early transition on the rods and higher noise levels. The next change was to provide various sharp flat-plate leading edges and fairing sections from the straight leading edge to the full circular shape of the rods in the hope of improving the transition performance of the open leading edge. These models did reduce the local-stream noise by 50 to 60 percent, but only at low Reynolds numbers. At higher Reynolds numbers ($R_\infty \gtrsim 1.6 \times 10^7$), the noise levels were not appreciable attenuated by the shield, partly because of premature transition in the boundary layers on the rods.

This report presents a brief review of some of the pertinent transition results from previous versions of the rectangular shield as well as more detailed results and analysis of the data obtained on a new modified version of the rectangular shield. Data were obtained at Mach 5 over the Reynolds number range of 0.5×10^7 to 8.0×10^7 per meter.

Use of trade names or names of manufacturers in this report does not constitute an official endorsement of such products or manufacturers, either expressed or implied, by the National Aeronautics and Space Administration.

SYMBOLS

A	amplitude of acoustic waves proportioned to rms pressure fluctuation
C_r	reflection coefficient for specific sound energy (ref. 7)
d	rod diameter, 0.635 cm
e	hot-wire voltage, mV
F	dimensionless frequency parameter, $\frac{2\pi f \nu_e}{u_e^2}$
f	frequency, kHz
g	minimum physical width of gaps between rods, cm
ℓ	longitudinal distance along nozzle centerline from beginning of uniform test rhombus, cm
M	Mach number

p	static pressure
p_o	stagnation pressure
$p_{t,w}$	surface pitot pressure on rods
p_t	pitot pressure
R_e	local Reynolds number, per meter
R_∞	free-stream Reynolds number, per meter
R_x	local free-stream Reynolds number based on wetted length from leading edge
R_δ	local free-stream Reynolds number based on boundary-layer thickness
r	nozzle radius, cm
T	absolute temperature
u	velocity in x direction
w	mass flow from hot wire, g/sec
x	distance from model leading edge (axial), cm
y	horizontal distance normal to model centerline, cm
z	vertical distance normal to model centerline, cm
α	angle of attack, deg
β	shock angle, deg
Δe_m	hot-wire sensitivity to mass-flow fluctuation
Δe_T	hot-wire sensitivity to total temperature fluctuations
δ	boundary-layer thickness, cm
δ^*	boundary-layer displacement thickness, cm
μ	Mach angle, deg
ν	kinematic viscosity

Subscripts:

a	acoustic-origin location
box	test-chamber condition

e	local value at edge of boundary layer
FP	flat-plate value
I	incident noise
o	stagnation condition
p	probe location
pl	plenum
pls	plenum side of rods
R	reflected noise
SL	windward stagnation line of rods (on side of rods facing into shield interior)
s	velocity of moving acoustic source in boundary layers
T	transition location
w	value at surface
∞	free-stream condition

Superscripts:

~	root mean square (rms) value
-	mean value

APPARATUS AND TESTS

The tests were made in the Mach 5 pilot quiet tunnel at the Langley Research Center (refs. 8 and 9). This tunnel (fig. 1(a)) consists of a settling chamber, a Mach 5 axisymmetric nozzle, an open jet test section within a vacuum chamber, and a diffuser section. The tunnel general layout and operating conditions are described in reference 8. The Mach 5 axisymmetric nozzle incorporates a boundary-layer suction slot just upstream of the throat. The purpose of the slot is to bleed off the settling-chamber turbulent boundary layer before it enters the nozzle so that a laminar boundary layer can be maintained on the downstream nozzle wall to higher Reynolds numbers (ref. 9). However, for the present tests, the bleed valves were closed. The slot lip then trips the nozzle-wall boundary layer so that the "transition peak" (ref. 10) in the nozzle input noise occurs at a much lower Reynolds number, which is below the range of interest for these tests.

The rectangular rod-wall sound shield is shown mounted in the tunnel in figure 1(a). A photograph of the shield used in the present investigation, Mod V, is shown in figure 1(b). The inside walls consisted of 0.635-cm diameter rods with 0.102-cm gaps between the rods and between the rods and corner fairings as indicated in figure 1(c). The leading edge of each rod-wall panel was a sharp flat-plate segment (fig. 1(b)) with a leading-edge thickness of less than 0.003 cm at the beginning of the tests. The present rod-wall sound shield (Mod V, fig. 1(b)) differs from the flat test panel and the previous model (Mod IV) in the fairing region between the sharp flat-plate leading edge and the round rods. The new fairing was designed to provide a nearly constant streamwise flow area between the leading-edge plate and the rods. This required that the rods be machined flat at the junctions with the leading edge. This flat section decreases in width until at 8.3 cm downstream of the leading edge the rods are cylindrical. (See fig. 8.) Surrounding the rectangular rod-wall sound shield is a plenum chamber (fig. 1(c)) ducted to a vacuum tank. The pressure ratio of the plenum side to the flow side of the rods is thereby maintained at 0.5 or less to provide sonic cross flow in the gaps. The shield is mounted with its sharp leading edge about 0.6 cm upstream of the exit of the Mach 5 nozzle.

Surface pitot pressures on the rods were measured with a three-tube pitot rake shown in figure 2(a). A traversing mechanism was used to move the pressure rake during a test run. Mean free-stream pitot pressures were measured inside the rod-wall sound shield with another three-tube rake. A sketch of this rake will be shown in a later figure. Free-stream pressures were measured in the vertical center plane of the model and in a horizontal plane 1.11 cm above the model centerline.

Pitot-pressure fluctuations at six different stations within the shielded region of the model were measured on-centerline and off-centerline by the method of reference 11. The basic calibration techniques and data reduction procedures are also given in reference 11. In the present tests, these pressures were measured using two different pitot probes containing piezoelectric transducers. Two 0.32-cm diameter transducers were mounted in a 0.64-cm diameter probe (see fig. 2(b)), and two 0.64-cm diameter transducers were mounted in a 1.28-cm diameter probe. In each probe one transducer (exposed), was mounted in the probe so that it was exposed to the flow, and the second transducer (covered) was mounted behind the exposed transducer to measure only the accelerations caused by vibration of the probe (ref. 11). The root mean square (rms) pressure was obtained by subtracting the mean square of the covered-transducer acceleration pressure from the mean square of the exposed-transducer pressure and taking the square root of the difference. Thus, probe acceleration effects are removed from the measurements. Low-pass filters of 150 kHz were used for all data. Specifications of the transducers used are given in the following table:

Probe diam, cm	Transducer diam, cm	Resolution,[a] Pa (b)	Resonant frequency, Hz (b)	Axial vibration sensivity, Pa/g (b)	Sensitivity,[c] Pa/mV	Position
0.640	0.318	68.95	250	20.68	552.5	Exposed
.640	.318	68.95	250	20.68	310.6	Covered
1.280	.635	27.58	300	13.79	140.4	Exposed
1.280	.635	27.58	300	13.79	139.3	Covered

[a]200 μV peak-to-peak broadband electrical noise.
[b]Manufacturer's specifications.
[c]Calibrated at 1000 Hz.

Hot-wire data were obtained at four stations in the shield for $R_\infty \approx 1.5 \times 10^7$. The data reduction techniques and probe design were the same as those described in reference 11.

Static pressures were measured on the flow side and the plenum side of the rods and in the gaps between selected rods. Static pressures were also measured on the nozzle wall. Tests were conducted at a nominal free-stream Mach number of 5 and at R_∞ from 0.5×10^7 to 8.0×10^7. The stagnation temperature was maintained at high enough levels to avoid condensation effects in the shield flow.

RESULTS AND DISCUSSION

Pressure measurements were made within the rectangular rod-wall sound shield installed in the open-jet test section of the Mach 5 pilot quiet tunnel. These tests were made with the nozzle bleed valves closed; therefore, the nozzle-wall boundary layer was tripped and completely turbulent for $R_\infty > 1.0 \times 10^7$ (refs. 9 and 10).

Static Pressures

The upper- and lower-surface rod static pressures on the bottom panel of the model, plenum pressure, and test-section chamber pressure, all normalized by the static pressure measured at 1.8 cm upstream of the nozzle exit, are shown in figure 3. If static pressures in the entire plenum are uniform, the inviscid cross flow in the gaps between the rods should be sonic (see fig. 3(a)), since pressures in the plenum were always less than 0.53 of free-stream static pressure. Sonic cross flow is desirable to reduce the plenum noise that may enter the internal shielded region of the rod-wall sound shield. The pressures on the bottom or the plenum sides of the rods are generally somewhat lower than the plenum pressure except at the two forward stations for the lower unit Reynolds numbers. The cross flow is presumably reduced for these conditions and some plenum noise could enter the shielded flow, but the internal test-section flow is not greatly disturbed, as evidenced by the top- or flow-side rod static pressures (fig.3 (b)). These pressures are nearly the same as the free-stream static pressures except for the downstream orifice

at $x = 30.2$. Figure 3(b) indicates that a pressure rise generally occurred between $x = 20.0$ and $x = 30.0$. This pressure rise is believed to be caused by the top leading-edge shock impinging on the rod surfaces at $x \approx 28.0$, as will be shown later.

The test-chamber box pressure provides an indication of boundary-layer separation in the nozzle. Figure 4 presents a collection of data obtained in the pilot quiet tunnel with several different models over a range of unit Reynolds numbers. When the static pressure at the nozzle wall exceeds free-stream static pressure p_∞, then separation at that orifice has presumably occurred. Thus, as shown by figure 4, if the ratio of test-chamber pressure to free-stream pressure is greater than approximately 2.3, then separation would be expected at the orifice closest to the nozzle exit. Nozzle boundary-layer separation is important because the corners of the leading edge are close to the nozzle boundary-layer edge as shown in figure 5. If separation does occur far enough upstream in the nozzle, the nozzle turbulent boundary layer may enter the model causing early transition in the rod-wall sound shield and free-stream disturbances. However, figure 4 indicates that no significant separation occurs at or upstream of the nozzle orifice 1.28 cm upstream of the nozzle exit when $p_{box}/p_\infty \leq 3.1$. Since figure 3(b) shows that $p_{box}/p_\infty \leq 2.8$ and figure 5 shows some clearance between the mean boundary-layer edge and the corner of the model (δ is based on pitot-pressure surveys in ref. 7 at $R_\infty = 7 \times 10^6$ to 30×10^6), it may be concluded that the spillage of boundary-layer air into the shield corners should not be a serious problem, even allowing for intermittency effects out to a distance from the wall of 15 percent greater that δ.

Free-Stream Pitot Pressures

A three-tube pitot rake (see sketch in fig. 6) was used to measure pitot pressures within the rod-wall sound shield. The pitot probe was installed on a traversing mechanism so that an axial survey of approximately 15.0 cm could be made during one run. Thus, to complete the survey to $x = 48.0$ required four different runs.

Pitot-pressure measurements with the rake in both the horizontal and vertical positions are presented in figure 6. The locations of the strong leading-edge shocks are noted in the figure. The locations of the peak pressures shown in figures 6(a) to 6(c) indicate that the top-wall and bottom-wall shock angles are approximately 12.2° and 12.9°, respectively. (These angles were calculated from the known tube spacing.) These calculated shock angles do not agree with the angle of 13.1° based on the magnitude of p_t/p_0 at the peaks. There could be several reasons for these discrepancies, of which probe tolerances and model misalignment may be mentioned. There is also evidence of rake misalignment or flow angularity. For example, if the locations of the pressure peaks from figure 6(a) for the centerline pitot tube are plotted versus distance, as shown in figure 7(a), it can be seen that the bottom-wall shock and top-wall shock do not impinge on the centerline tube at a common axial station. Also shown in figure 7 are several other points denoting the locations of the peaks in the pitot-pressure distributions from figures 6(a) and 6(d). The dashed lines connecting these points should represent the location of the actual leading-

edge shocks and their downstream reflections. Comparison of these lines in figure 7(a) with the long-short dashed lines which are drawn through the leading edge at an angle of 13° shows again that the rake may be misaligned or that the flow is not symmetrical. Extrapolation of the dashed lines forward indicates that the top- and bottom-wall leading-edge shocks may be stronger at the leading edge than further downstream. On the other hand, the peak pressure points from figure 6(d) (with the rake horizontal) shown in figure 7(b) fall almost exactly on the 13° lines, indicating very little flow asymmetry or misalignment problems for these particular data. The pitot surveys (fig. 6) show that there is a core region (2.5-cm square) of relatively undisturbed flow over an axial distance of about 16.0 cm starting at $x \approx 22.0$. The pressure peaks at $x = 48.5$ (figs. 6(a) to 6(c)) occur because a shock disturbance is generated at the junction of the rods and the rear flat plate ($x = 33.3$).

Comparisons of the locations of the peak pressure points for the bottom-wall shock in figures 6(a) to 6(c) indicate that this shock moves downstream significant distances with increasing Reynolds number. The side-wall shocks (figs. 6(a) to 6(f)) also appear to shift downstream somewhat with increasing Reynolds number. The top-wall shock remains essentially at a fixed location. These shock movements may be caused by changes in suction flow rates over the forward portions of the rod-wall panels. There is additional indirect evidence from figure 3 of increases in suction flow rates with increasing R_{∞} in the forward region of the bottom panel. This figure shows that the pressure ratio across the rods (p_{pls}/p_{SL}) at the forward orifice decreases from about 1.0 at $R_{\infty} \approx 1.0 \times 10^{7}$ to about 0.4 at the highest Reynolds number. Thus, at the lower Reynolds numbers, suction flow rates may be quite small back to 10.0 cm from the leading edge, at least on the bottom panel.

Transition

Figure 8 shows a top view of the bottom panel. The projected location of the leading-edge shocks with $\beta = 13.1^{\circ}$ (based on data of fig. 6) and also the leading-edge Mach lines ($\mu = 11.8^{\circ}$) are shown. The actual intersection locus of the side-wall shocks with the bottom panel would be slightly greater than 13.1°, as indicated by the sketch in figure 9 which shows the estimated shock structure inside the shield, assuming "regular reflection" of the intersecting shocks in the corners based on results from reference 12. Also shown in figure 8 is an approximate locus of the "acoustic origins" (ref. 11) on the panel for a typical probe location at $x_p = 33.0$ on the model centerline. This locus is a hyperbola which is the intersection of a Mach cone with the panel surface with the vertex of the cone at the probe tip on the shield centerline at $x_p = 33.0$. Note also that the rods are numbered in figure 8.

The location of transition on the top of the rods as indicated in figure 8 was determined from surface pitot data. Typical distributions of $p_{t,w}/p_o$ along rods 1 to 6 and rod 8 are shown in figure 10. The approximate locations of the pressure rise due to the leading-edge shocks are indicated in this figure. The location of transition, denoted by the crosshatched areas, is taken as the region where the surface pitot pressure begins to increase with increasing downstream distance, but is generally outside regions influenced by the leading-edge shocks, except on rods 4 and 8. Also, careful examination of

figure 10 indicates the location of the leading-edge shocks is not noticeably affected by unit Reynolds number, whereas the designated location of transition generally moves forward with increasing unit Reynolds number except on rod 1 for $R_\infty \geq 1.6 \times 10^7$. It is clear that the surface pitot technique is subject to uncertainties in the present application due to the very-thin boundary layer, the small radius of the rods, the presence of leading-edge shocks, and other flow disturbances. Nevertheless, it may be concluded that transition did not occur on the rods for $R_\infty \leq 1.0 \times 10^7$, the lowest value of the unit Reynolds number. At $R_\infty = 1.6 \times 10^7$, transition moved ahead of the acoustic-origin locus for $x_p = 33.0$ on rod 6 (figs. 8 and 10(f)), whereas at $R_\infty = 2.4 \times 10^7$ and 2.9×10^7, transition moved ahead of this acoustic-origin locus on rods 4, 5, 6, and 8. (The acoustic-origin locations for $x_p = 33.0$ are also shown in figure 10.)

A cross plot of the data of figure 10 is shown in figure 11. Again in reference to figure 8, note that the acoustic-origin locus for the fluctuating pitot probe on the model centerline at $x_p = 33.0$ intersects the rods at varying distances from the leading edge. If the surface pitot pressure measured at these acoustic-origin locations x_a for each rod is plotted versus unit Reynolds number, then figure 11 is obtained. Data values for rod 2 are not shown because they coincided with those of rod 3. Transition occurs on rods 4, 5, 6, and 8 for $R_\infty \approx 1.5$ to 1.8×10^7 for the acoustic-origin locations corresponding to this probe location. Thus, if transition in the rod boundary layers along the top of the rods contributes to the noise levels in the shield, then the noise level measured at this probe location may be expected to increase over this range of unit Reynolds numbers. The noise measurements (fluctuating pressure) will be presented in the next section of this report.

The results of using a hot-wire probe in the boundary layer on the center rod of the test panel with Mod IV are presented in figure 12. The high rms voltage levels on Mod IV indicate early transition to turbulent flow and the much lower levels on the test panel indicate laminar flow to at least $x = 45.0$. The leading-edge configuration for Mod IV was essentially the same as that for the test panel (refs. 4 to 6). The sharp flat-plate section on these models was 3.8-cm long, and this flat section was followed by a 3.0-cm long fairing contoured into the gaps. However, the surface finish on Mod IV was not as smooth as that on the test panel. In figure 13, transition locations from the surface pitot data on rods 1, 4, and 6 of the present rod-wall sound shield (Mod V) are compared with flat-plate data and with data from the test panel (refs. 4 to 6) and earlier versions of the rectangular rod-wall shield (Mod III and Mod IV). The flat-plate leading-edge section of Mod III had the same cross-section dimensions as Mod IV (see fig. 5) but was only 0.63-cm long (in the streamwise direction) followed by a short fairing of 1.9 cm into the gaps between the rods. Possible causes of the early transition on the rectangular model (Mod III, Mod IV, and Mod V) compared with that on the test panel are low suction flow rates near the model leading edges (see section "Free-Stream Pitot Pressures"), leading-edge shock interference, the leading-edge fairing and roughness effects (Mod IV), cross-flow instability on the rods (ref. 6), and instability of the boundary layer on the top of the rods (treated by analogy with linear flat-plate amplification). Both the cross-flow instability and flat-plate type instability could be affected by the different boundary-layer thicknesses on the rods in the rectangular model and the test

panel and the different noise spectra in the pilot quiet tunnel (refs. 8 to 10) and the Langley 20-Inch Mach 6 Tunnel. These different boundary-layer thicknesses and noise spectra will be discussed in a later section of this report.

Another factor involved in the different transition results for Mod V and the test panel that must be considered is "cross-stream contamination" from rod to rod as influenced by the leading-edge shocks for Mod V. Thus, figure 8 shows that transition for $R_\infty \geq 2.4 \times 10^7$ on rods 5 and 6 is ahead of the leading-edge shocks but at the same x location as on rod 4, where transition has moved forward to the shock location. However, for the same Reynolds number range, transition on rods 2 and 3 is always farther from the leading edge and downstream of the shock location. Hence, it may be speculated that the shock disturbance was of just sufficient strength to move transition up to the shock location on rod 4, and that because this shock had greater destabilizing effects on rods 5 and 6 than on rods 2 and 3 (because of the larger downstream distances of the shock locations on rods 5 and 6), transition moved ahead of the shock locations on rods 5 and 6 due to cross-stream contamination from rod 4. There would have to be a cross-stream contamination mechanism between rods 4, 5, and 6 that would be enhanced by the downstream shocks. Involved in the cross-stream contamination is the observed result (ref. 6) that transition occurs in the gaps upstream of transition on the top side of the rods based on comparisons of heat-transfer data along the stagnation line (or top side) of the rods with noise data in the flow field of the flat test panel. This phenomenon probably also occurs in the present model and would help account for the increased noise levels at higher Reynolds numbers and large x stations (discussed in a later section).

Transition on rod 1 (figs. 8 and 10(a)) may be controlled by a different mechanism since it is fixed at $x \approx 11.0$ for $R_\infty \geq 1.6 \times 10^7$. This mechanism is probably related to the corner vortices that would form due to the intersecting shocks as sketched in figure 9.

Fluctuating Pitot-Pressure Measurements

The fluctuating pitot pressures in the flow field of the rod model were measured with 0.64-cm diameter and 1.28-cm diameter pressure probes described previously. Typical data from the two probes expressed as the square of the rms pitot pressure normalized by the mean pitot pressure plotted against unit Reynolds number are given in figure 14. For the 0.64-cm diameter probe (fig. 14(a)), the exposed and covered transducers follow the same trends. At low Reynolds numbers the transducer measurements are fairly large, with the exposed transducer being an order of magnitude larger than the covered transducer. With increasing Reynolds number the measured values decrease up to about $R_\infty \approx 1.7 \times 10^7$; then both transducers show increasing values, but now the covered transducer value tends to approach that of the exposed transducer. As can be seen, significant errors may be incurred above $R_\infty \approx 2 \times 10^7$ as the values of the exposed and covered transducer approach each other. For the 1.28-cm diameter probe (fig. 14(b)), the normalized signal from the covered transducer increases with unit Reynolds number but is always nearly an order of magnitude below the exposed value. For this larger probe, the errors due to probe vibrations are much smaller than for the 0.64-cm diameter probe.

A schematic side view of the shield mounted at the exit of the Mach 5 nozzle is shown in figure 15. The shielded region is donwstream of the shield leading-edge shocks, and four typical probe stations at x_p = 22.9, 27.9, 33.0, and 38.1 are designated by points 1 through 4 on the shield centerline. According to present theory on noise propagation and reflection in supersonic shields (ref. 7), the local-stream noise at any of these stations would consist mostly of noise originating at or reflected from corresponding regions on the shield wall. These regions are also designated by points 1 through 4 on the bottom panel, but here they are shown near the average streamwise location of the corresponding acoustic-origin loci. (See fig. 8.) The reflected noise originates upstream in the nozzle, and here again, for the purpose of discussion, the corresponding points on the nozzle centerline can be considered as the approximate centers of regions where representative "input" noise levels would be measured. All data shown in figure 15 are for $R_\infty \approx 1.5 \times 10^7$ and are expressed as the ratios of rms pitot pressures to mean pitot pressures. (The hot-wire data were converted to this form by the method of ref. 11.) Some of the apparent scatter in the nozzle data is caused by sharp peaks in noise levels focused along the centerline in the axisymmetric nozzle (ref. 10). Downstream of the nozzle exit, there is less scatter in the nozzle data and the shield noise levels are about 40 to 80 percent of the local nozzle noise levels that would have been measured at the shield stations without the shield in place. However, if we consider the nozzle "input" noise as the levels measured at the corresponding upstream nozzle centerline region, it is clear that much less attenuation of this input noise has occurred. The line labeled "Laminar flat-plate prediction" is based on the faired dashed line of nozzle input noise levels indicated and the shield theory of reference 7 with a reflection coefficient of $C_r = 0.36$, which is a mean value from laminar flat-plate data at the appropriate values of Mach number and boundary-layer thickness Reynolds number (See fig. 10(b) of ref. 7.) Since the shield noise levels measured with the hot wire are above this predicted level, there may be additional sources of noise associated with transition on the rods, with jittering shocklets including the leading-edge shocks, or with other possible sources such as corner disturbances. The pitot-probe data are significantly lower than the hot-wire data for $x > 28$ partly because of the smaller response of the pitot probe at high frequencies. Note the corresponding nozzle input data as measured with the pitot probe are also lower than the hot-wire data.

The normalized rms pitot pressures measured with the two probes over the test range of unit Reynolds number for x_p = 25.4, 27.9, 30.5, 33.0, 35.6, and 38.1 are shown in figure 16. The cross-hatched regions are the approximate nozzle input noise levels (ref. 10) as defined above. Thus, for example, at $x_p = 35.6$ (fig. 16(e)), the shield noise levels are essentially the same as the input noise from $R_\infty = 9.0 \times 10^6$ to 2.0×10^7, where an increase in noise levels is observed. The surface pitot data (figs. 8 and 10) indicate that this increase in noise may be caused by transition moving forward to about x_a = 15.0 to 17.0, at least on the center rods. At $x_p = 33.0$ (fig. 16(d)), this rise occurs at $R_\infty \approx 2.5 \times 10^7$ which again is consistent with the picture of transition behavior with respect to the acoustic-origin loci from the surface pitot data (fig. 8) for rods 4, 5, and 6. This increase in noise level (greater than nozzle input noise), as measured with the 0.64-cm diameter probe, is observed at all on-centerline stations except $x_p = 38.1$ (fig. 16(f)) for which the rod-wall model noise is apparently roughly equal to the nozzle input

noise at all Reynolds numbers. Figure 16(b) shows the results of three different attempts to obtain data at $x_p = 27.9$. Some of these data show a slight noise reduction but the majority of the data again indicate a noise increase above $R_\infty = 2 \times 10^7$.

Also, shown in figure 16 are data obtained by using the 1.28-cm diameter probe. For the first three probe stations, the 1.28-cm diameter probe data are lower than the 0.64-cm diameter probe data. This result may be due partly to the larger vibration errors in the small probe at the forward stations where the probe sting support was longer. However, the response of the larger probe to the high frequencies (small scale) of the reflected input noise is certainly not as good as that of the small probe. The response of the hot-wire probe to the high frequencies is better than either pitot probe. This better high-frequency response probably accounts for the higher noise levels obtained from the hot wire compared with the pitot-probe levels shown in figure 15 for $x_p > 32.0$.

The fluctuating pitot-pressure probe was also placed off the centerline and a complete set of data over the same ranges of Reynolds numbers and x_p as with the probe on the centerline are presented in figure 17. Comparison of these data with the on-centerline data from figure 16 shows generally similar trends and levels in noise. While the scatter in both sets of data is quite large, the noise field intensities do not appear to vary greatly with y or z, so any strong centerline focusing of the noise field does not occur.

Effect of Noise Input Frequencies on Attentuation of Reflected Noise

The sound-forcing theory of Mack (ref. 13) for a flat plate at $M_\infty = 4.5$ was applied to the stagnation-line flow on the rods of the flat test panel and the rectangular sound-shield model by equating the boundary-layer thickness Reynolds number in the flat-plate calculation to that of the rods along their stagnation line. The laminar boundary-layer thickness on the rods was obtained with the computer code of reference 14. In this calculation, the flow on the rods is assumed to be the same as on swept infinite cylinders. The velocity distribution around the rods normal to their axes (in the "chordwise" direction) was based on pressure data and theory of reference 4 corrected for the displacement-thickness effect as described in reference 5. Typical results of these calculations are shown in figure 18 for the conditions of the rectangular sound-shield model, which are $M_\infty = 5.0$, $g/d = 0.16$, $T_w/T_o = 0.88$, and $d = 0.635$. The boundary layer is thicker along the stagnation line (top) of the rods than in the gaps. It is of interest to note that the gap is filled with boundary layer at $R_\infty < 5 \times 10^6$ which is near the lower end of the range of present test conditions.

The computed results for the boundary-layer thickness on the stagnation line (with the δ^* correction included) are represented by the curve-fit equation

$$\left(\frac{2\delta}{g}\right)_{SL} = (1.7 \times 10^4) R_\infty^{-0.586} \qquad (1)$$

or in terms of the boundary-layer thickness Reynolds number where $g = 0.102$,

$$R_{\delta_{SL}} = 8.67 R_{\infty}^{0.414} \tag{2}$$

Similarly, for the flat test panel with the conditions $M_{\infty} = 6.0$, $\alpha = 10^{o}$, $M_e = 4.7$, $g/d = 0.16$, $T_w/T_o = 0.62$, and $d = 0.635$, computed results given in references 4 and 5 have been adjusted to include a δ^* correction. The boundary layer thickness Reynolds number is then given by the relation

$$R_{\delta_{SL}} = 7.71 R_{\infty}^{0.414} \tag{3}$$

Thus, at the same unit Reynolds number, the computed boundary-layer thickness in the present rectangular rod-wall sound-shield model is about 13 percent thicker than on the flat test panel. This thicker boundary layer in the rectangular model is due partly to the higher local Mach number, but the main cause is the higher value of T_w/T_o.

The boundary-layer thickness Reynolds number for a flat plate with the conditions to be used here (adiabatic wall and $M_{\infty} = 4.5$) from the calculations of Mack (ref. 13) as well as the data of Kendall (private communication with J. M. Kendall, Jet Propulsion Laboratory, Pasadena, CA) is

$$R_{\delta_{FP}} = 14.6\sqrt{R_{x_{FP}}} \tag{4}$$

Thus, for a given R_{∞} in the rod-wall tests, an equivalent flat-plate Reynolds number is found by equating $R_{\delta_{SL}}$, equations (2) or (3), to $R_{\delta_{FP}}$, equation (4).

New calculations provided by Mack (ref. 13) for the amplitude of the reflected wave normalized by the amplitude of the incident wave are compared with narrow-band experimental data of Kendall (private communication) in figure 19. The source speed used in the calculations was 65 percent of free-stream velocity and the wave-obliqueness angle was zero. The data were obtained in the same way as described for the frequency response results of reference 15 except that here the wire used to obtain A was just outside the boundary layer at the local x whereas the other wire used to obtain A_{∞} was in the free stream slightly ahead of and below the plate leading edge, just as in reference 15. The filled data points of figure 19 represent data for which the corresponding free-stream levels were not measured. Each of the sets of points has been jointly multiplied by a factor so as to bring it to the level of other measurements in the overlapping R_x range for which the stream level was known. For the present purposes, the ratio of A/A_{∞} is essentially the same as the ratio of the rms reflected noise to rms incident noise. (See refs. 13 and 15.) Thus, both the theory and data in figure 19 show that noise reflected from a laminar flat-plate boundary layer is attenuated, or reduced, below the incident noise level but to an extent that is highly dependent on the frequency and the Reynolds number. The frequency parameter F in figure 19 is defined as

$$F = \frac{2\pi f \nu_e}{u_e^2} \tag{5}$$

or, if you solve for f,

$$f = \frac{F u_e R_e}{2\pi} \tag{6}$$

So for given wind-tunnel conditions, the required frequency can be found. The intensity of the reflected noise depends on boundary-layer thickness, the incident-noise wavelength, and presumably, to some extent, on the boundary-layer profile shapes. However, in the absence of more complete calculations or data, it is assumed that the profile shapes in the windward region of the rods are the same as the flat-plate profiles.

Application to test panel.- The theory and data from the faired curves of figure 19 were applied to the test panel as described previously and the results, in terms of the ratio of the rms reflected noise to the rms incident noise as a function of frequency at various unit Reynolds numbers, are presented in figure 20. Thus, the theory predicts that there should be attenuation of reflected noise at frequencies below about 40 kHz (fig. 20(a)), whereas the data indicate that the rod-wall test panel should attenuate noise at frequencies below approximately 80 kHz (fig. 20(b)) at the three largest values of unit Reynolds numbers.

A typical frequency spectrum of the free-stream noise measured with a 0.64-cm diameter fluctuating-pitot-pressure probe on the centerline of the Langley 20-Inch Mach 6 Tunnel for $R_\infty = 1.6 \times 10^7$ is presented in figure 21. From the upper frequency limits for noise attenuation from figure 20, figure 21 indicates that a significant part of the noise in the tunnel should be attenuated by using a rod-wall shield in agreement with measured noise data on the flat test panel (refs. 4 to 7). To show that the spectrum of figure 21 is not peculiar to the wind tunnel or instrument, a spectrum from the JPL 20-inch continuous flow tunnel taken from reference 15 is shown in figure 22. The attenuation limits from figure 20 are noted in figure 22 and the conclusion that a significant part of the free-stream noise energy should be attenuated by a rod-wall shield similar to the test panel is also valid in the JPL tunnel.

Application to rectangular sound shield.- Figure 23 was derived in the same way as figure 20 but equation (2) was used instead of equation (3). Application of the theory (fig. 23 (a)) indicates that the rectangular rod-wall sound shield could be effective in reducing noise levels provided the frequencies of the input noise are below about 30 kHz. Application of Kendall's data to this problem (fig. 20(b)) shows that attenuation of the reflected noise should occur at input frequencies below about 50 kHz for $R_\infty \leq 3.1 \times 10^{-7}$. Unfortunately, free-stream noise spectra in the rapid-expansion Mach 5 nozzle (figs. 24 and 25)

show that there is considerable energy present in the upstream input regions of this nozzle above these frequencies. Hence, it can be concluded that overall attenuation of the reflected noise in the rectangular rod model would be considerably less than for the test panel due to the high frequencies of the nozzle input noise from the Mach 5 nozzle.

Noise Spectra in the Shielded Region

Typical spectra obtained with the fluctuating-pitot-pressure probes on the model centerline at several x stations and Reynolds numbers are shown in figure 26. In all cases the lower trace is from the covered transducer, which responds only to vibration of the probe. (See ref. 11 for details of probe construction and calibration procedures.) The ordinate is the normalized mean square output of the transducers in terms of $(\tilde{p}_t/\bar{p}_t)^2$.

Figure 26(a) was obtained with the 0.64-cm diameter probe at six different x stations for $R_\infty \approx 1.5 \times 10^7$. At frequencies below 10 kHz, the probe acceleration or vibration contribution is large and tends to dominate the exposed- or flow-transducer output except for a peak of $f \approx 2$ kHz, which evidently originates in the upstream nozzle flow as shown by the prominent peak of $f \approx 2$ kHz in figure 25. The hot-wire spectra (fig. 24) do not show any evidence of a peak at this low frequency. Another flow-related peak is evident in figure 26(a) at $f \approx 22$ kHz which is also present in the nozzle flow (fig. 25). A significant increase in energy between 30 and 40 kHz is evident for $x \geq 30.5$. The "tail" of the spectra for $f > 40$ kHz also appears to increase with increasing x beyond 30.5 cm. These last two effects are caused by increases in shield-noise properties that are related to transition and the development of turbulent boundary-layer flow on the rods at the larger x stations as discussed previously and as shown by the hot-wire data in figure 15 and the flagged symbols in figure 16. These flagged symbols are the rms values corresponding the same runs as for the spectral data of figure 26(a).

Figure 26(b) shows the spectra from the 0.64-cm and 1.28-cm diameter probes at $x = 33.0$ and $R_\infty \approx 1.5 \times 10^7$. While the relative vibration levels for the larger-diameter probe are much smaller than for the small probe, the flow disturbances for $f > 20$ are not detected by the large probe. It is obvious that the large probe cannot respond to spectral details or levels at higher frequencies.

Figure 26(c) shows variations of the spectra with Reynolds number at $x = 33.0$ as measured with the 0.64-cm diameter probe. The rms values corresponding to these runs are plotted as flagged symbols in figure 16(d). The large increases in energy with increasing Reynolds number for $R_\infty > 2.33 \times 10^7$ are again caused to a considerable extent by increases at the higher frequencies from about 30 kHz to 80 or 90 kHz. At the highest Reynolds number of 5.4×10^7, an increase in energy around $f = 70$ is apparent. These increases in energy with increasing Reynolds number at high frequencies are definitely caused by turbulent flow on the rods since no corresponding increases occurred in the nozzle rms noise input values. (See fig. 2, ref. 10.)

Hot-Wire Mode Diagrams and Source Velocities

Hot-wire data in this report have been provided by John B. Anders, Jr., of Langley Research Center. Hot-wire mode diagrams with the probe set on the model centerline are shown in figure 27. The variables used are well known (see ref. 11, for example) and will not be discussed here except to point out that a straight line with a positive slope and positive intercept indicates that the dominant disturbances are acoustic waves radiated from moving sources. The slopes of the straight lines are the rms mass-flow fluctuations $\tilde{m}/\bar{m}$. The pressure-fluctuation levels are approximately proportional to $\tilde{m}/\bar{m}$ as indicated by comparing the values of $\tilde{p}_t/\bar{p}_t$ listed in the figure with the apparent slopes of the faired lines. Thus, it is clear that a significant increase in noise level has occurred between $x = 27.9$ and $x = 33.0$. This increase in noise is presumably caused by transitional and turbulent flow on the rods and in the gaps that would have moved up to or ahead of the acoustic origin for the probe at $x = 33.0$ on rods 1 and 6. (See fig. 8 and previous discussion in "Transition" section.) These hot-wire data are plotted in figure 15 and the noise levels for $x \geq 33.0$ are considerably higher than the pitot data in that figure. Unfortunately, hot-wire spectra were not obtained, but these higher noise levels from the hot-wire data may be attributed at least partly to the increases in energy at high frequencies associated with turbulent flow on rods as discussed previously and the inherent capability of the hot-wire probe to respond more correctly to the higher frequencies as compared with the pitot-pressure probe. This better response of the hot wire is due not only to the smaller physical size of the probe itself but also to the low resonant frequencies of the piezoelectric pressure transducers and their sensitivity to vibration disturbances. (See refs. 11 and 16 and previous discussion in this report.)

The hot-wire probe can also be used to obtain the apparent velocity of the sources when the dominant disturbances are acoustic (refs. 17 to 19). A comparison of source velocities measured by several methods from $M_\infty = 2$ to 8 is given in reference 20. By using the technique of cross correlation between the two wires spaced a known streamwise distance apart (refs. 18 and 19), the results at $M_\infty \approx 5$ vary from $\bar{u}_s/\bar{u}_\infty \approx 0.57$ to 0.70 (ref. 20). The single-wire technique (ref. 17) is not as accurate as the two-wire technique, but it can be used to indicate approximate levels and trends.

The single-wire technique was used to obtain values of $\bar{u}_s/\bar{u}_\infty$ inside the rectangular rod-wall shield. Typical results for Mod II through Mod V are shown in figure 28. A sketch of the leading-edge configuration for these modifications is given in figure 5 which shows that Mod II is essentially the same as Mod I.

Data for Mod I (ref. 7) showed that strong outflow occurred in the leading-edge region. This outflow apparently caused early transition. The source velocities for Mod II increase from zero at small R_∞ to large values of 0.5 to 0.7 (in the range of free-stream wind-tunnel values) at $R_\infty \approx 3.2 \times 10^7$. These results imply that for low Reynolds numbers, the noise in the shield was dominated by fixed sources that were probably caused by shimmering shocklets from disturbed flow in the leading-edge region. The trend of the $\bar{u}_s/\bar{u}_\infty$ values with varying Reynolds number for Mod III, Mod IV, and Mod V is just the opposite of that for Mod II. At low R_∞ the values are comparable to free-stream wind-

tunnel values of 0.5 to 0.7, but as R_∞ increases the source velocities consistently decrease. Thus, at low Reynolds numbers and for the upstream x stations, the rod boundary layers at the acoustic origins are mostly laminar and the probe measures noise reflected from the rods at the same source speeds as the nozzle input noise. As the Reynolds number increases, the flow on the rods and in the gaps becomes turbulent and the average source velocity decreases. It seems reasonable that the source velocities in the gap region would decrease due to merging of the adjoining rod boundary layers as the flow approaches and enters the gap. (See refs. 4 and 5 for further discussion and calculations of rod boundary-layer characteristics.)

CONCLUDING REMARKS

A rod-wall sound-shield model was tested at Mach 5 over a range of unit Reynolds number of 0.5×10^7 to 8.0×10^7 per meter. The model consisted of a rectangular array of 0.635-cm diameter rods aligned in the flow direction with 0.102-cm gaps between the rods for boundary-layer suction.

Static-pressure measurements in the nozzle, the test chamber, the model vacuum plenum, and on the rods showed that the flow in the shield was fully started over the range of test conditions. These data also showed that the inviscid cross flow in the gaps was sonic except near the leading edge at the lowest Reynolds number where the cross flow was subsonic. The suction mass flow in this region was presumably reduced below desired values.

Surveys of mean pitot pressure within the shielded region inside the model showed that the leading-edge shocks were strong, but no centerline focusing effects as had occurred in previous tests of an axisymmetric rod-wall shield were present. Leading-edge shocks (side wall and bottom) were observed to move downstream with increasing Reynolds number. A reasonably uniform-flow core was found in the shielded region of the present model. This core was about 16-cm long by 2.5-cm square in cross section.

Transition in the rod boundary layers was obtained from surface pitot-pressure surveys along the windward ray of the rods. Comparison of these data with results from previous tests on a flat rod-wall panel showed that transition occurred much farther forward than in the previous tests. This early transition in the present tests was probably caused by the leading-edge shock disturbances and/or the reduced suction in the upstream regions of the rod-walls.

The noise field in the model was measured with fluctuating pitot-pressure probes utilizing piezoelectric transducers and with hot-wire probes. The hot-wire data showed that the dominant disturbance mode was acoustic. At the lower Reynolds numbers the source velocities for Mod IV and Mod V were within the range of values measured in wind tunnels. At the higher Reynolds numbers the values of the source velocities for Mod III and Mod IV showed a decreasing trend with increasing Reynolds number probably due to increasing noise radiation from the three-dimensional turbulent boundary layers on the rods.

At the lower Reynolds numbers and when the fluctuating pitot-pressure probe "sees" mostly laminar flow on the rods, the local free-stream noise

levels were reduced from about 1.5 percent down to about 0.6 percent by the shield. However, the actual nozzle "input" noise as measured upstream before reflection at the shield wall was not attenuated significantly even when the rod boundary layers were laminar. When the rod boundary layers were transitional or turbulent the shield noise levels at higher Reynold numbers were above nozzle input levels due at least partly to the increase in high frequency energy radiated from the very thin rod boundary layers.

Analysis of theory and data for reflection of noise from flat-plate laminar boundary layers indicates that the lack of significant attenuation when the rod boundary layers were laminar may be attributed to the very high frequencies of the nozzle input noise. These high frequencies are unique to the rapid expansion nozzle and are not found in larger conventional nozzles.

Langley Research Center
National Aeronautics and Space Administration
Hampton, VA 23665
April 25, 1980

REFERENCES

1. Morkovin, Mark V.: Critical Evaluation of Transition From Laminar to Turbulent Shear Layers With Emphasis on Hypersonically Traveling Bodies. AFFDL-TR-68-149, U.S. Air Force, Mar. 1969. (Available from DTIC as AD 686 178.)

2. Pate, S. R.; and Schueler, C. J.: Radiated Aerodynamic Noise Effects on Boundary-Layer Transition in Supersonic and Hypersonic Wind Tunnels. AIAA J., vol. 7, no. 3, Mar. 1969, pp. 450-457.

3. Stainback, P. Calvin: Hypersonic Boundary-Layer Transition in the Presence of Wind-Tunnel Noise. AIAA J., vol. 9, no. 12, Dec. 1971, pp. 2475-2476.

4. Harvey, W. D.; Berger, M. H.; and Stainback, P. C.: Experimental and Theoretical Investigation of a Slotted Noise Shield Model for Wind Tunnel Walls. AIAA Paper No. 74-624, July 1974.

5. Stainback, P. Calvin; Harvey, William D.; and Srokowski, Andrew J.: Effect of Slot Width on Transition and Noise Attenuation of a Flat Sound Shield in a Mach 6 Wind Tunnel. NASA TN D-8081, 1975.

6. Harvey, W. D.; Stainback, P. C.; and Srokowski, A. J.: Effect of Slot Width on Transition and Noise Attenuation of a Sound Shield Panel for Supersonic Wind Tunnels. Proceedings - AIAA 9th Aerodynamic Testing Conference, June 1976, pp. 198-222.

7. Beckwith, I. E.; Anders, J. B.; Stainback, P. C.; Harvey W. D.; and Srokowski, A. J.: Progress in the Development of a Mach 5 Quiet Tunnel. Laminar-Turbulent Transition, AGARD-CPP-224, 1977, pp. 28-1 - 28-14.

8. Beckwith, I. E.: Development of a High Reynolds Number Quiet Tunnel For Transition Research. AIAA J., vol. 13, no. 3, Mar. 1975, pp. 300-306.

9. Anders, J. B.; Stainback, P. C.; Keefe, L. R.; and Beckwith, I. E.: Fluctuating Disturbances in a Mach 5 Wind Tunnel. AIAA J., vol. 15, no. 8, Aug. 1977, pp. 1123-1129.

10. Anders, J. B.; Stainback, P. C.; and Beckwith, I. E.: A New Technique for Reducing Test Section Noise in Supersonic Wind Tunnels. A Collection of Technical Papers - AIAA 10th Aerodynamic Testing Conference, Apr. 1978. pp. 354-364. (Available as AIAA Paper 78-817.)

11. Anders, J. B.; Stainback, P. C.; Keefe, L. R.; and Beckwith, I. E.: Sound and Fluctuating Disturbance Measurements in the Settling Chamber and Test Section of a Small, Mach 5 Wind Tunnel. ICIASF '75 Record, IEEE Publ. 75 CHO 993-6 AES, pp. 329-340.

12. Marconi, Frank: Supersonic, Inviscid, Conical Corner Flowfields. AIAA J., vol. 18, no. 1, Jan. 1980, pp. 78-83.

13. Mack, Leslie M.: Progress in Compressible Boundary Layer Stability Computations. Proceedings of the Boundary Layer Transition Workshop, Volume IV, TOR-0172(S2816-16)-5 (Contract No. F04701-71-C-0172), Aerosp. Corp., Dec. 20, 1971, pp. 1-1 - 1-19.

14. Hixon, Barbara A.; Beckwith, Ivan E.; and Bushnell, Dennis M.: Computer Program for Compressible Laminar or Turbulent Nonsimilar Boundary Layers. NASA TM X-2140, 1971.

15. Kendall, J. M.: Wind Tunnel Experiments Relating to Supersonic and Hypersonic Boundary-Layer Transition. AIAA J., vol. 13, no. 3, Mar. 1975, pp. 290-299.

16. Steenken, W. G.: Effect of Transducer Diameter on Resolution of Total Pressure Fluctuations in a Turbulent Flow. Instrumentation for Air-breathing Propulsion, Allen E. Fuhs and Marshall Kingery, eds., MIT Press, c.1974, pp. 167-177.

17. Laufer, John: Aerodynamic Noise In Supersonic Wind Tunnels. Aerosp. Sci., vol. 28, no. 9, Sept. 1961, pp. 685-692.

18. Laufer, John: Some Statistical Properties of the Pressure Field Radiated by a Turbulent Boundary Layer. Phys. Fluids, vol. 7, no. 8, Aug. 1964, pp. 1191-1197.

19. Kendall, James M., Jr.: JPL Experimental Investigations. Proceedings of the Boundary Layer Transition Workshop, Volume IV, TOR-0172(S2816-16)-5 (Contract No. F04701-71-C-0172), Aerosp. Corp., Dec. 20, 1971, pp. 2-1 - 2-16.

20. Schopper, M. R.: A Model for the Noise Radiated by Turbulent Boundary Layers and Its Interaction With Laminar Layers in Supersonic Flow. AIAA Paper 79-1523, July 1979.

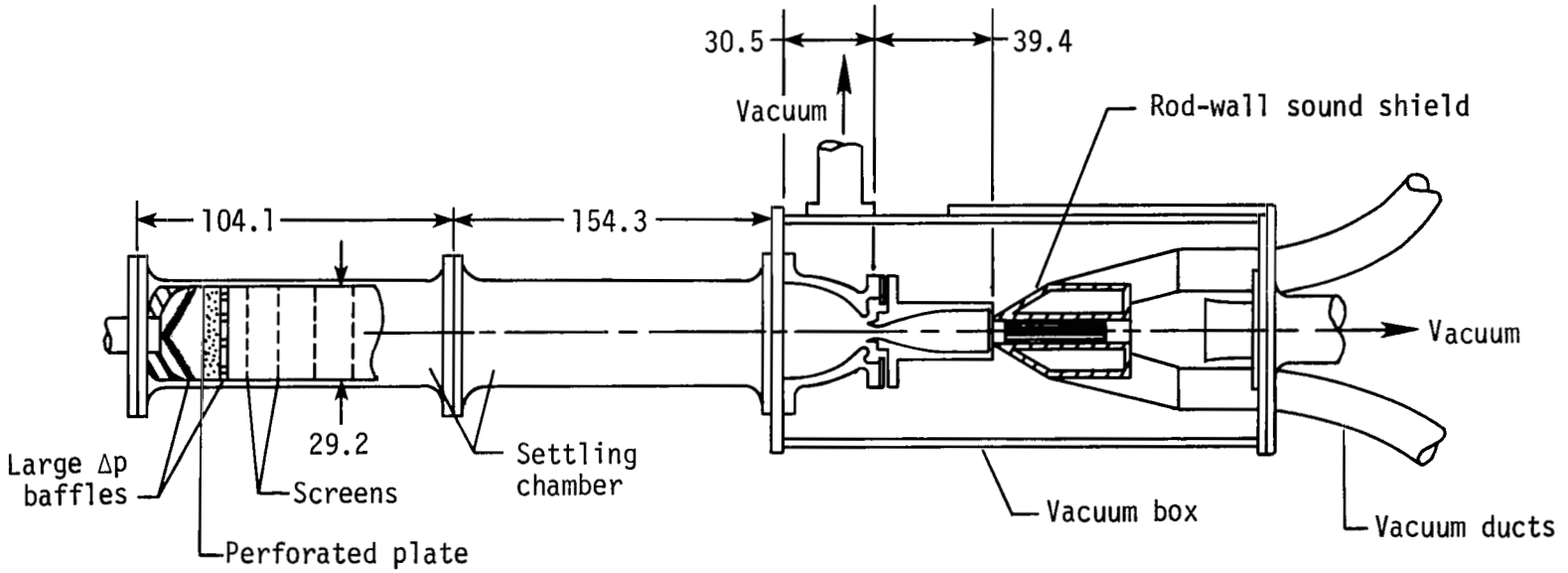

(a) Schematic of test facility showing location of rod-wall sound shield.

Figure 1.- General arrangement of test facility and rod-wall sound shield. Dimensions are in centimeters.

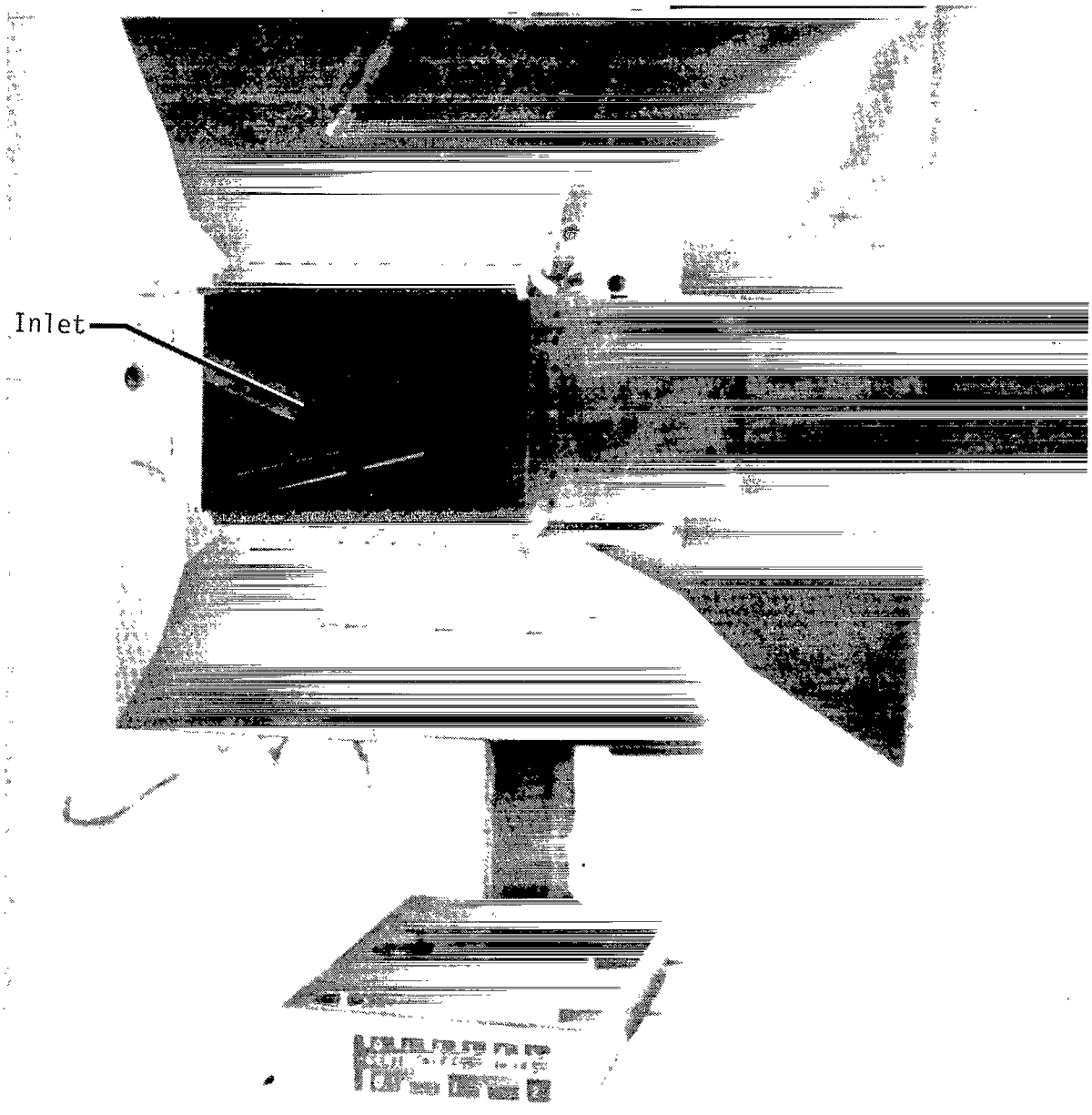

L-78-4006.1

(b) Rod-wall sound shield, Mod V with plenum ducts removed.

Figure 1.- Continued.

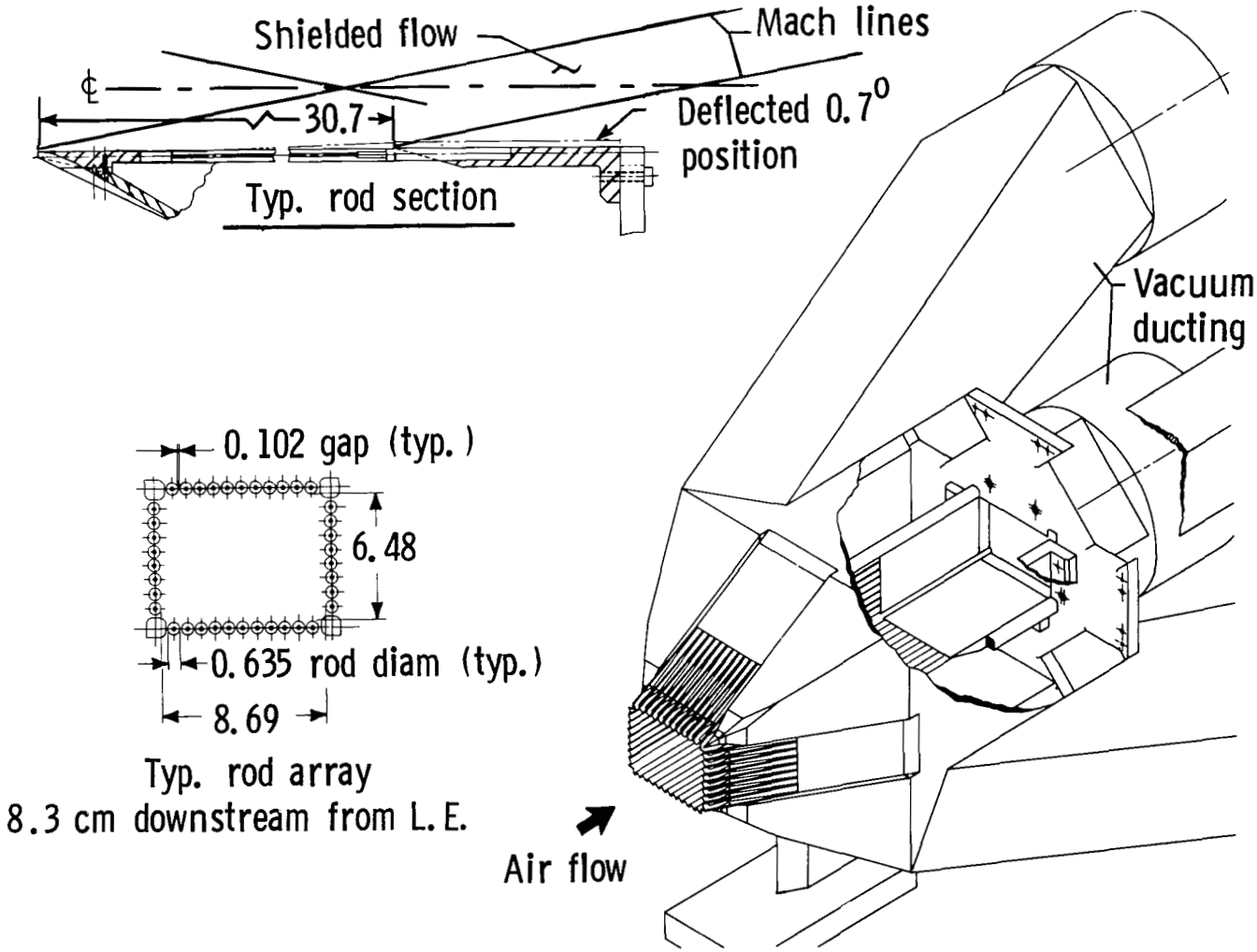

(c) Cut-away view of rod-wall sound shield, Mod I.

Figure 1.- Concluded.

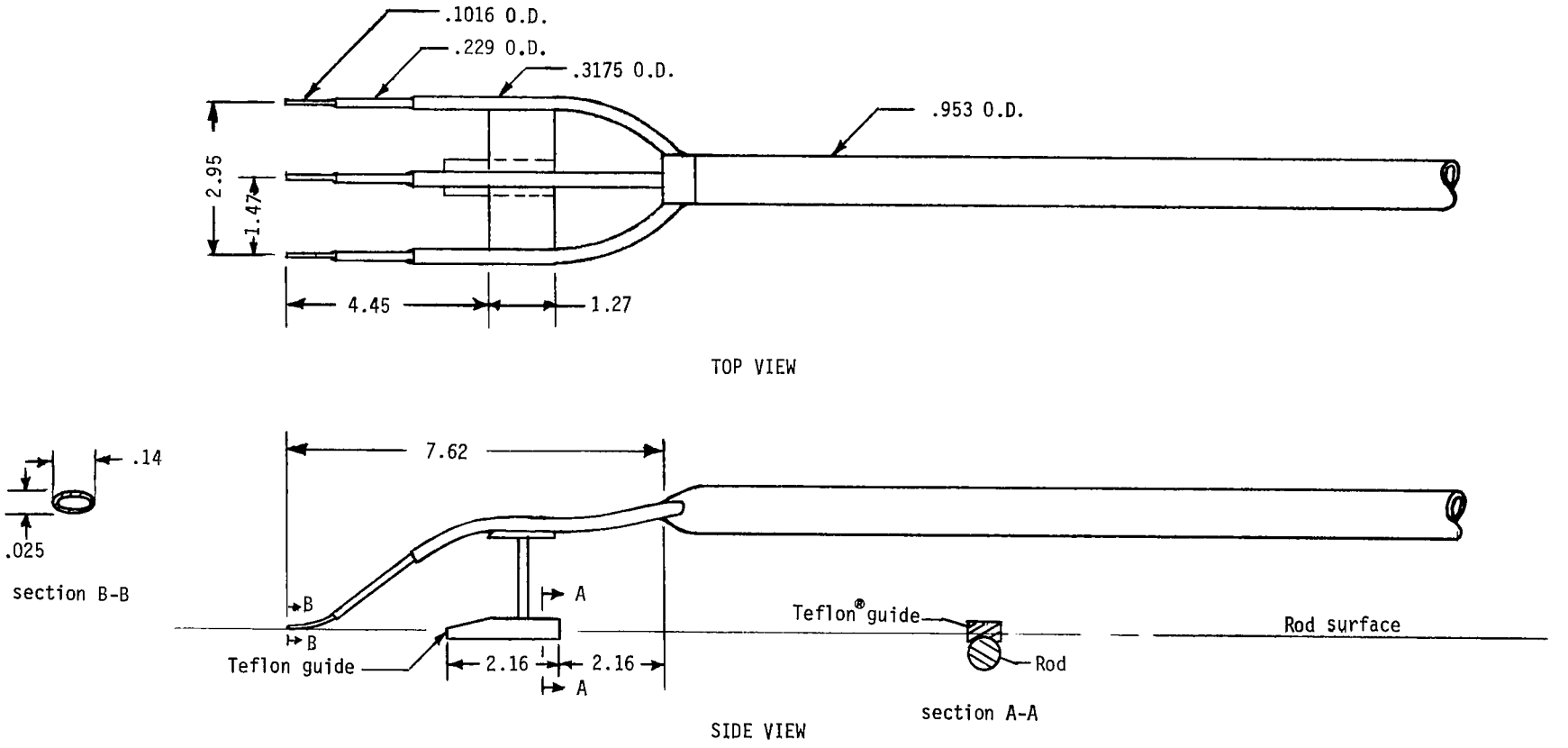

(a) Three-tube surface pitot rake. ®Teflon: registered trademark of E. I. du Pont de Nemours & Co., Inc.

Figure 2.- Pressure probes. All dimensions are in centimeters.

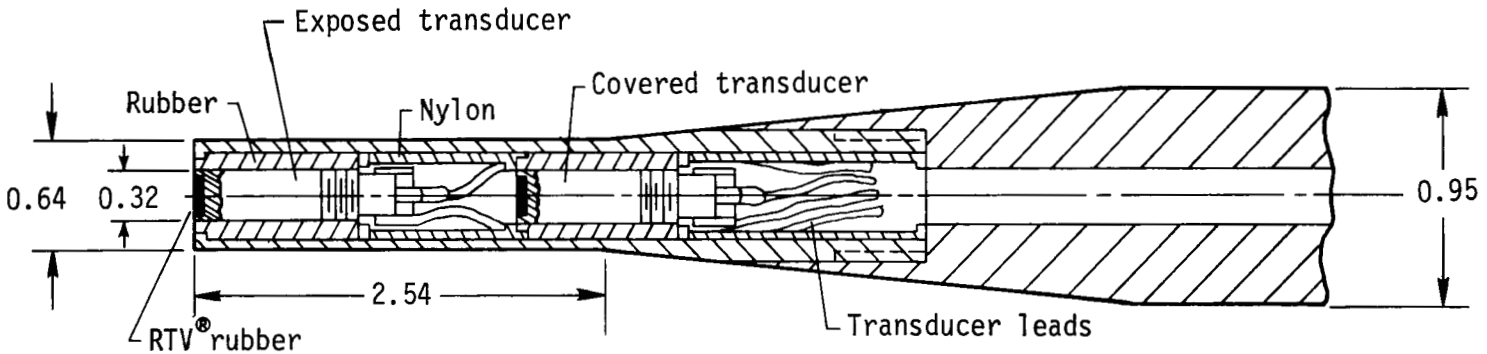

(b) Details of fluctuating pitot-pressure probe. ®RTV: registered trademark of General Electric Co.

Figure 2.- Concluded.

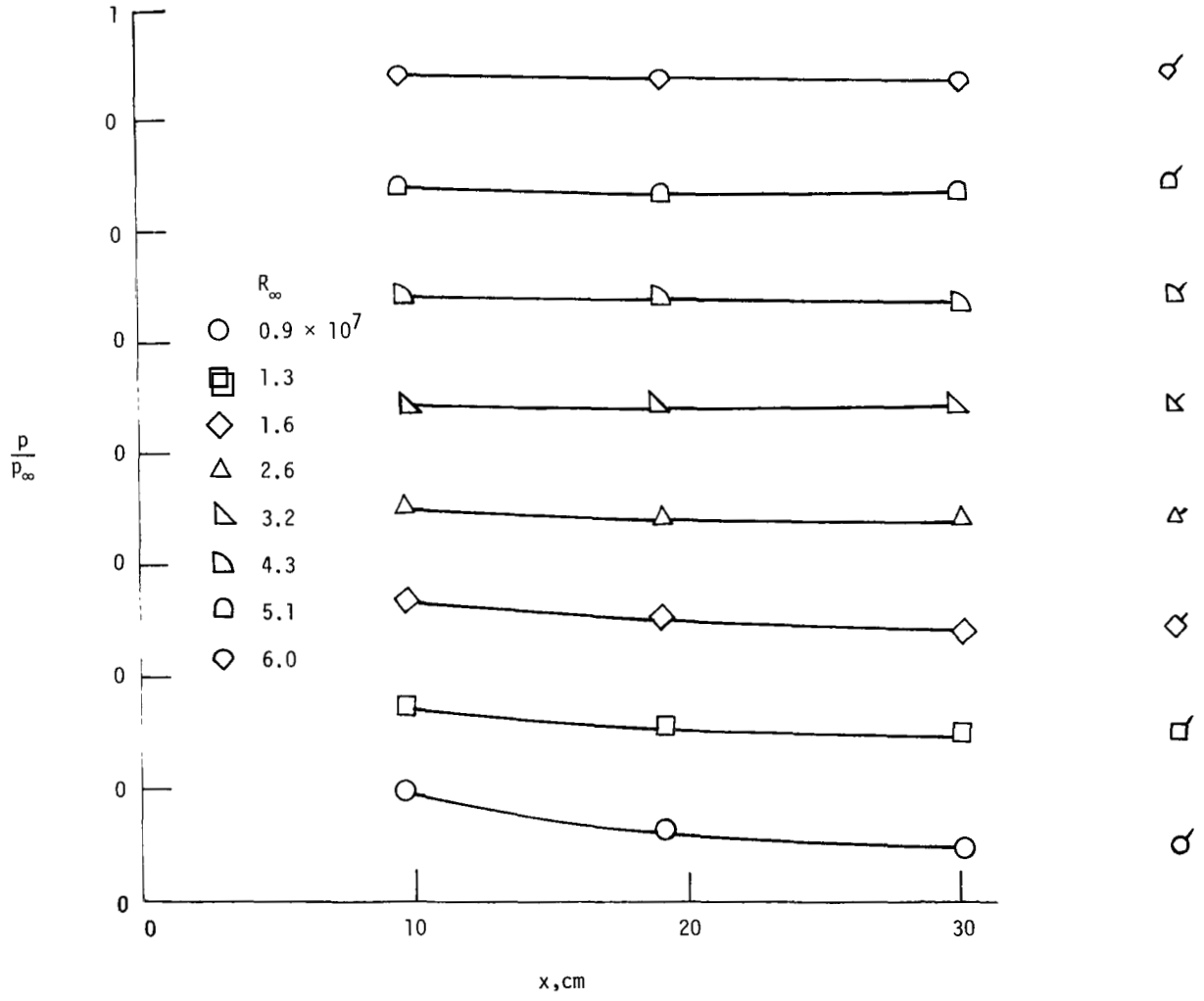

(a) Bottom surface of rods. Flagged symbols are for P_{pls}/P_{SL} at x = 33.0 cm.

Figure 3.- Static pressures on rod-wall sound shield, Mod V.

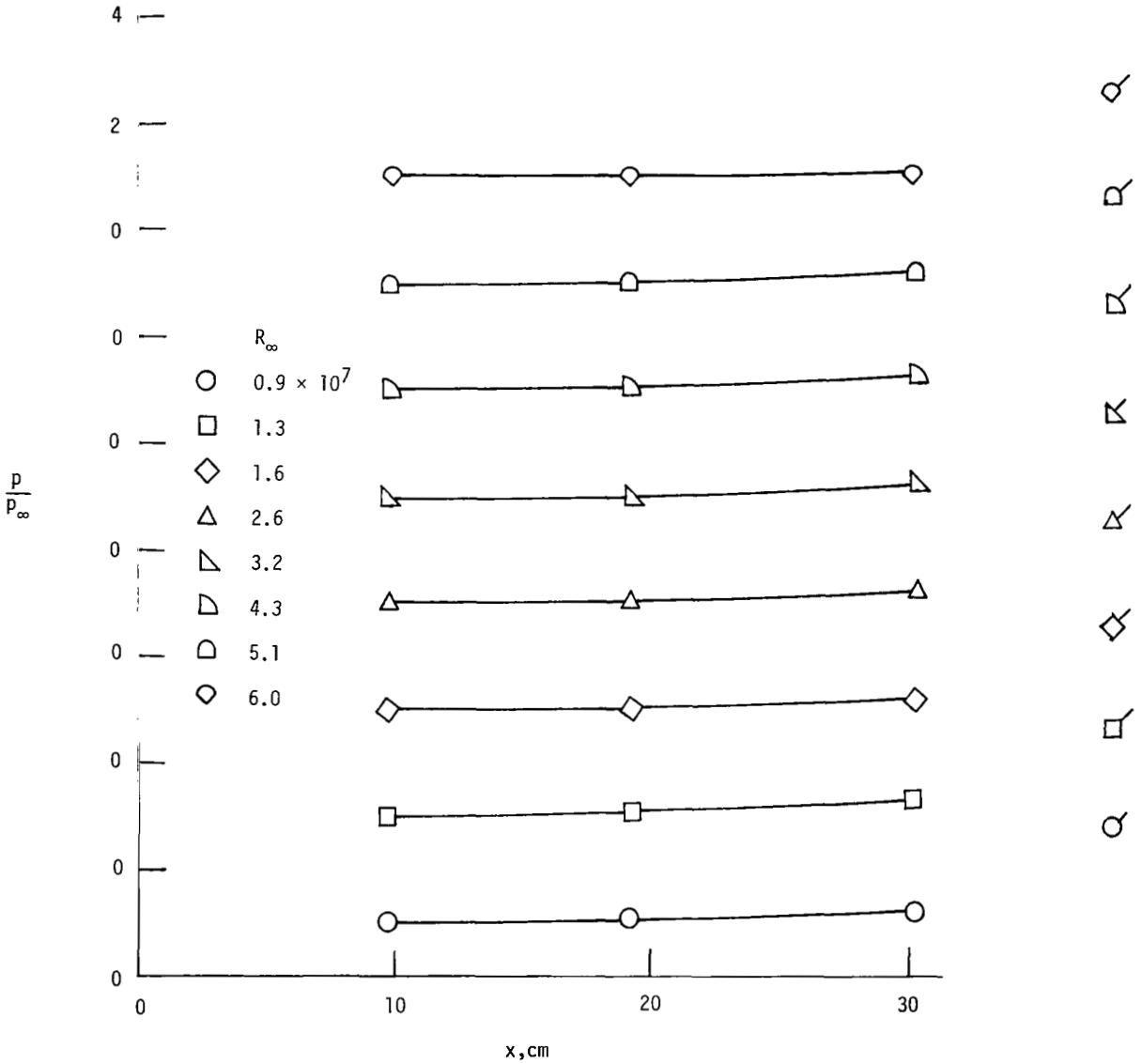

(b) Top surface of rods. Flagged symbols for p_{box}/p_∞ upstream of nozzle.

Figure 3.- Concluded.

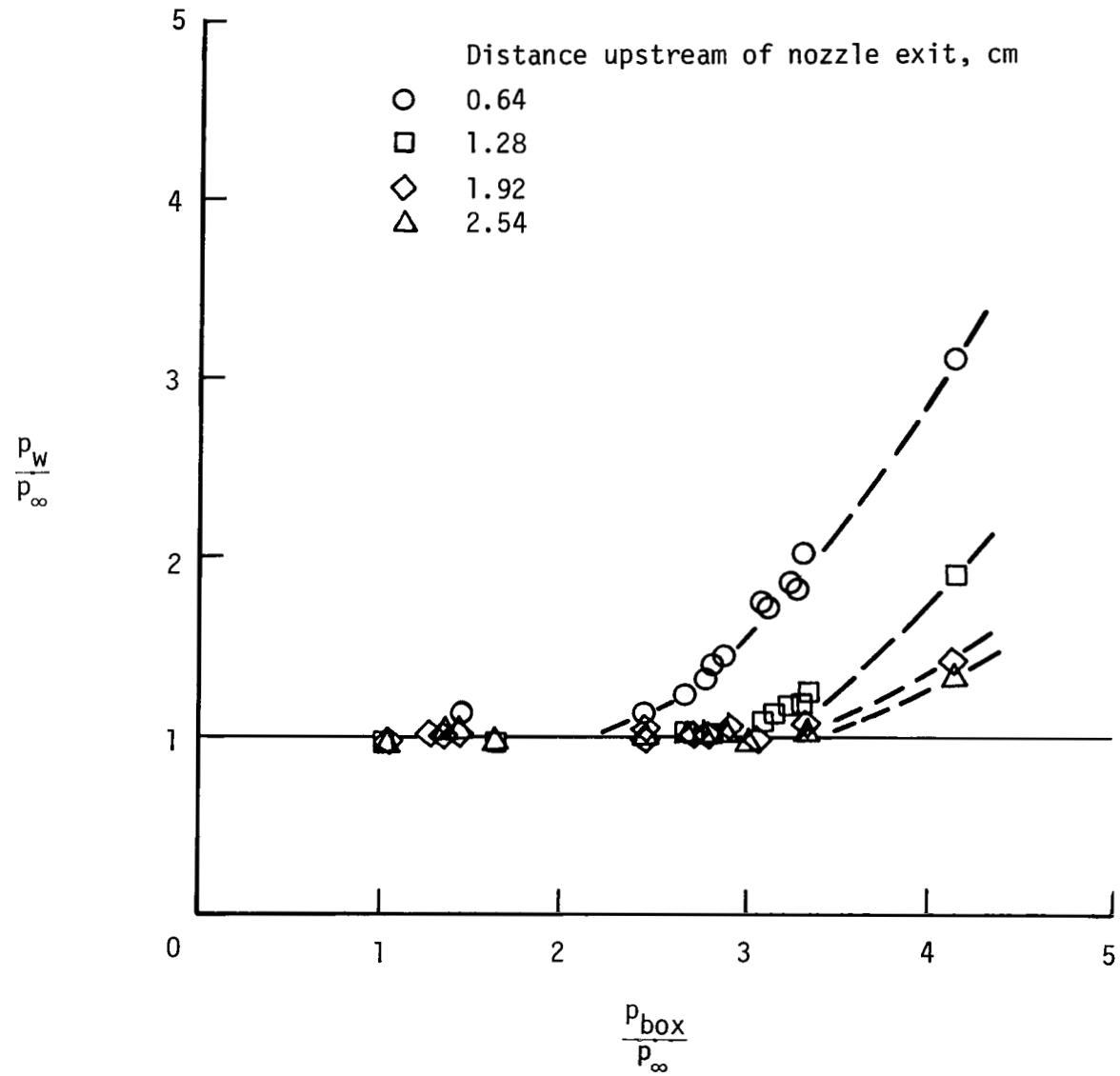

Figure 4.- Effect of test-chamber box pressure on nozzle-wall pressure and boundary-layer separation. M = 5.

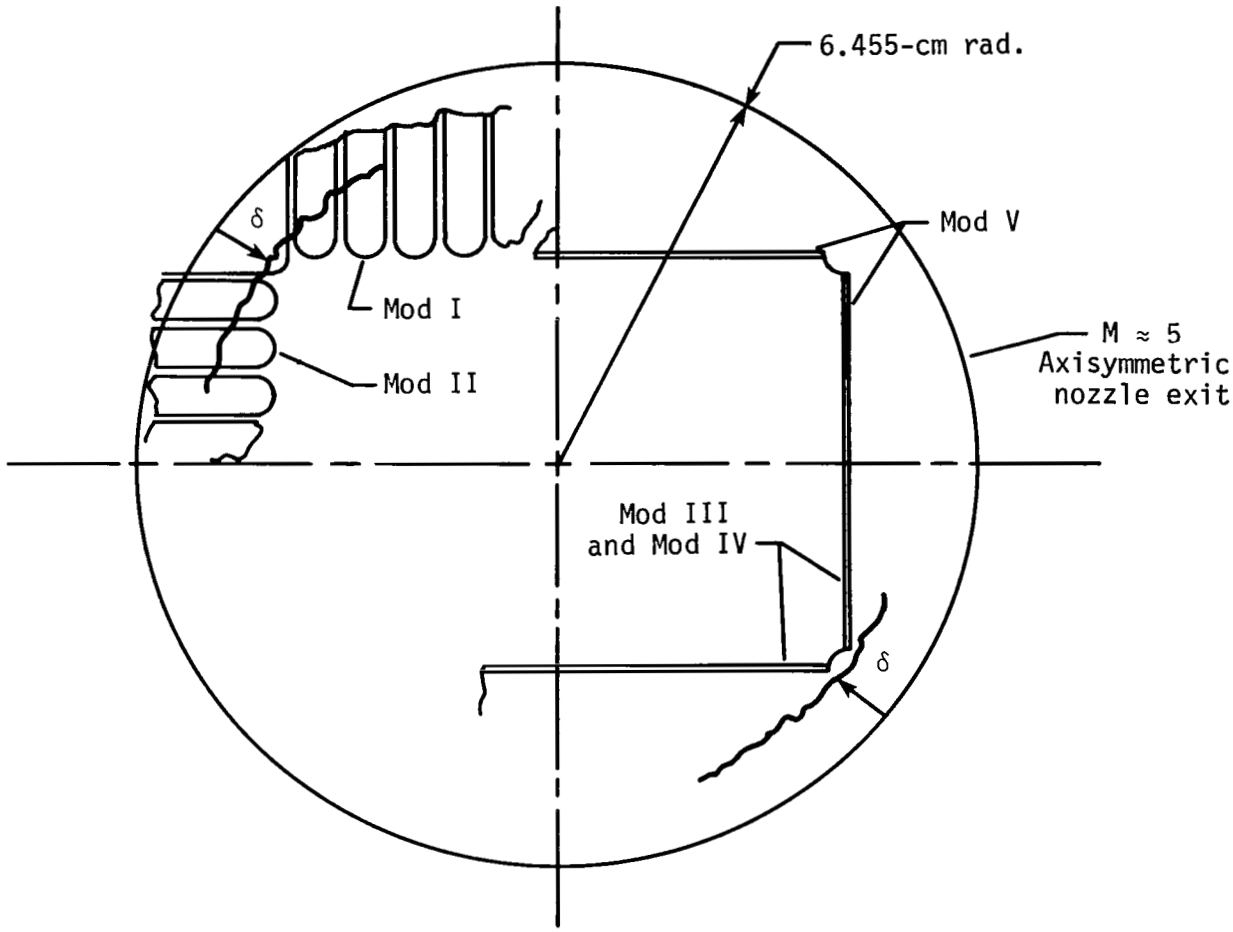

Figure 5.- Leading edges of rod-wall shields compared with nozzle exit. Inside dimensions of leading edges: Mod III and Mod IV - 8.687-cm wide by 6.477-cm high; Mod V - 8.890-cm wide by 6.680-cm high. $\delta \approx 1.0$ cm (ref. 7).

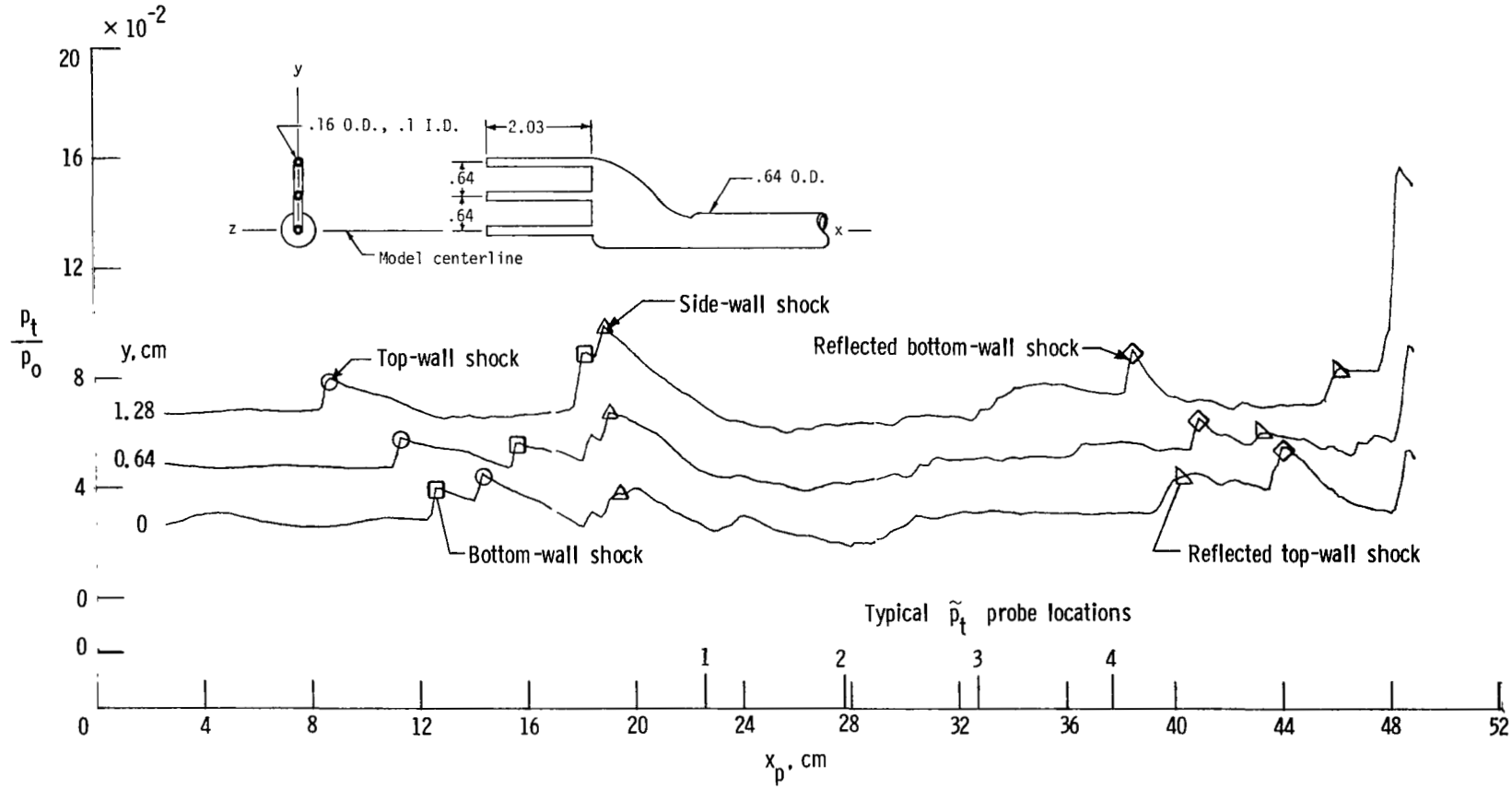

(a) Three-probe rake vertical; $R_\infty \approx 1.0 \times 10^7$.

Figure 6.- Mean pitot pressures in rod-wall sound shield, Mod V. $M_\infty \approx 4.9$.

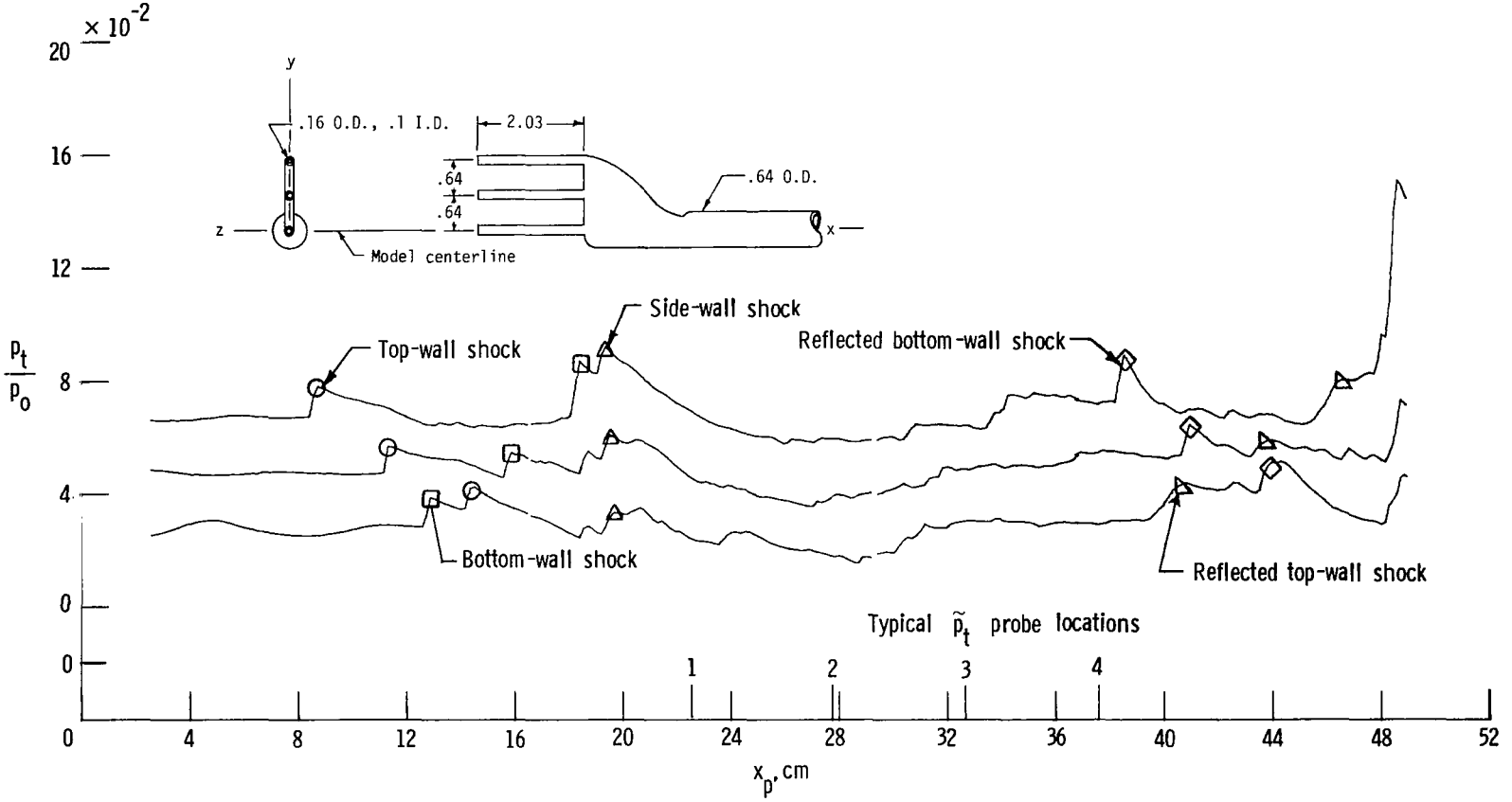

(b) Three-probe rake vertical; $R_\infty \approx 1.6 \times 10^7$.

Figure 6.- Continued.

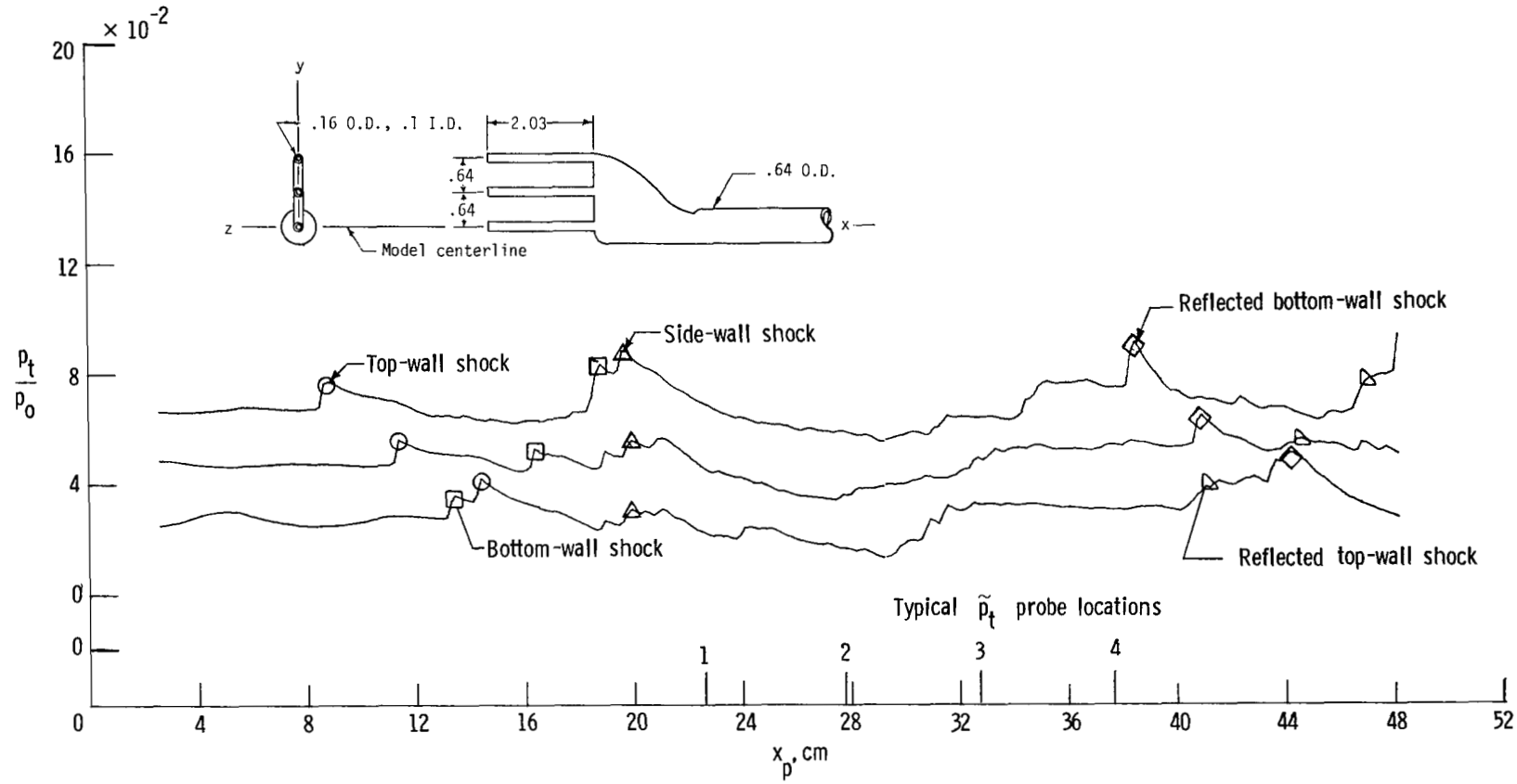

(c) Three-probe rake vertical; $R_\infty \approx 2.9 \times 10^7$.

Figure 6.- Continued.

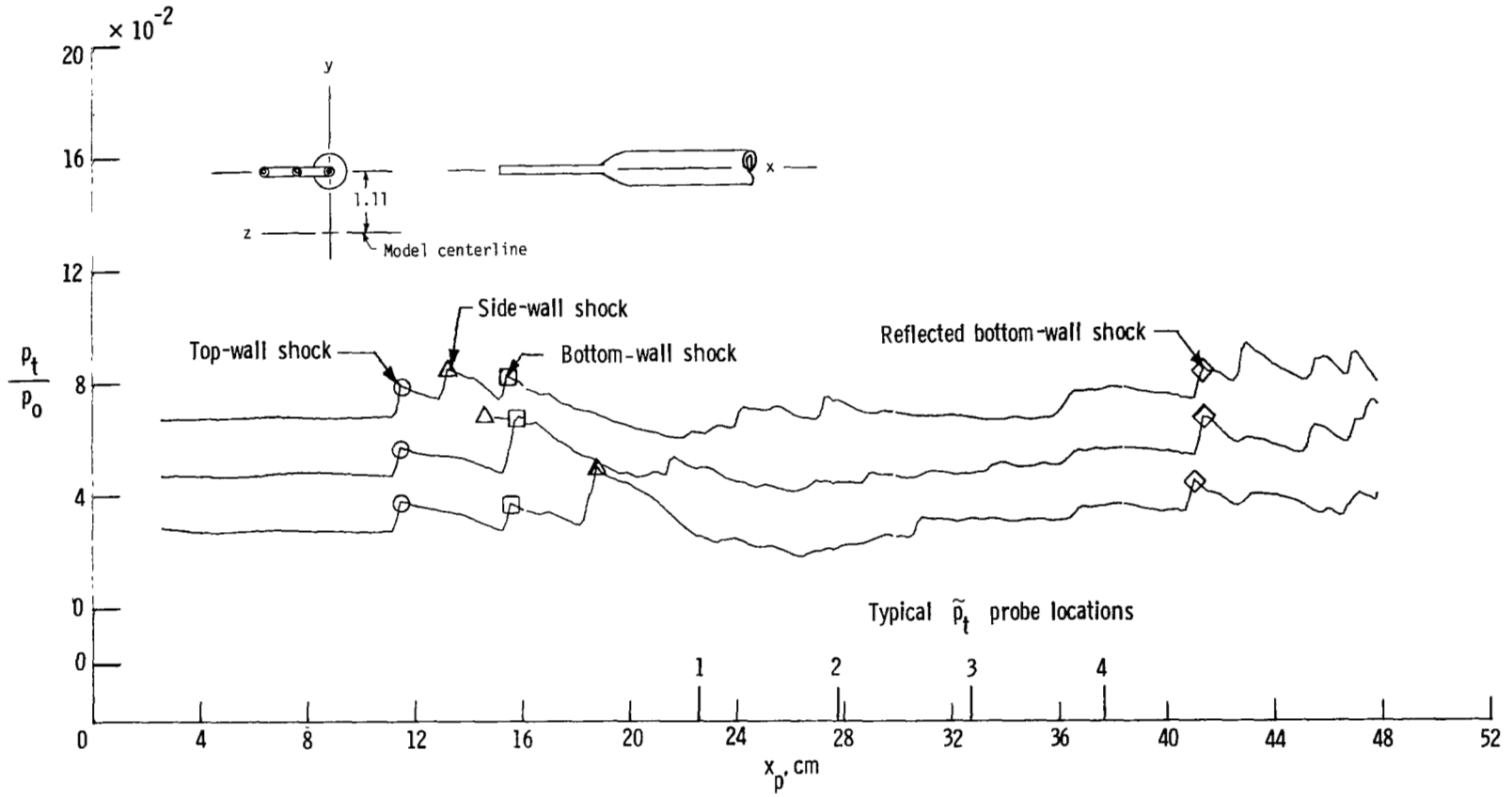

(d) Three-probe rake horizontal, 1.11 cm above centerline; $R_\infty \approx 1.0 \times 10^7$.

Figure 6.- Continued.

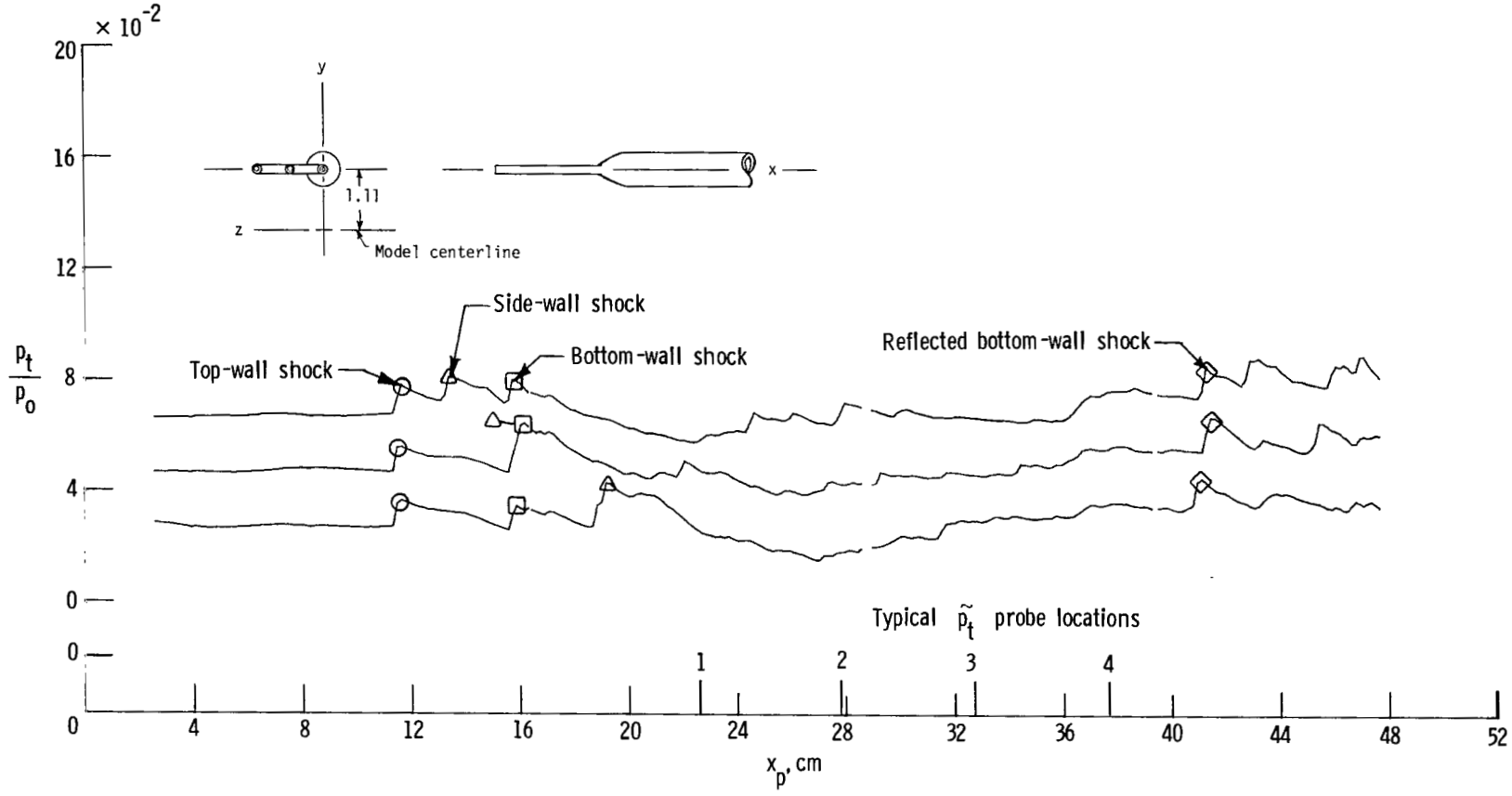

(e) Three-probe rake horizontal, 1.11 cm above centerline; $R_\infty \approx 1.6 \times 10^7$.

Figure 6.- Continued.

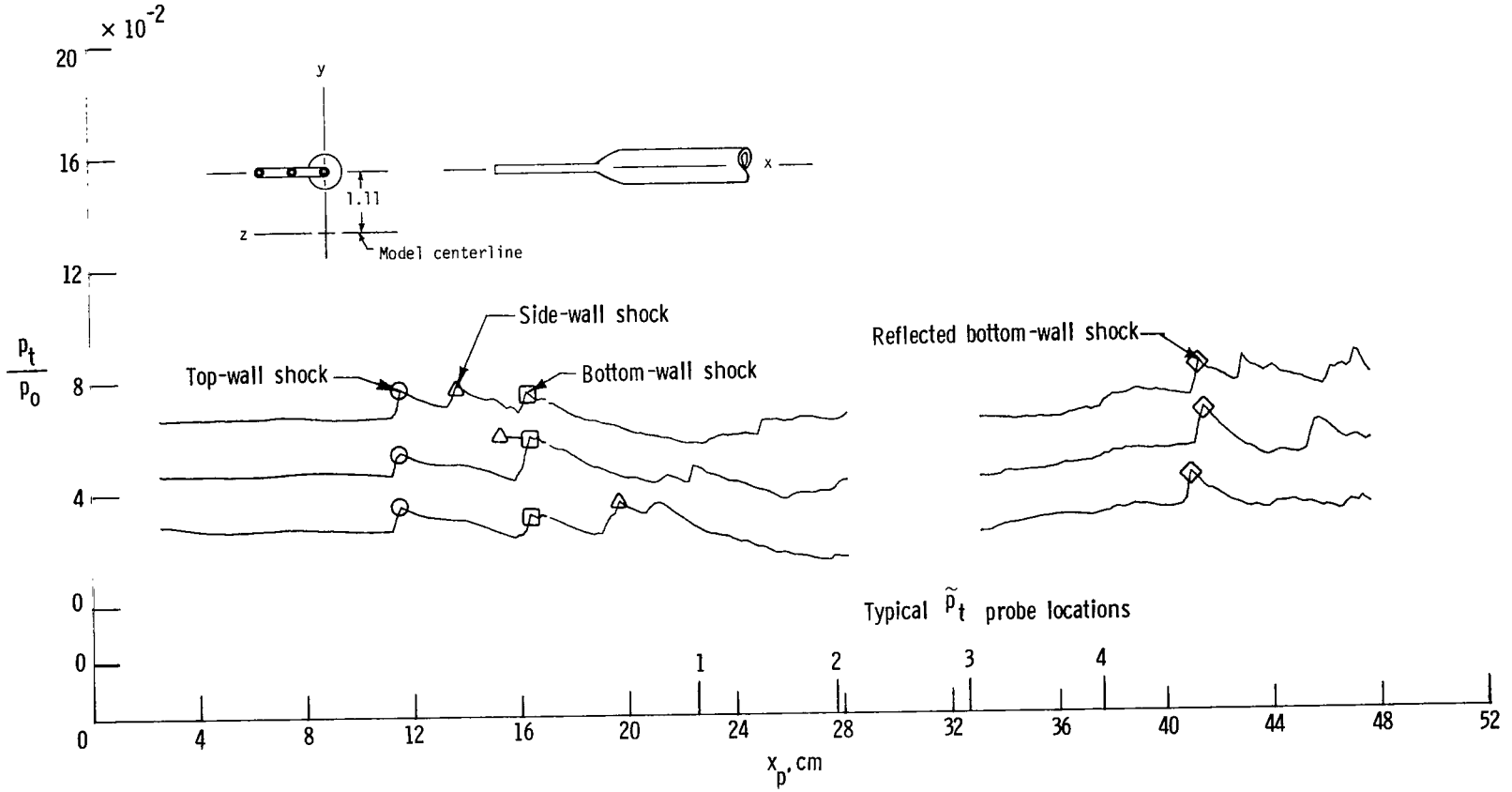

(f) Three-probe rake horizontal, 1.11 cm above centerline; $R_\infty \approx 2.9 \times 10^7$.

Figure 6.- Concluded.

× Location of pressure peaks from fig. 6(a)

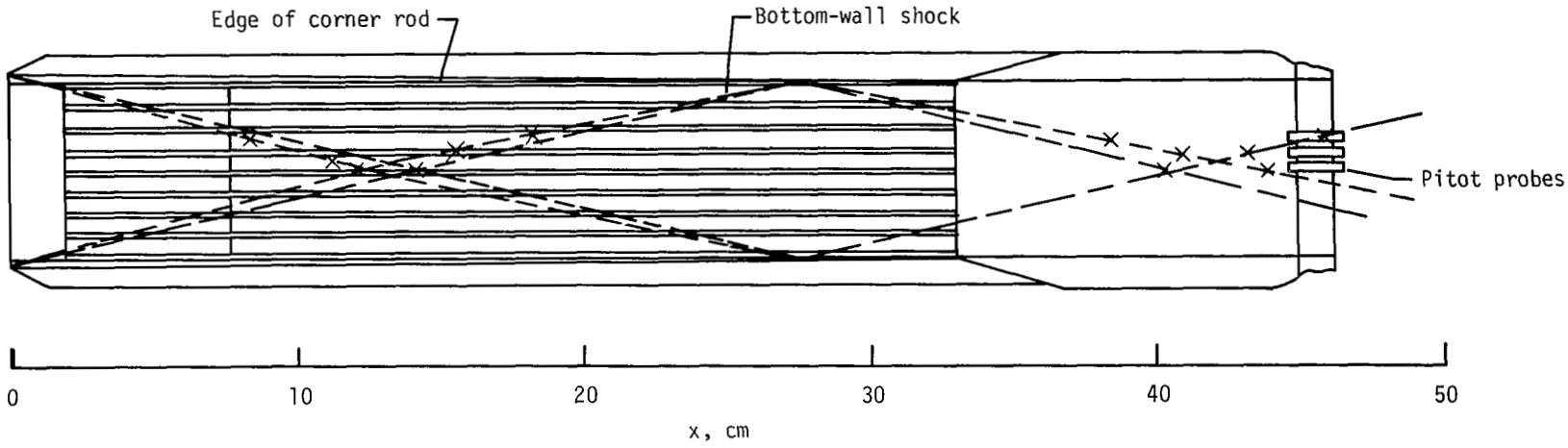

(a) Side view.

Figure 7.- Simplified shock structure inside rod-wall sound shield, Mod V. M ≈ 4.9.

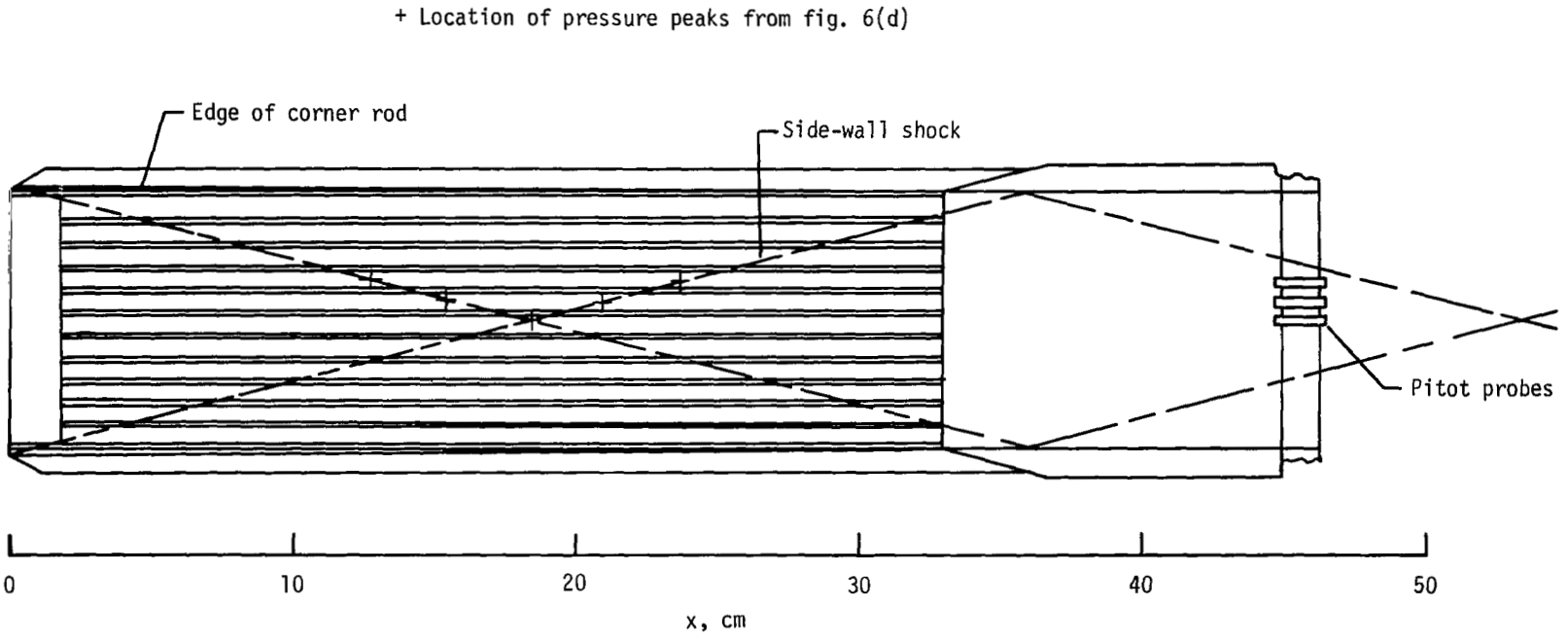

(b) Top view.

Figure 7.- Concluded.

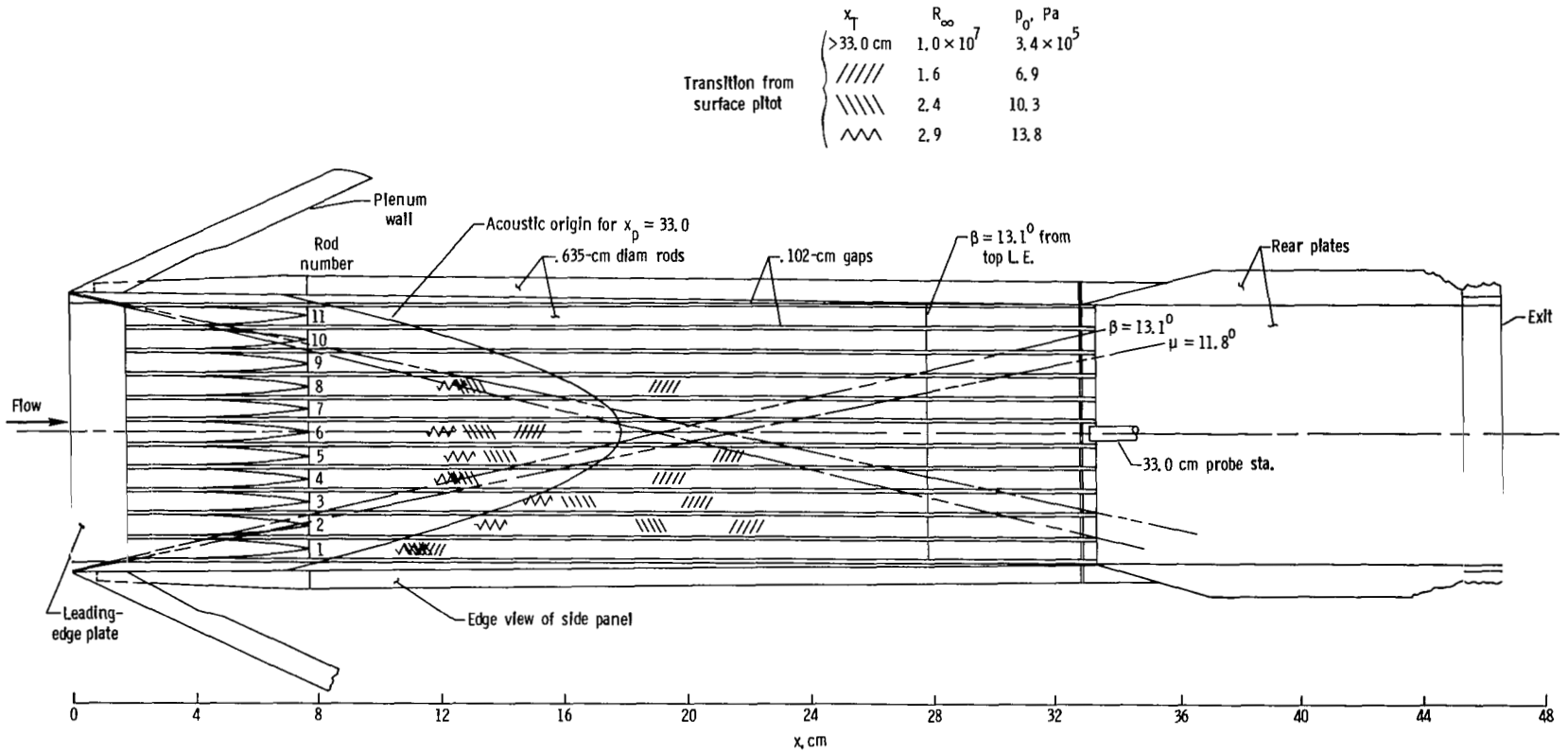

Figure 8.- Bottom panel of shield with projected locations of side-wall shocks and acoustic-origin locus for probe at x_p = 33.0, Mod V.

Top

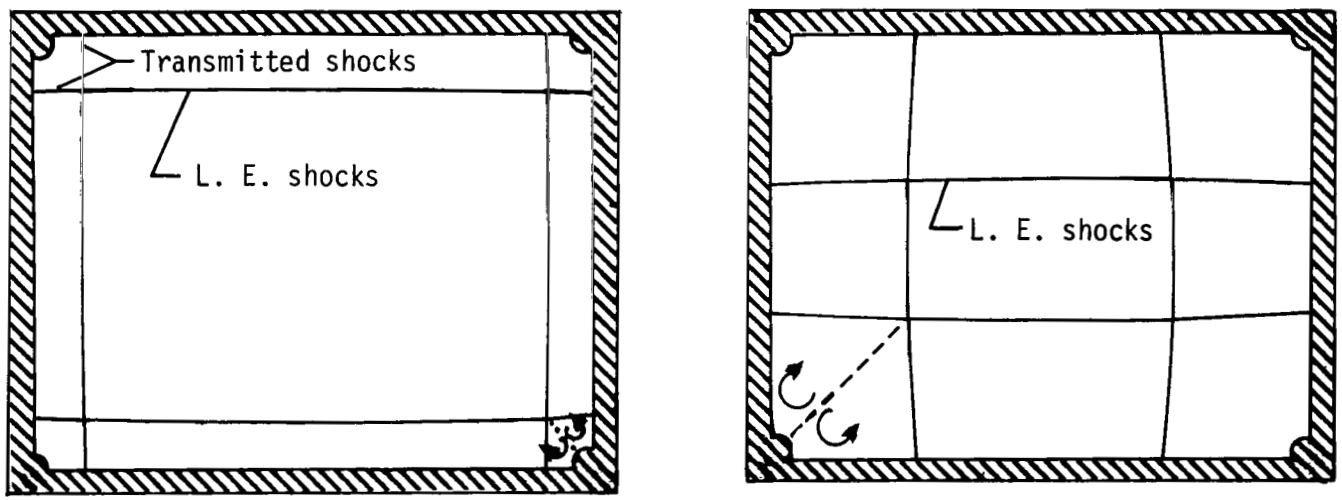

Figure 9.- Estimated shock structure (ref. 12) in rectangular sound shield, Mod V. M ≈ 5.

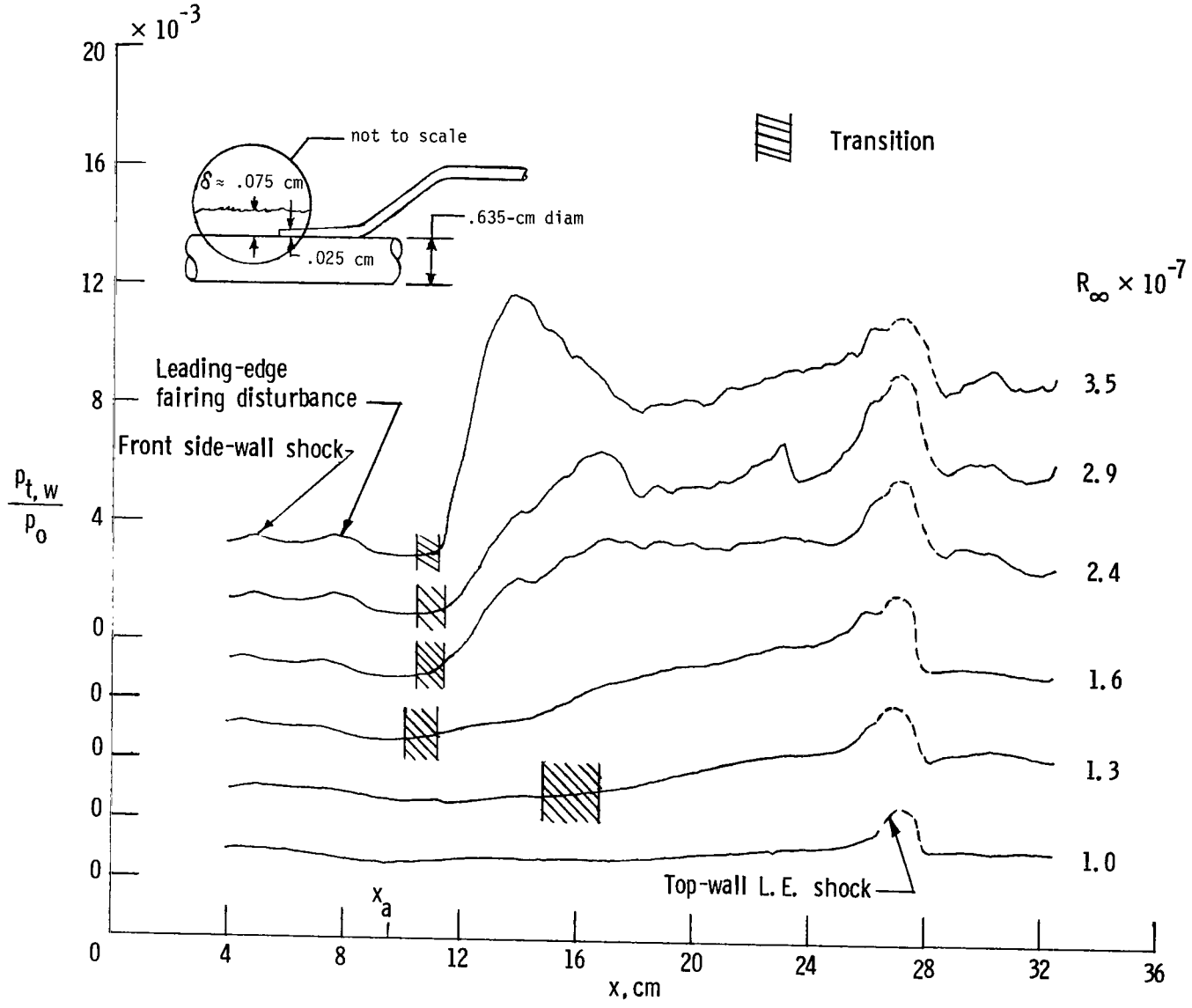

(a) Rod 1.

Figure 10.- Typical surface pitot pressures on bottom panel of rod-wall sound shield, Mod V. $M_\infty \approx 4.9$.

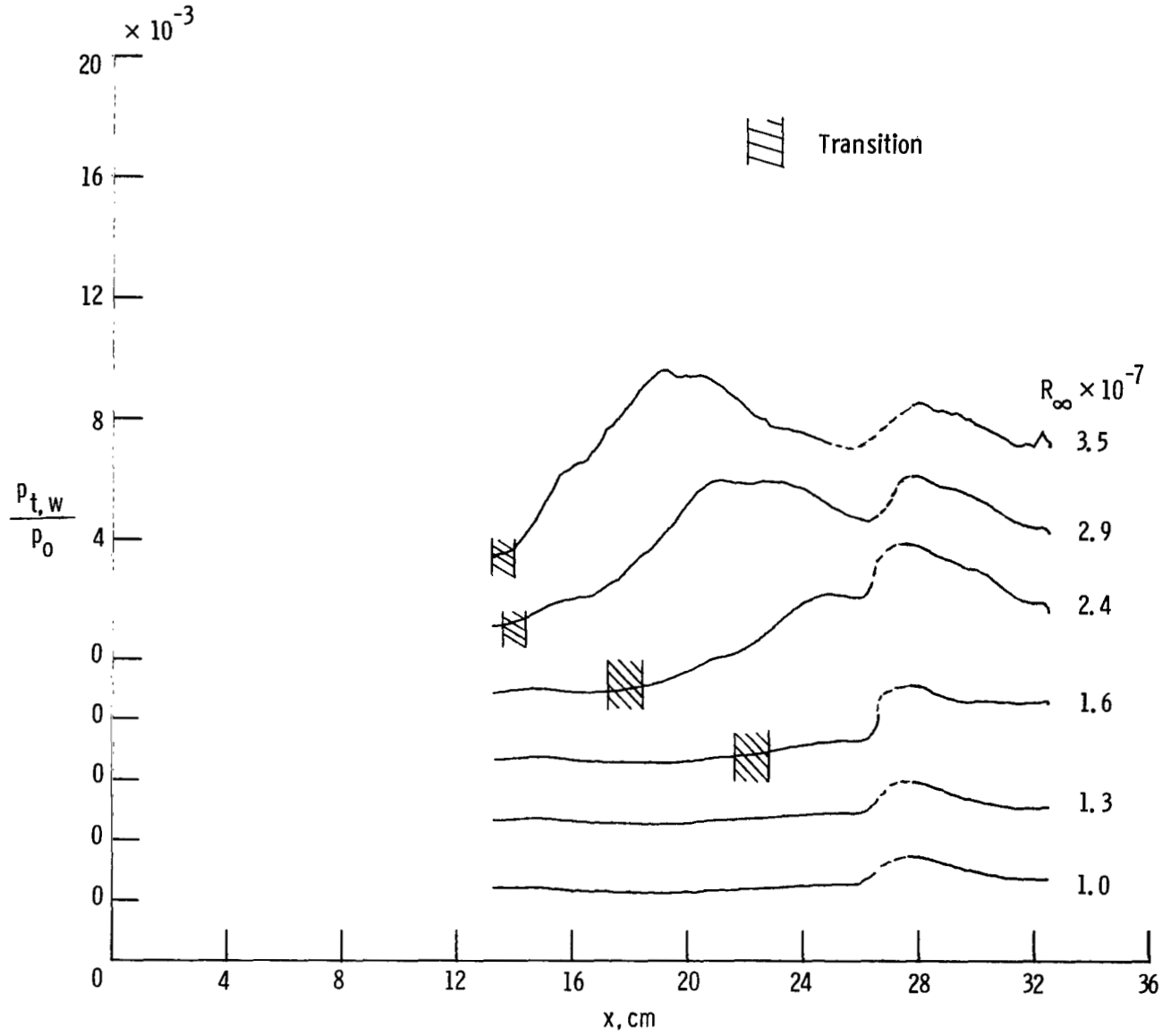

(b) Rod 2.

Figure 10.- Continued.

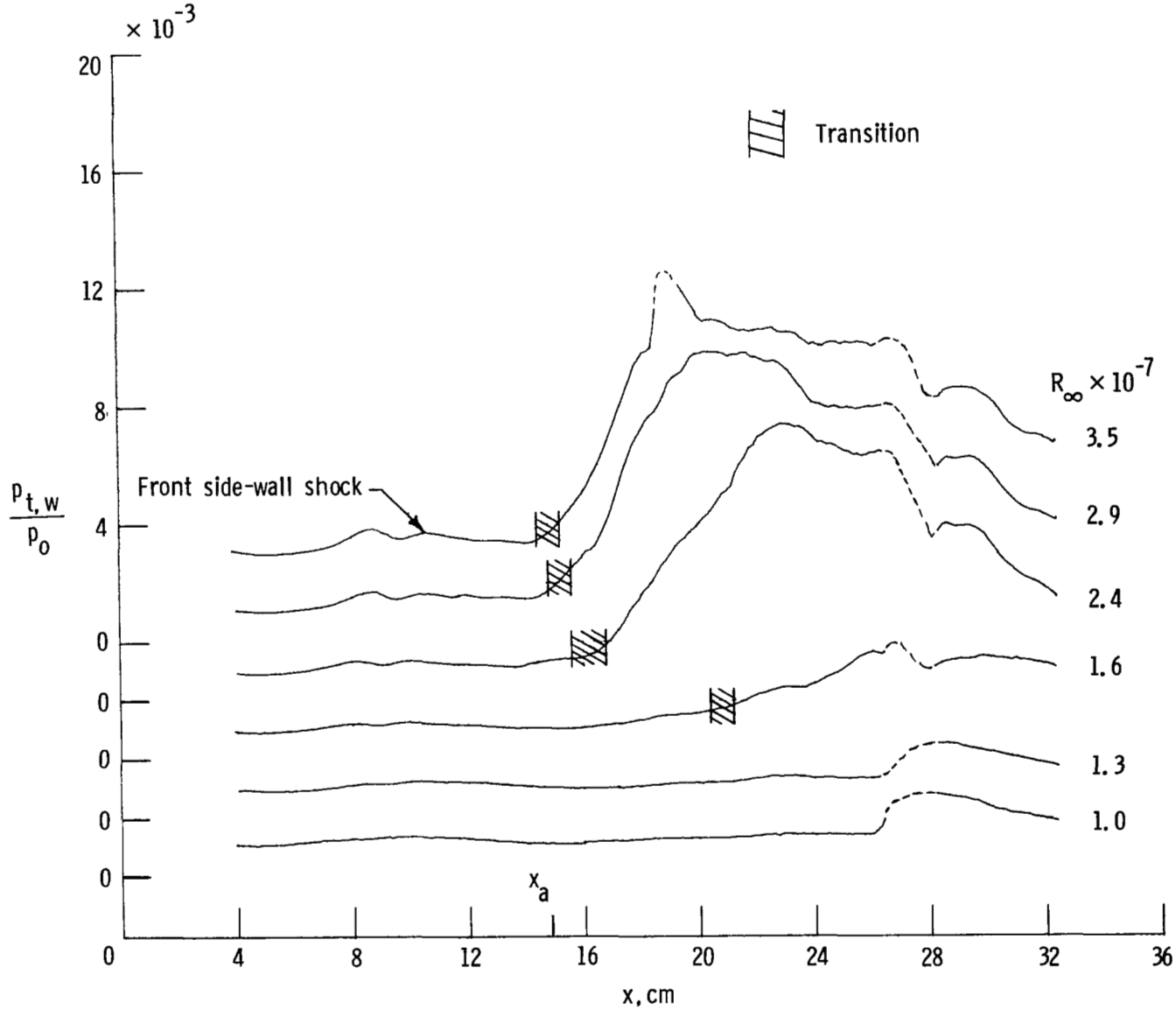

(c) Rod 3.

Figure 10.- Continued.

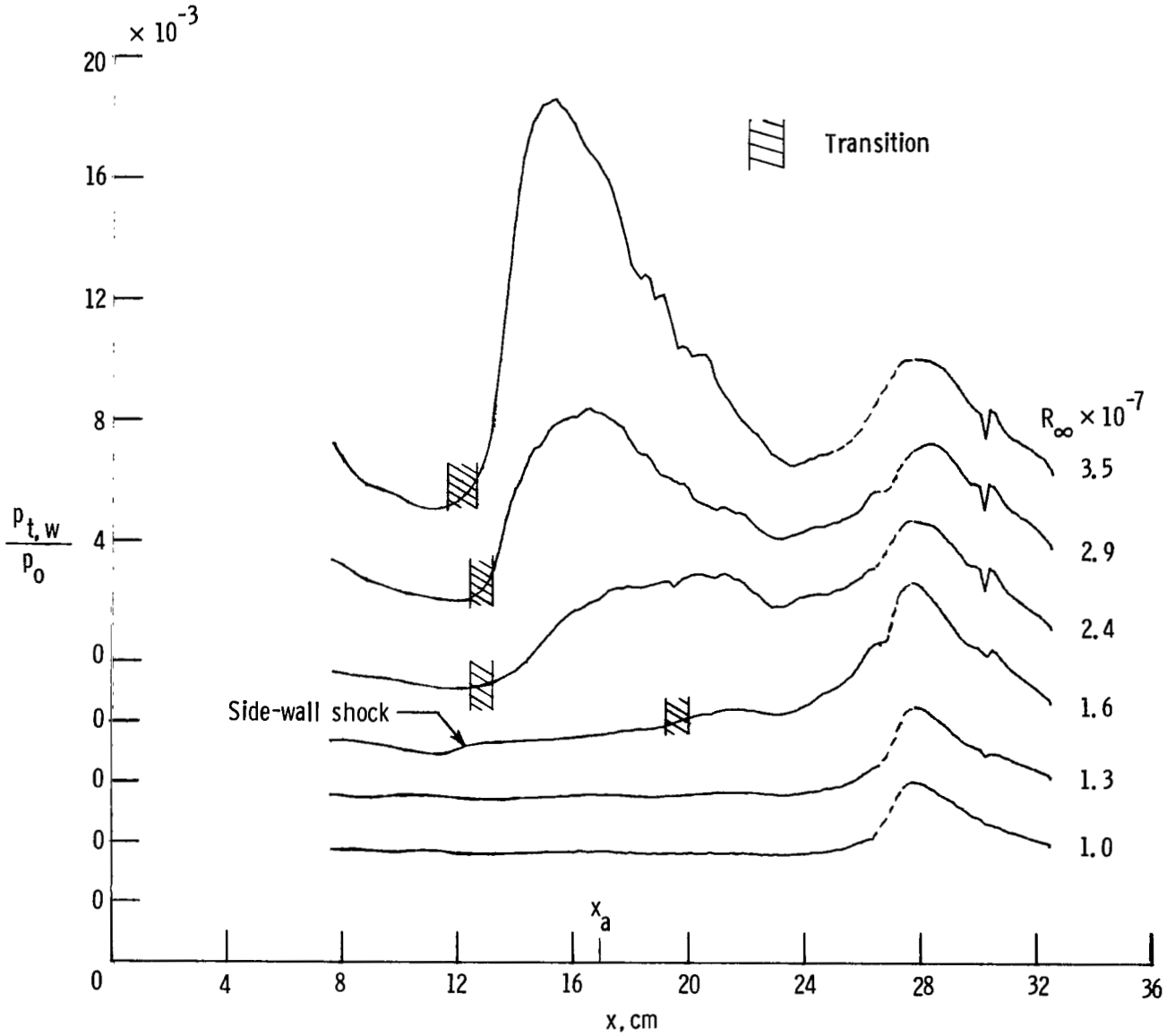

(d) Rod 4.

Figure 10.- Continued.

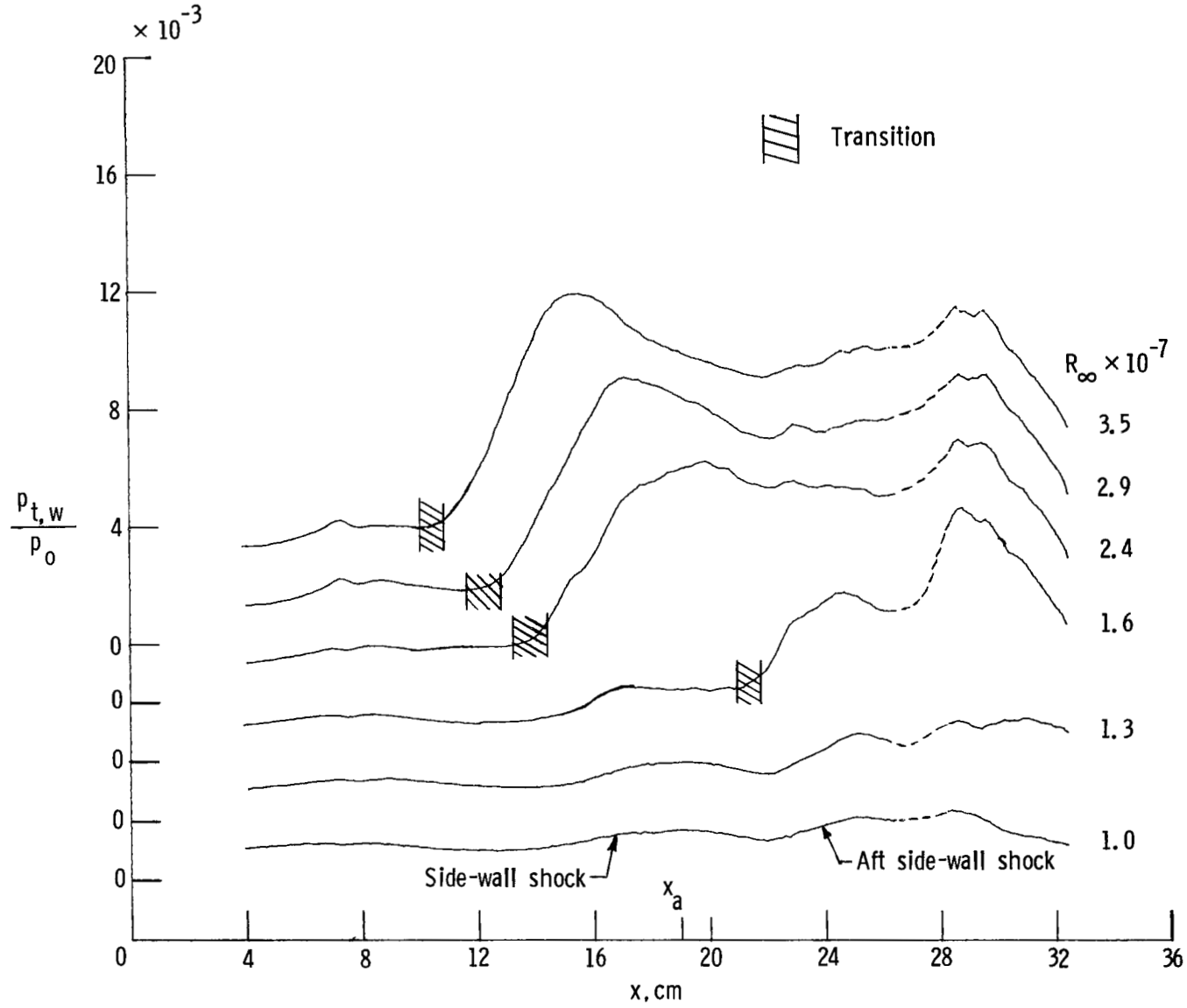

(e) Rod 5.

Figure 10.- Continued.

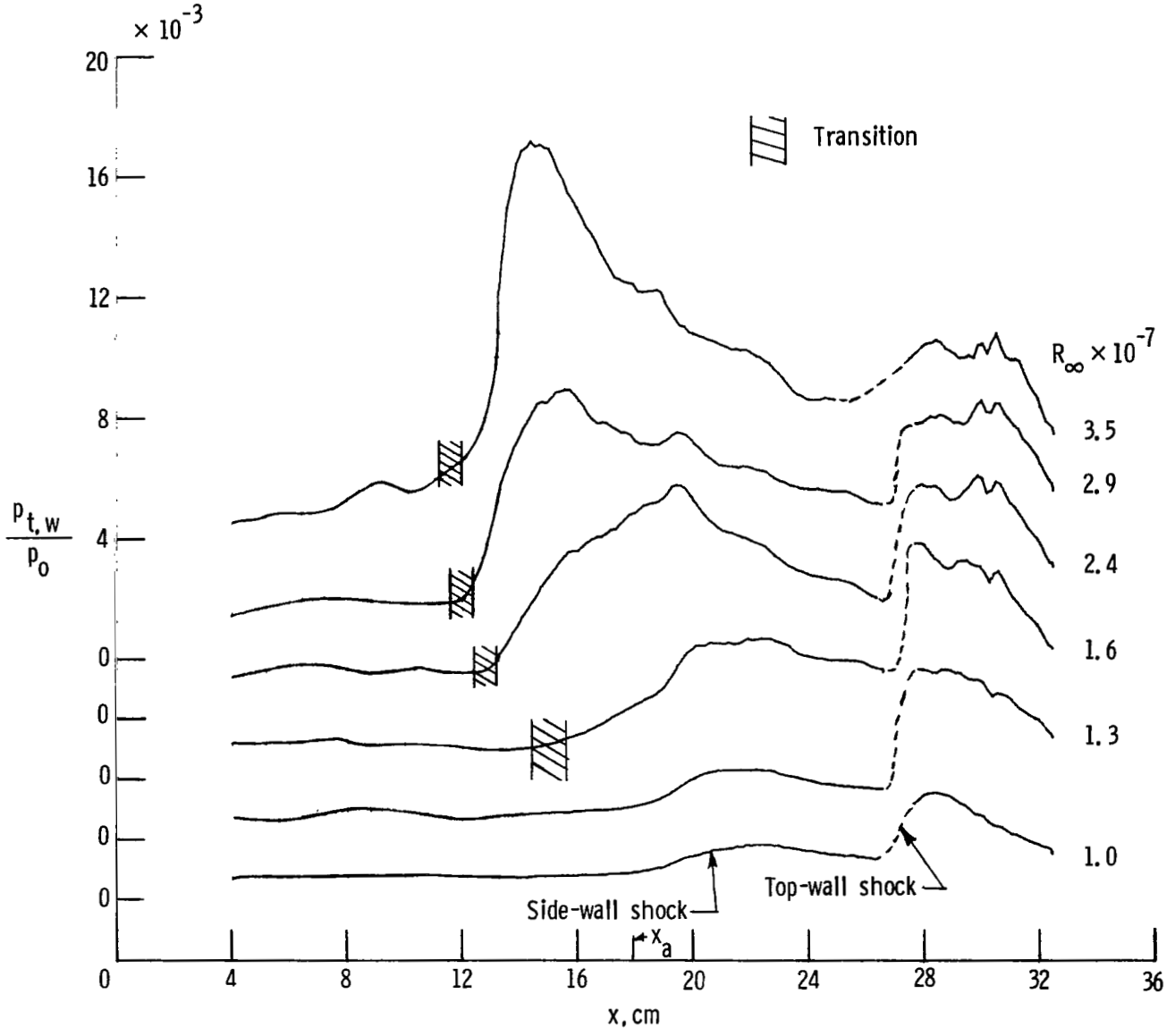

(f) Rod 6 (center rod).

Figure 10.- Continued.

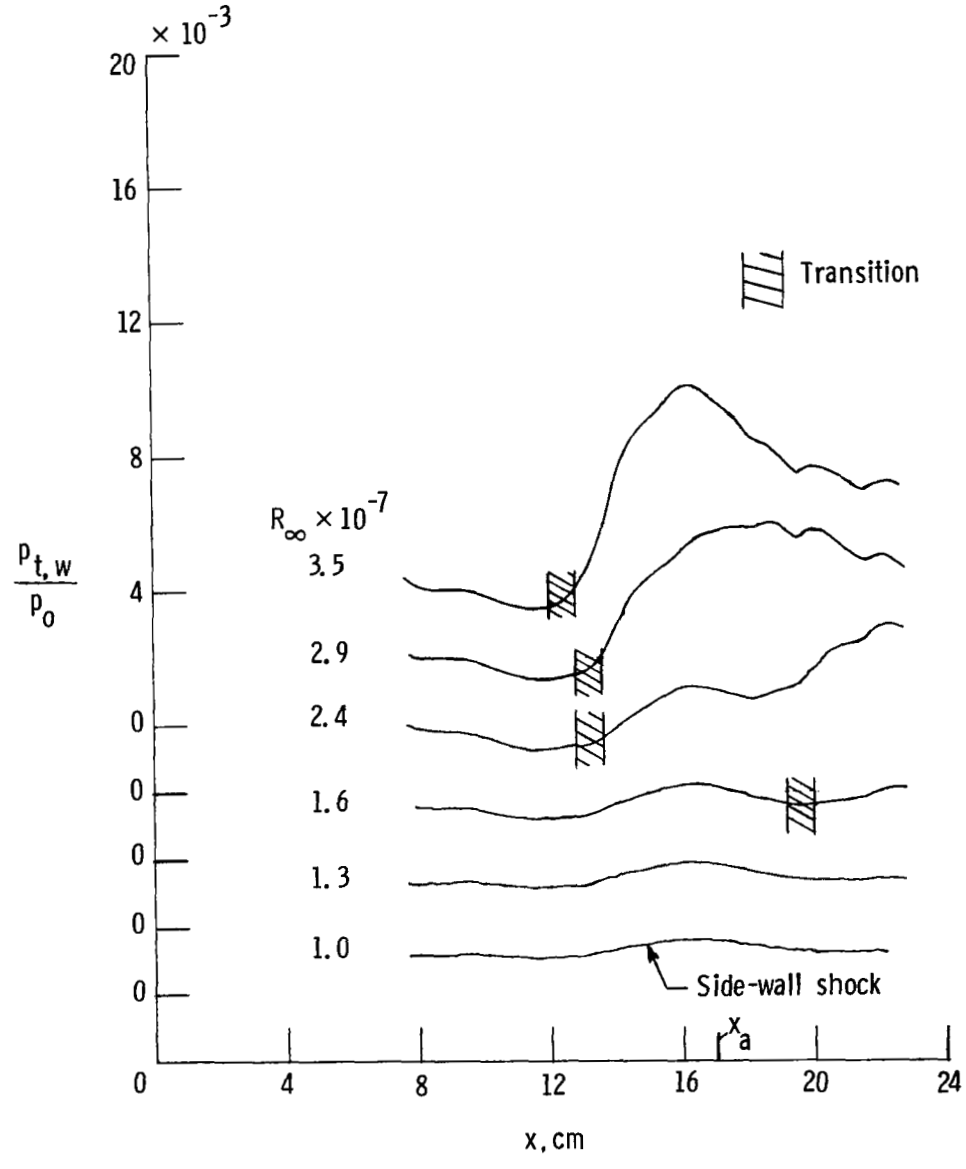

(g) Rod 8.

Figure 10.- Concluded.

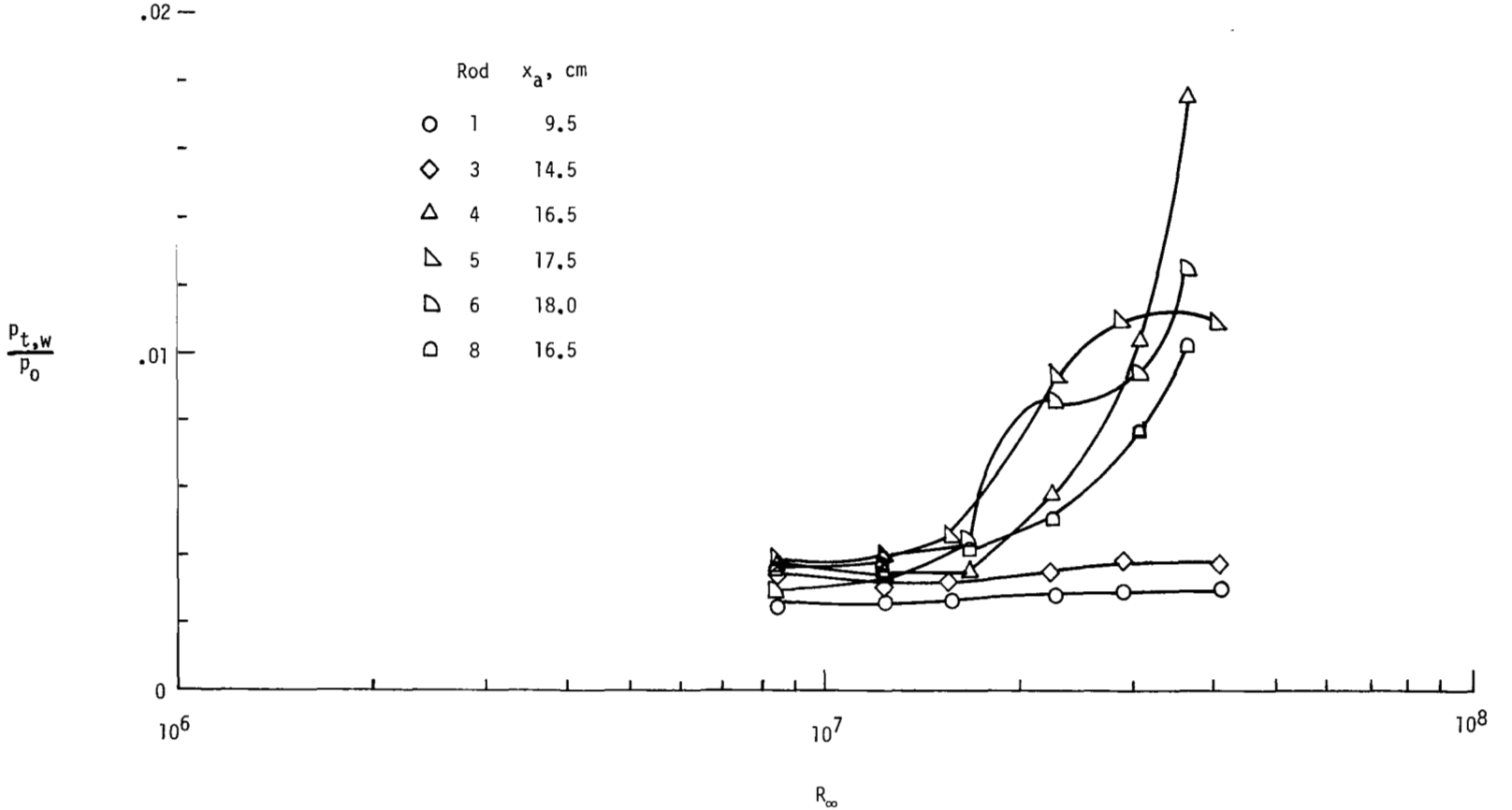

Figure 11.- Variation of surface pitot pressure with Reynolds number on bottom panel of rod-wall sound shield at acoustic origin for $x_p = 33.0$.

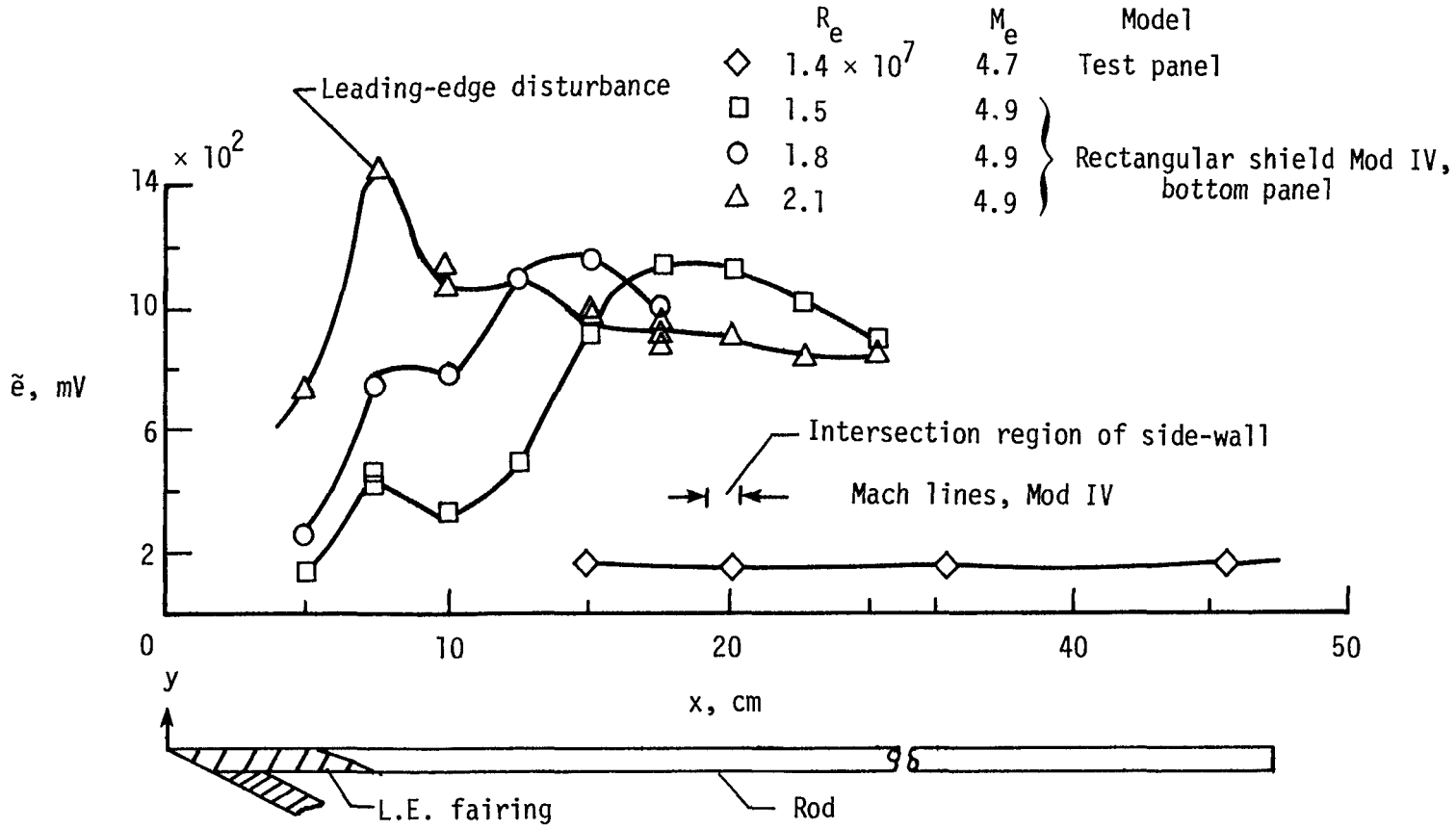

Figure 12.- Hot-wire probe in boundary layer of center rod at rod stagnation line, Mod IV. $y \approx 0.025$; $\delta \approx 0.062$.

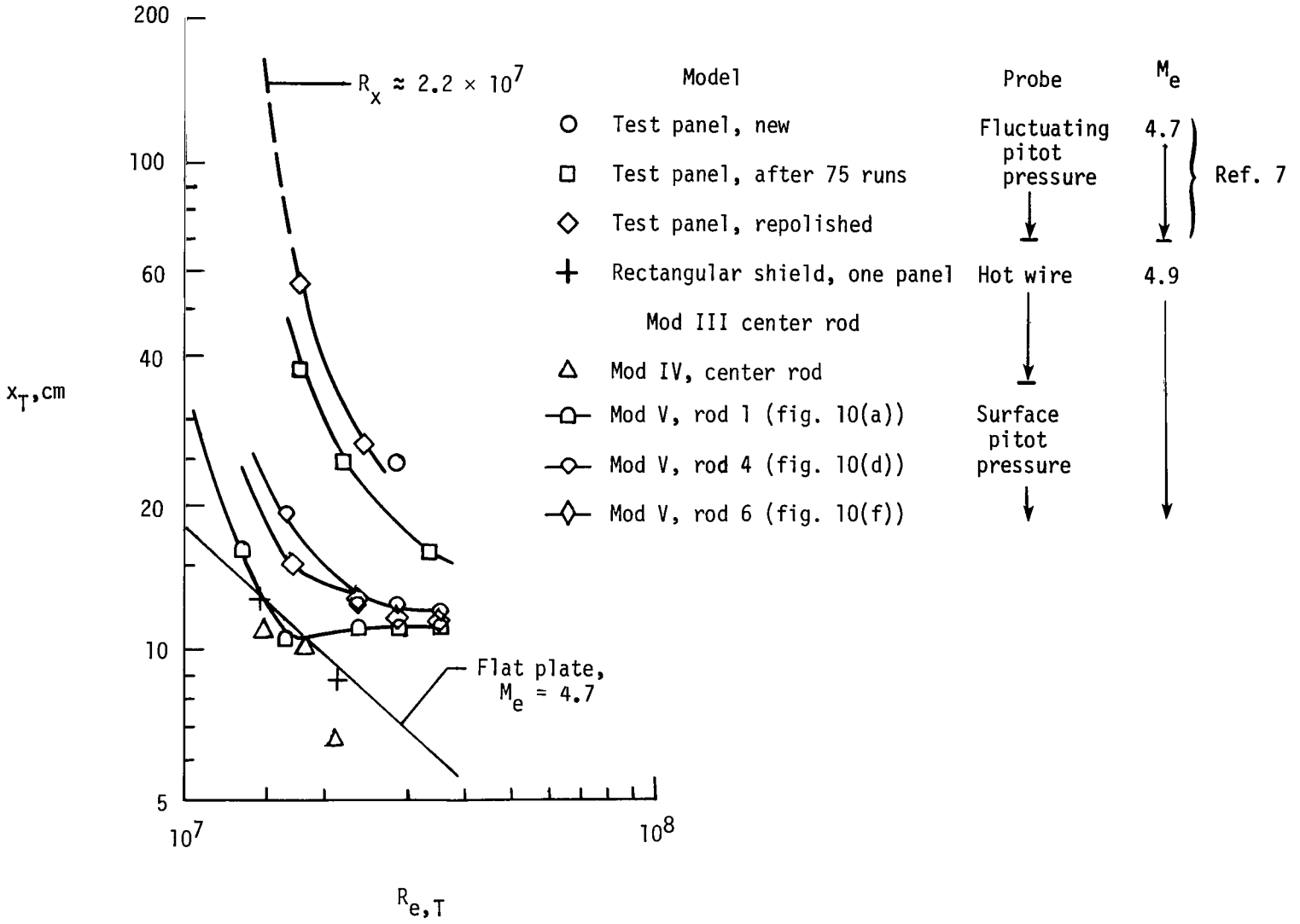

Figure 13.- Transition on rod walls.

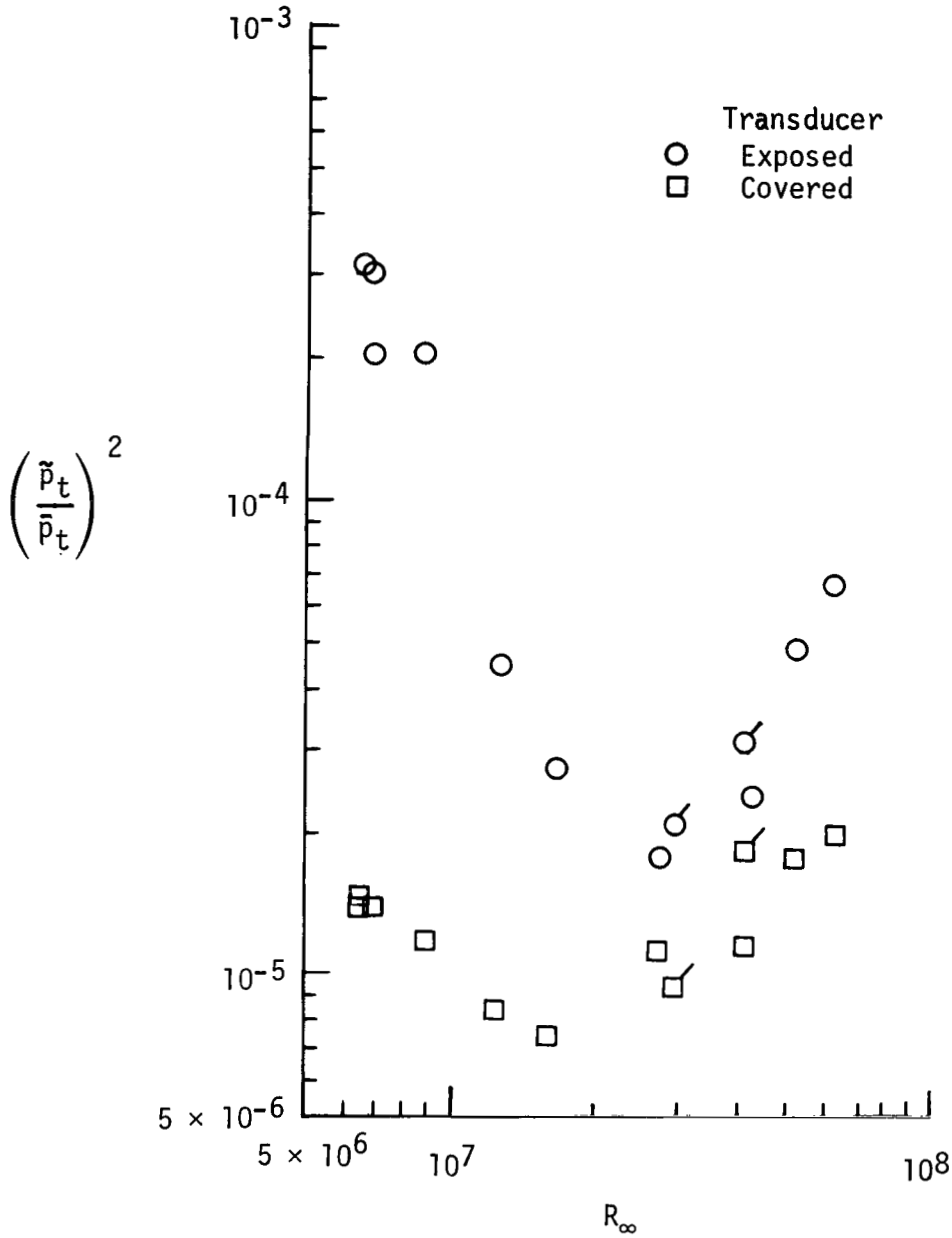

(a) 0.64-cm diameter probe.

Figure 14.- Comparison of acceleration signal (covered transducer) to fluctuating-pressure signal (exposed transducer). Flagged symbols denote repeat runs. x = 25.4 on centerline.

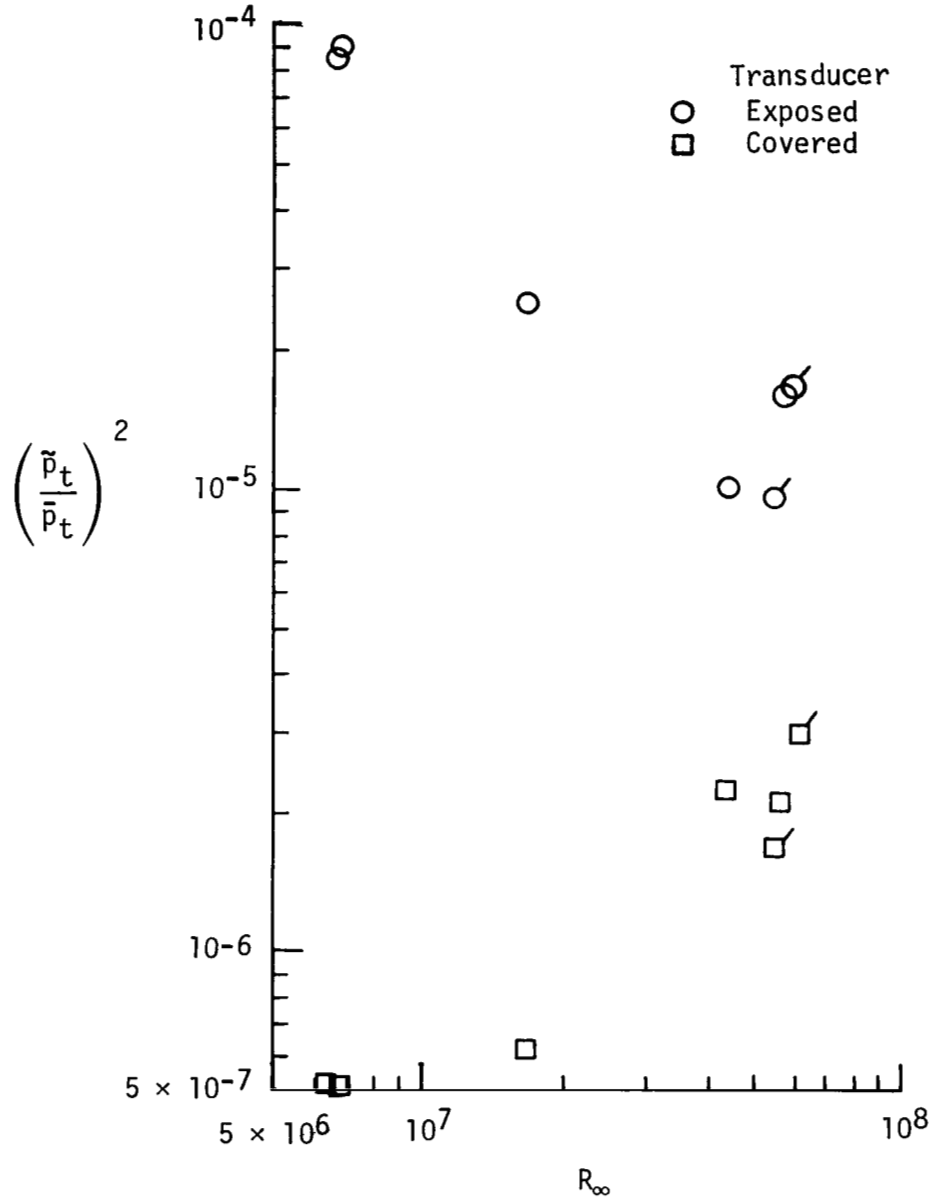

(b) 1.28-cm diameter probe.

Figure 14.- Concluded.

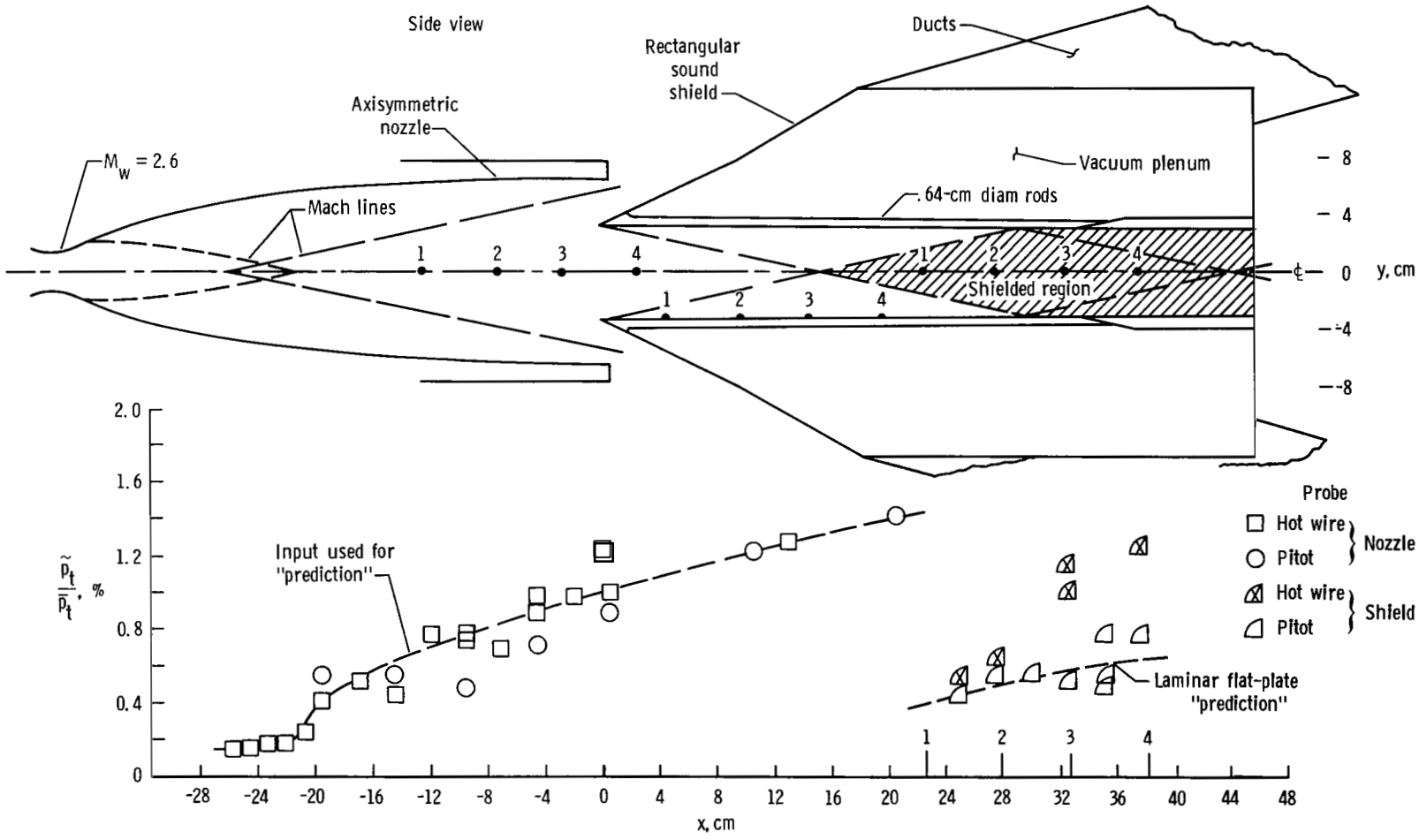

Figure 15.- Normalized pitot-pressure fluctuations along centerline of rectangular rod-wall sound shield, Mod V. Numbers 1 to 4 indicate probe locations. Diameter of fluctuating pitot-pressure probe was 0.635 cm. $M_\infty = 4.9$; $R_\infty = 1.5 \times 10^7$.

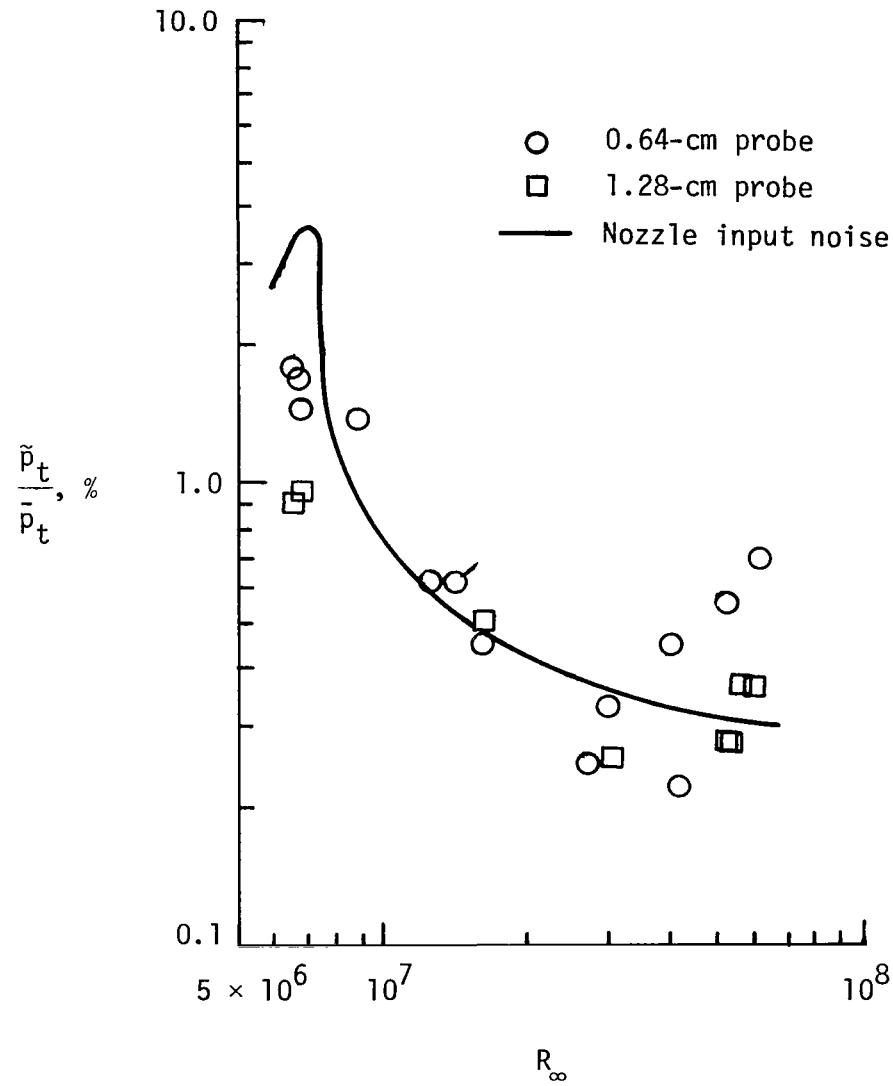

(a) $x_p = 25.4$.

Figure 16.- Variation of normalized fluctuating pitot pressure with unit Reynolds number compared with nozzle input noise. Probes on centerline. Flagged symbols show rms values. y = 0; z = 0.

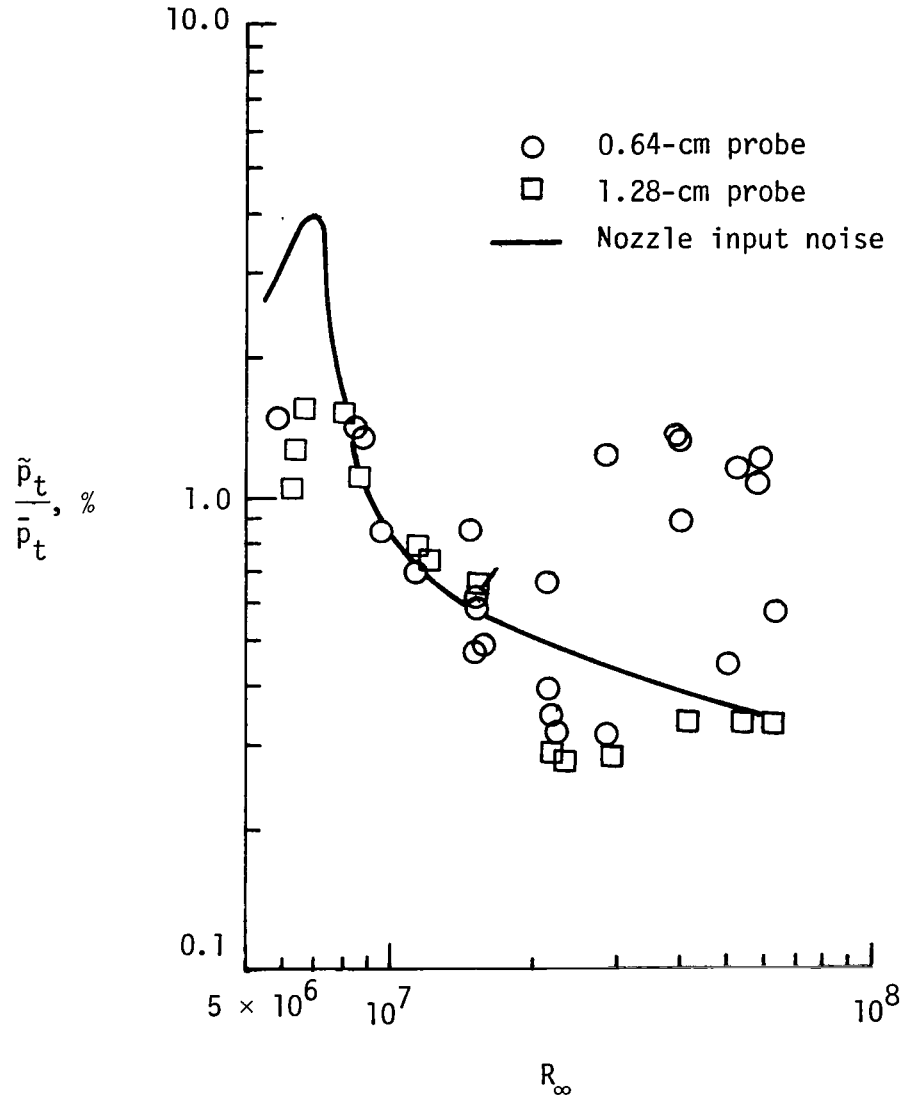

(b) x_p = 27.9.

Figure 16.- Continued.

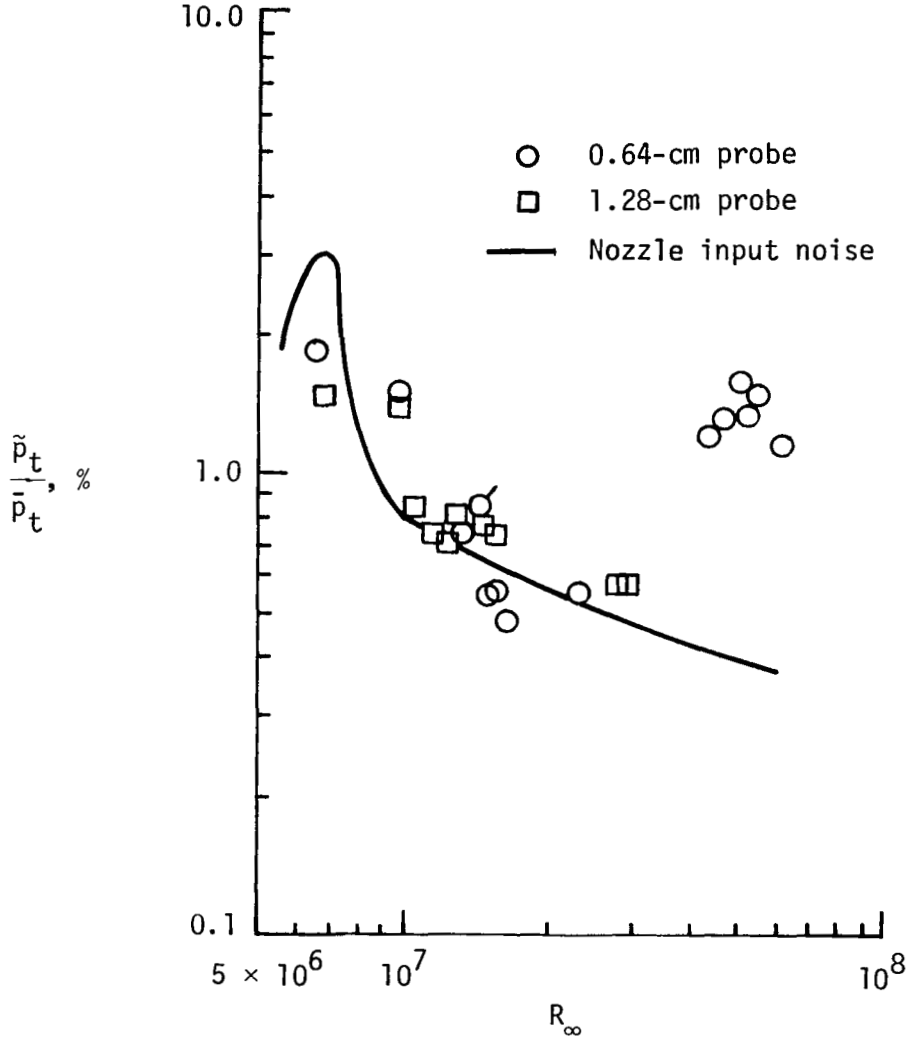

(c) $x_p = 30.5$.

Figure 16.- Continued.

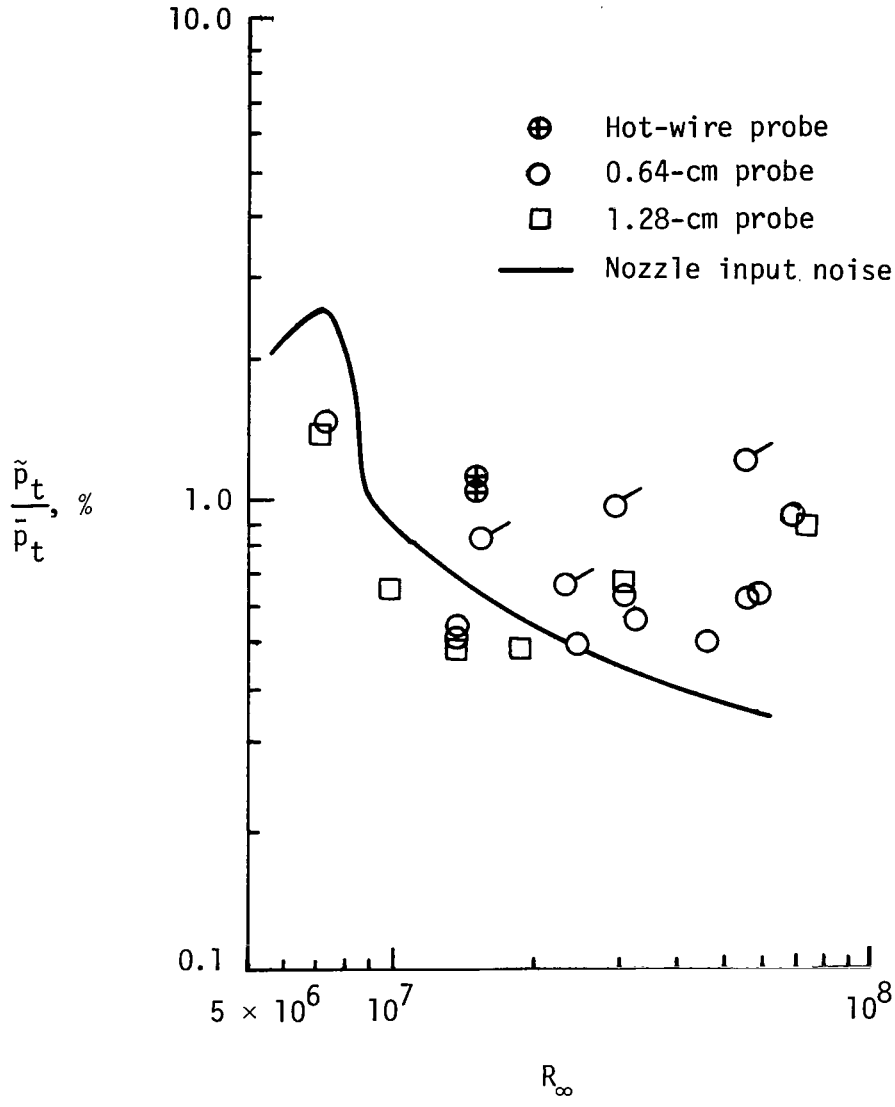

(d) x_p = 33.0.

Figure 16.- Continued.

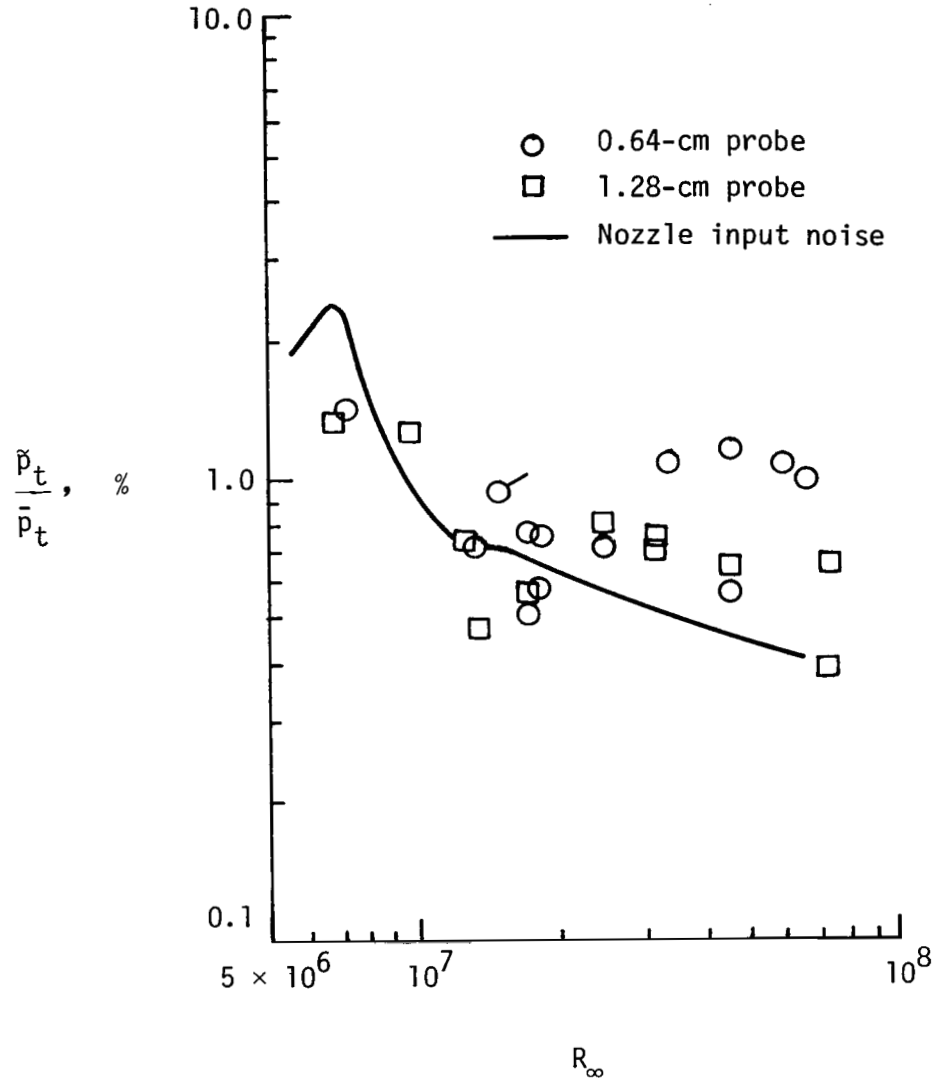

(e) $x_p = 35.6$.

Figure 16.- Continued.

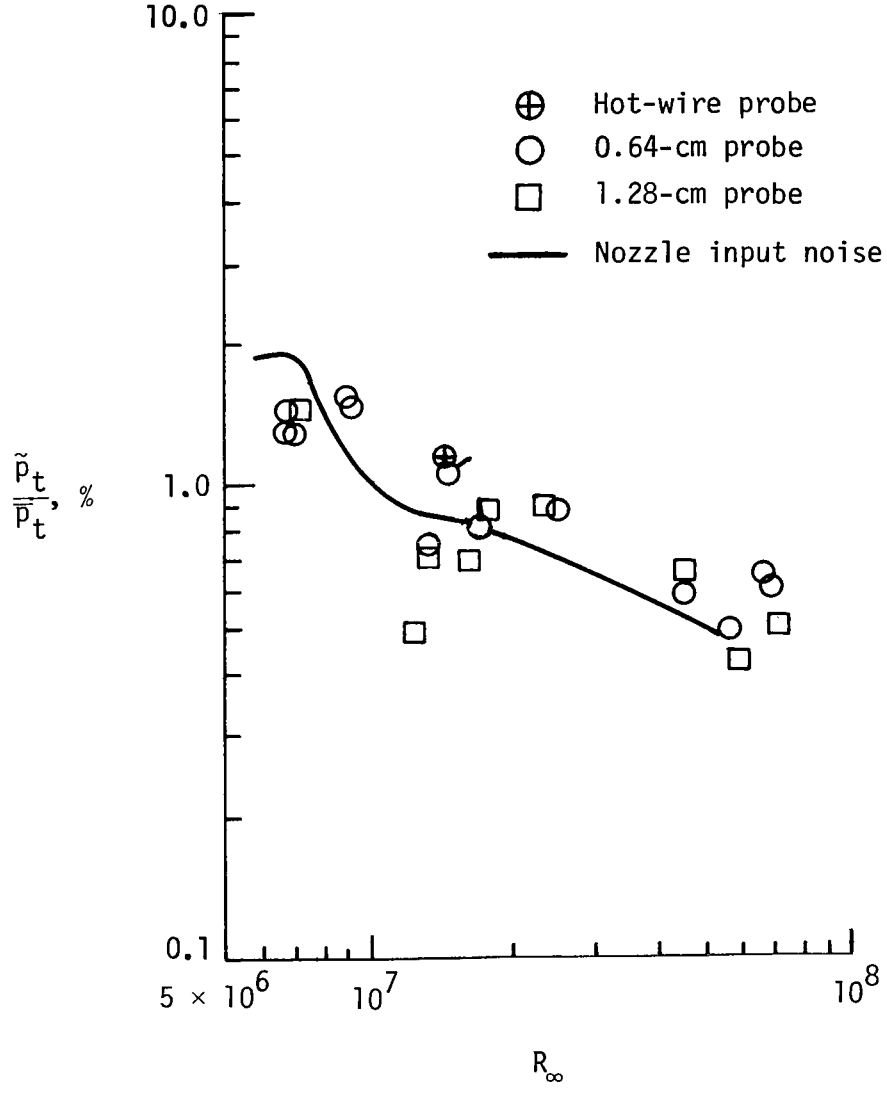

(f) x_p = 38.1.

Figure 16.- Concluded.

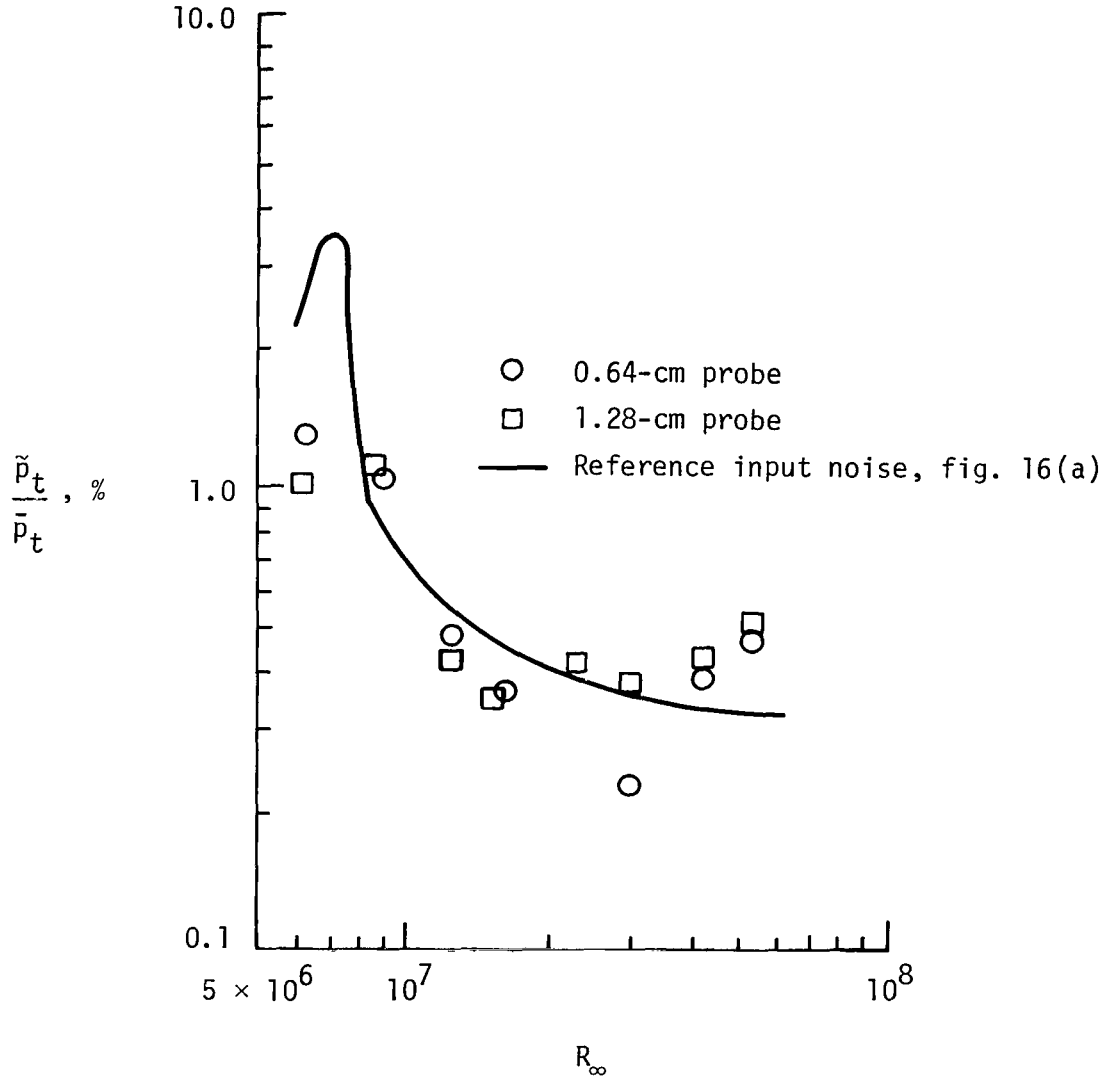

(a) $x_p = 25.4$.

Figure 17.- Variation of normalized fluctuating pitot pressure with unit Reynolds number. Probes off centerline. y = 0.64; z = 1.11.

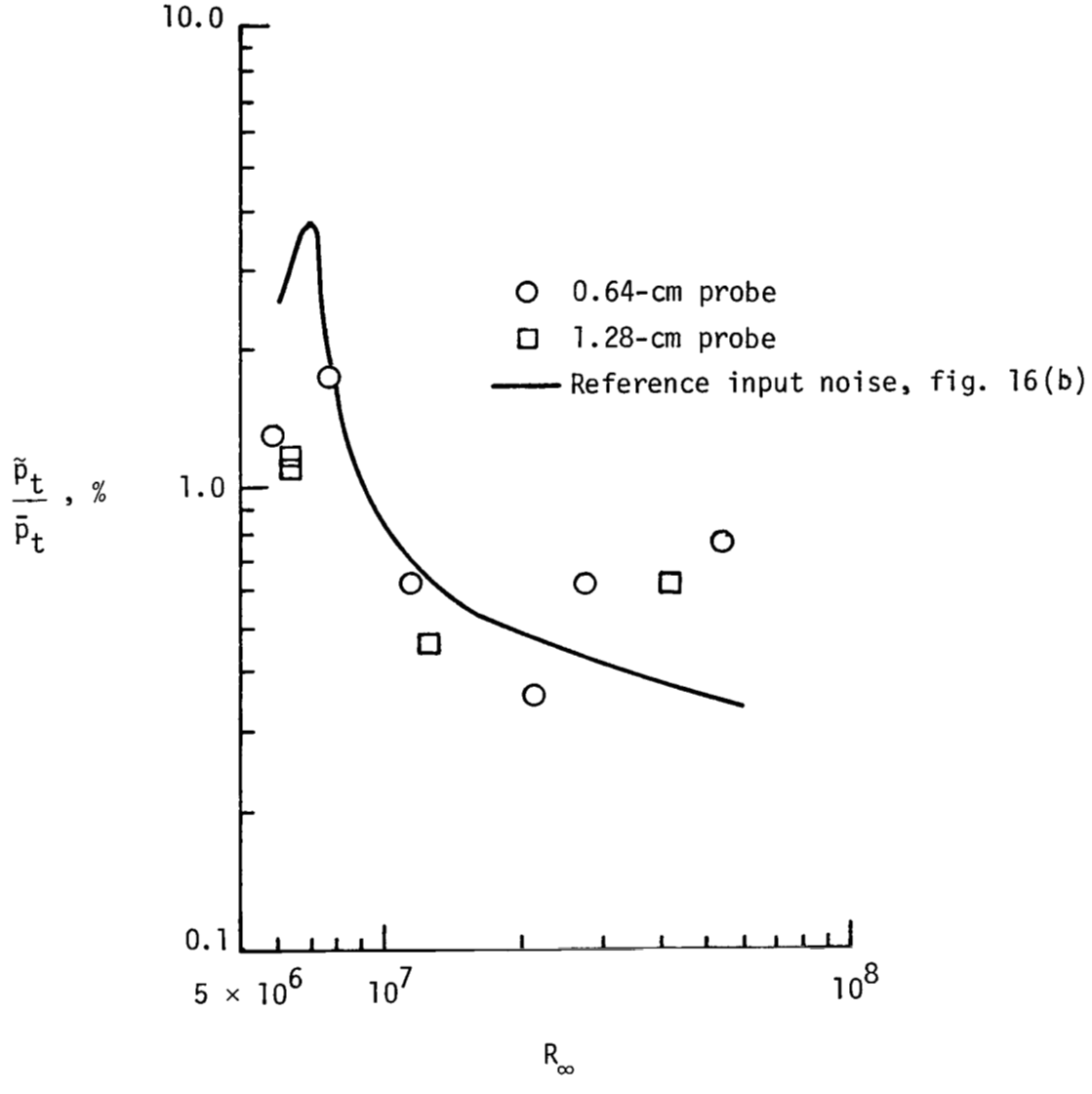

(b) $x_p = 27.9$.

Figure 17.- Continued.

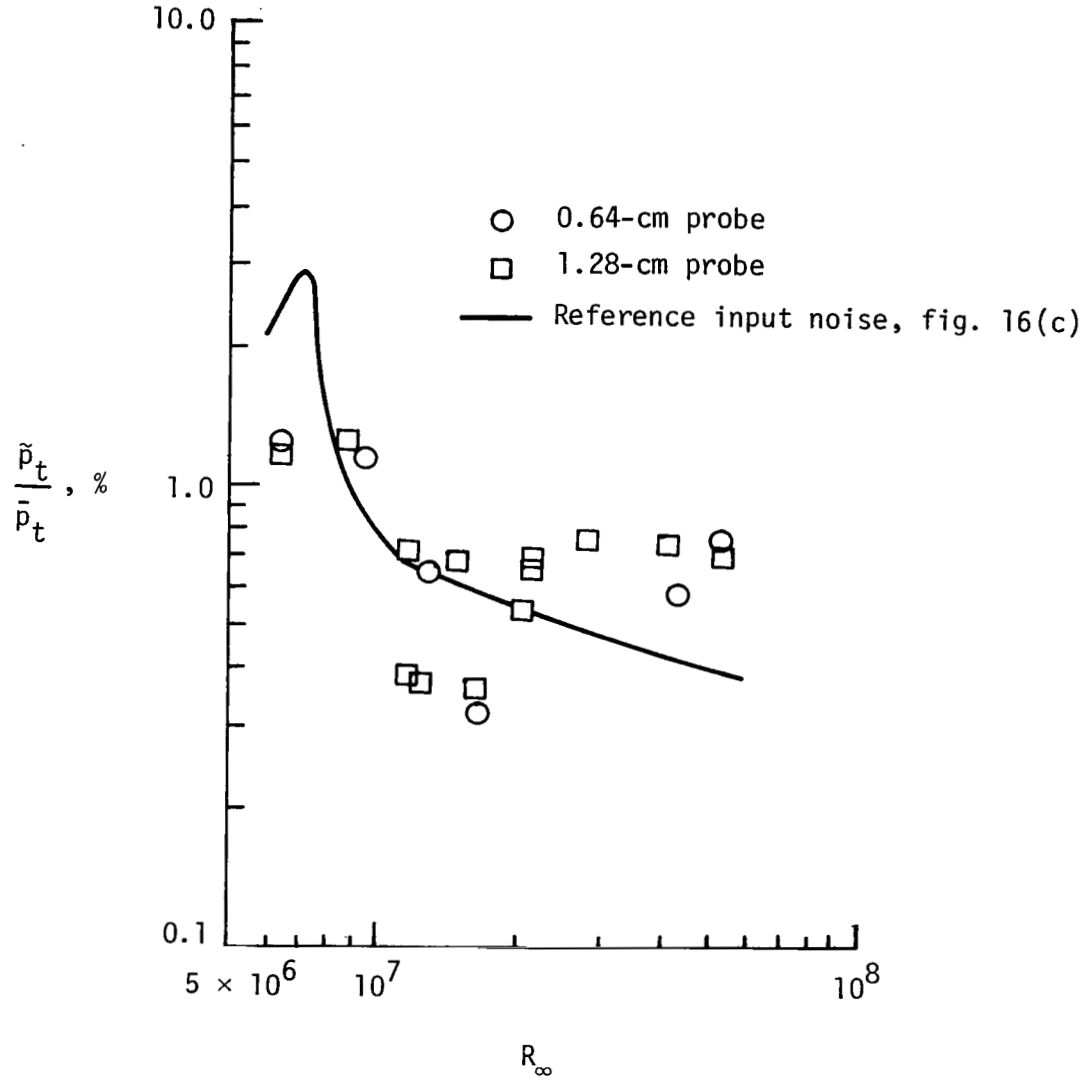

(c) x_p = 30.5.

Figure 17.- Continued.

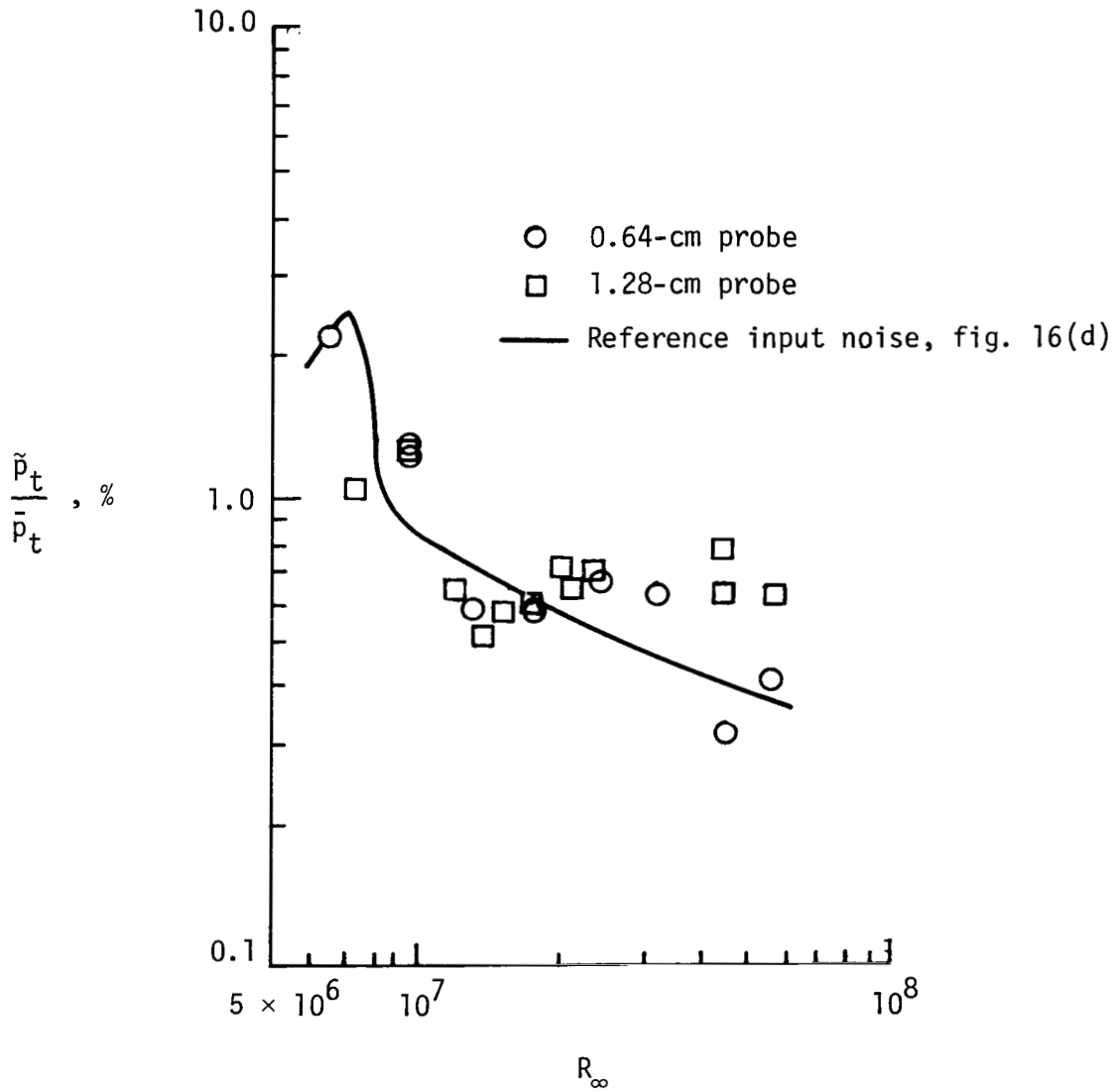

(d) x_p = 33.0.

Figure 17.- Continued.

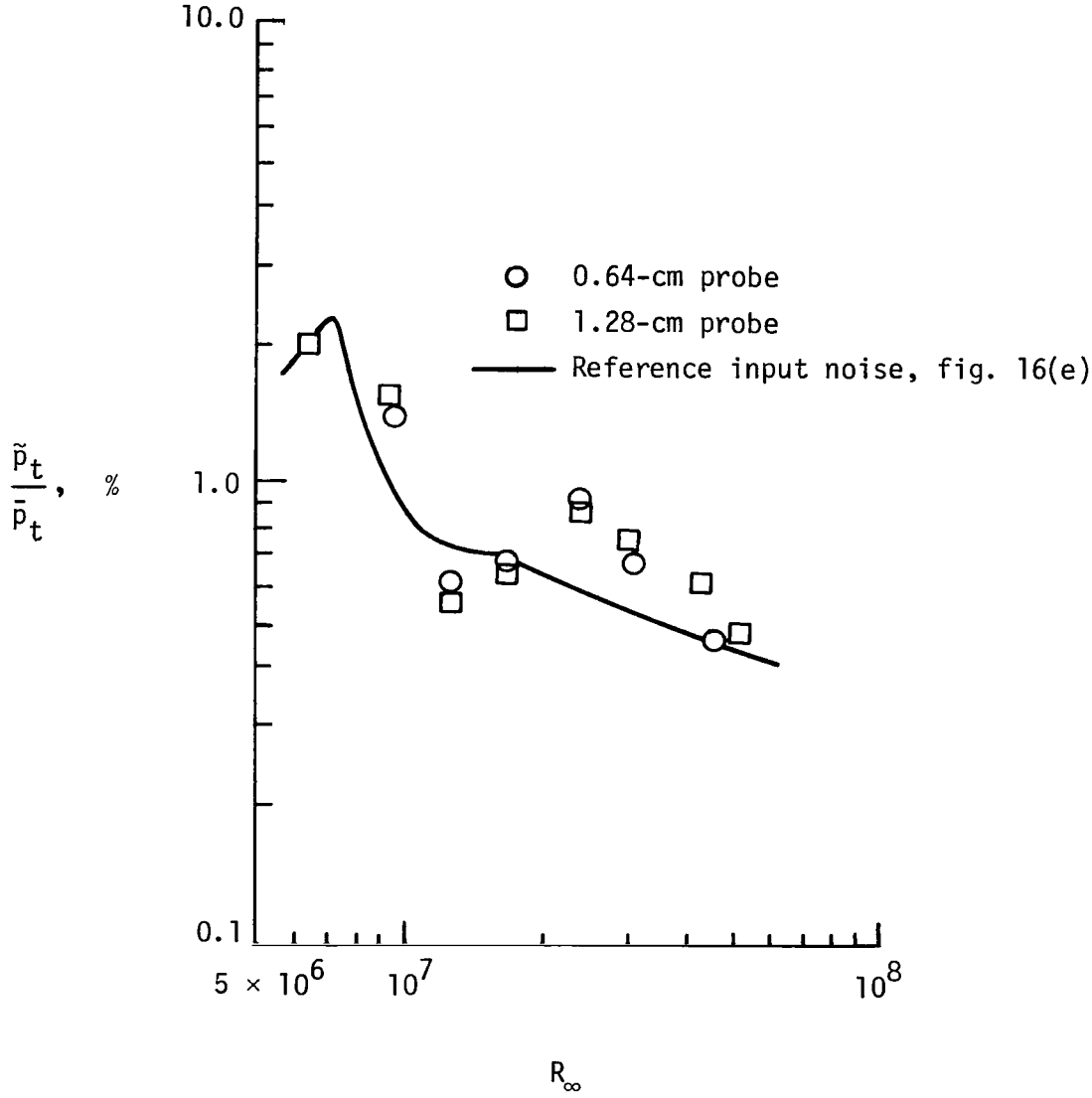

(e) $x_p = 35.6$.

Figure 17.- Continued.

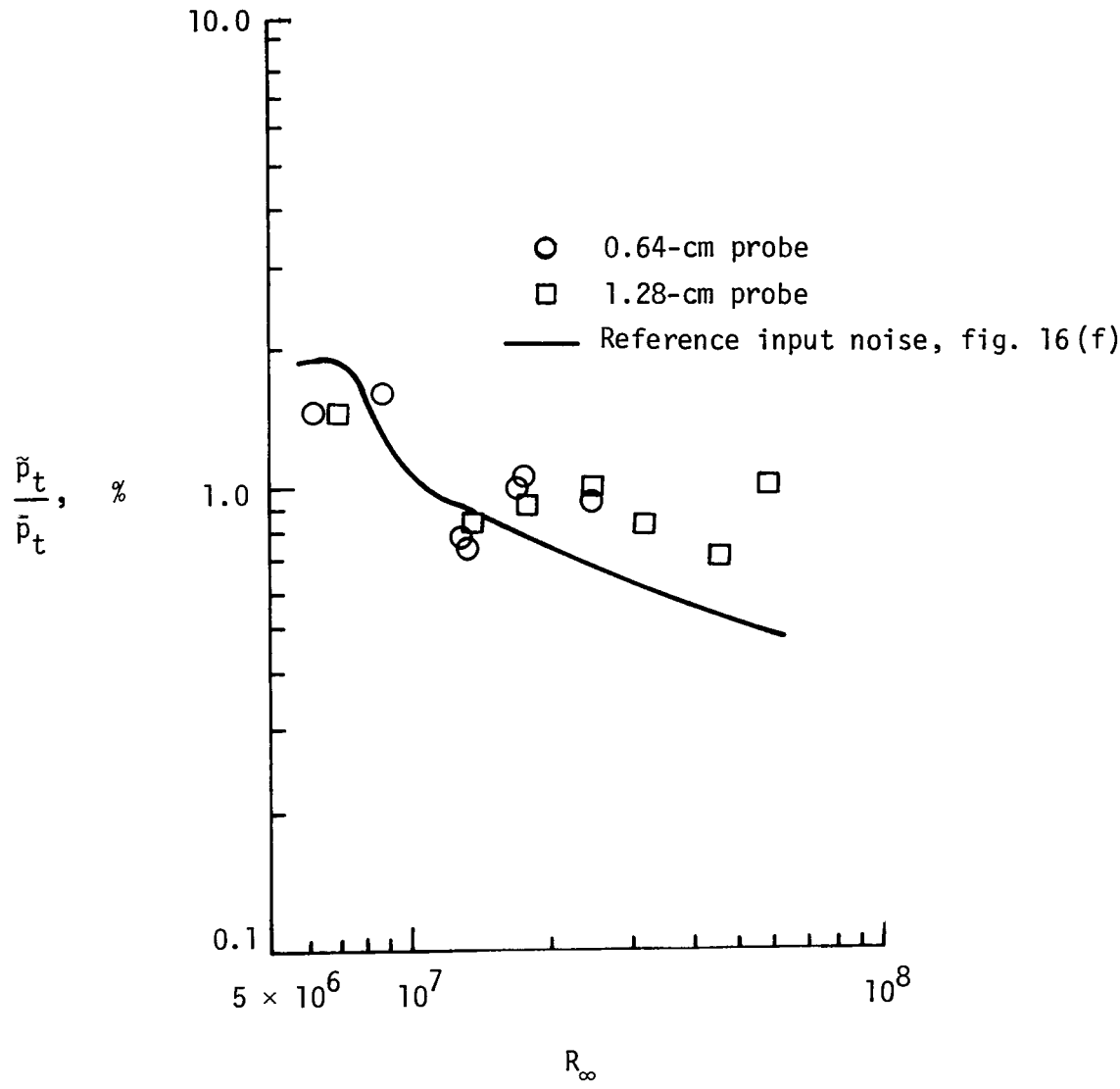

(f) x_p = 38.1.

Figure 17.- Concluded.

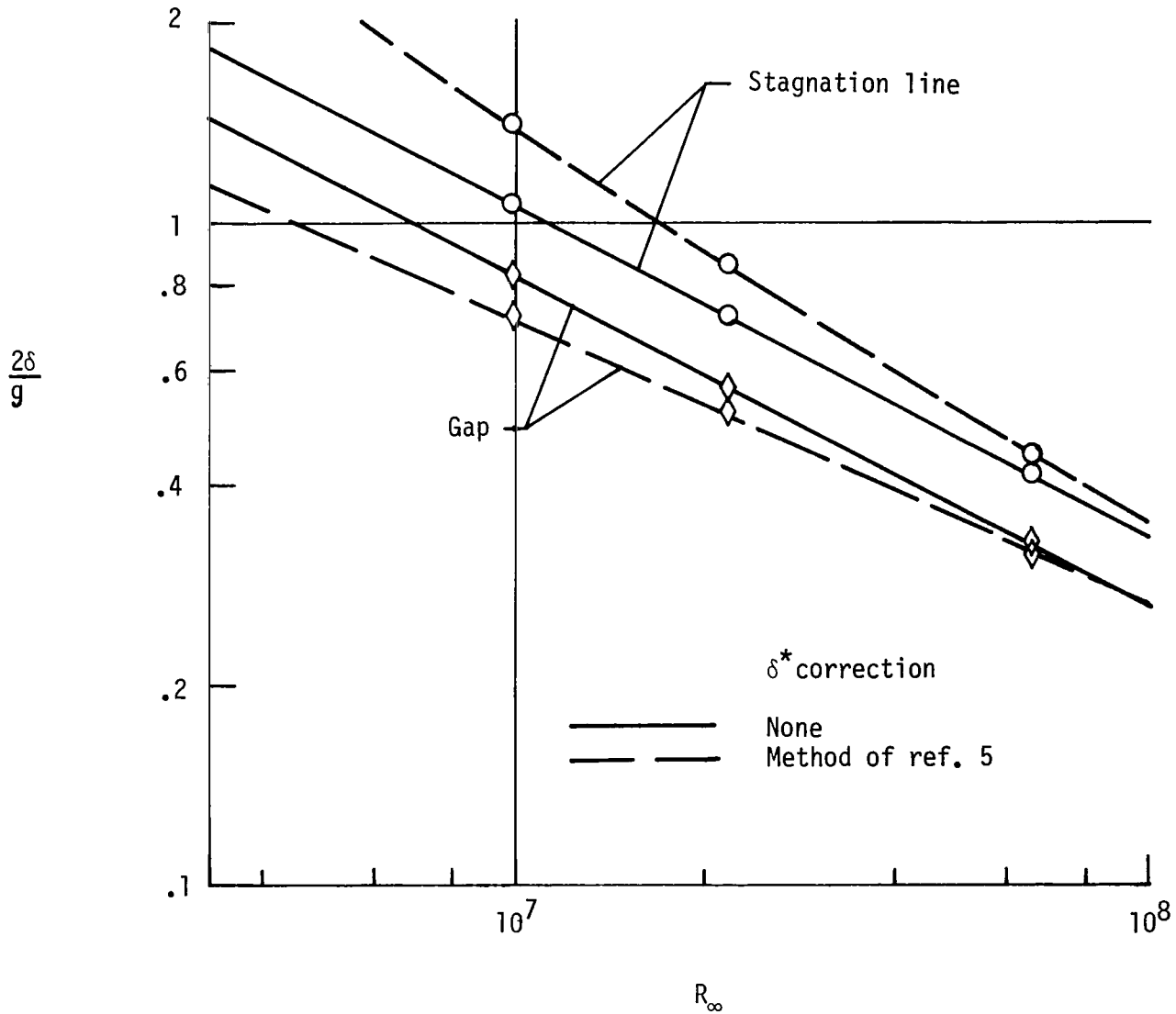

Figure 18.- Variation of laminar boundary-layer thickness with unit Reynolds number on rods of rectangular sound-shield model. Symbols are values computed with code of reference 14. $M_\infty = 5.0$; $T_w/T_o = 0.88$; $g/d = 0.16$; $d = 0.635$.

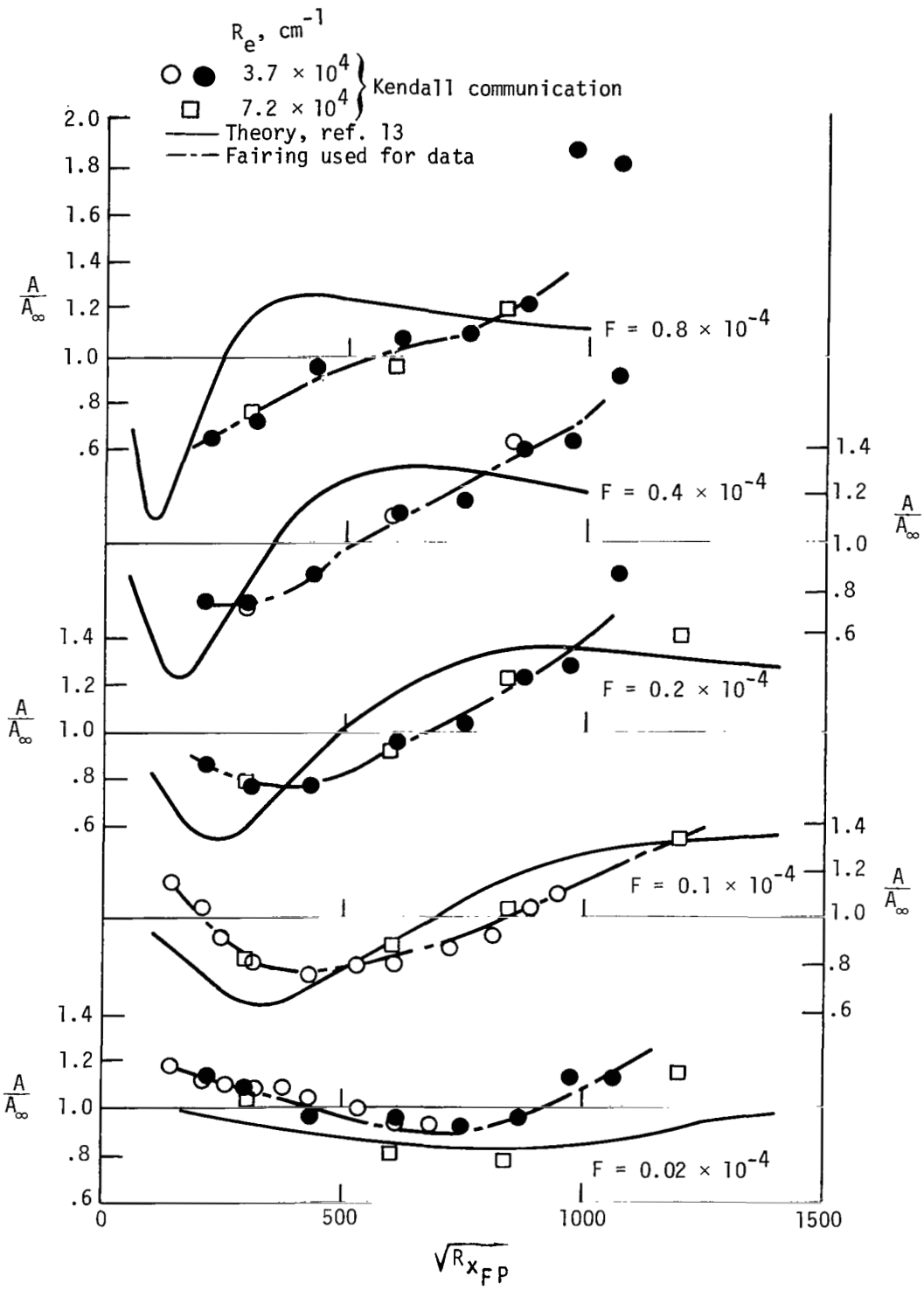

Figure 19.- Fluctuation amplitude outside boundary-layer edge on flat plate (ref. 13 and Kendall communication). Solid symbols are adjusted. (See text.) $M_\infty = 4.5$.

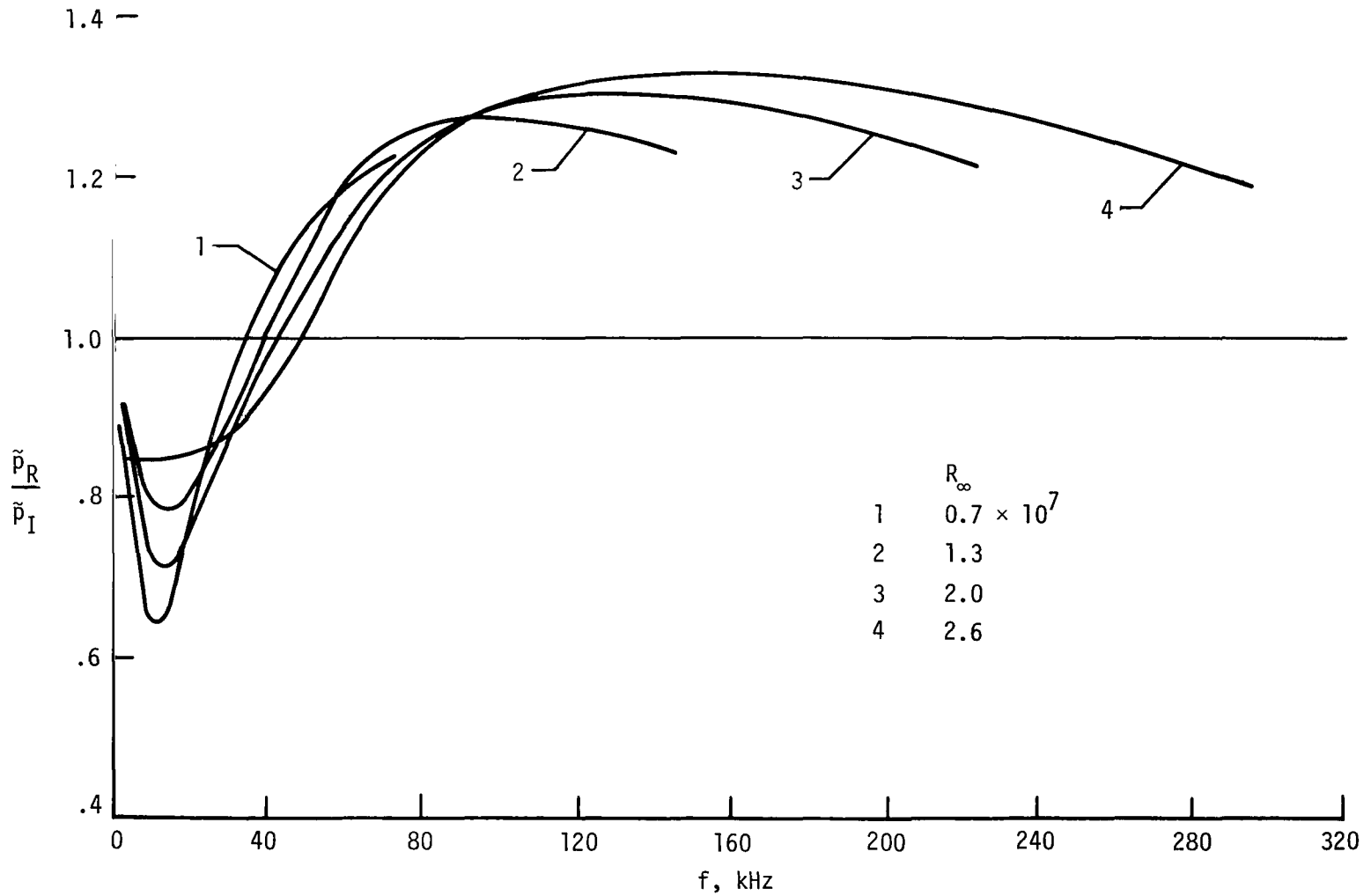

(a) Theory, reference 13 and private communication.

Figure 20.- Application of sound-reflection theory and data for adiabatic flat plate (M = 4.5) to rod-wall test panel. $M_\infty = 6.0$; $\alpha = 10$; $g/d = 0.16$; $M_e = 4.74$.

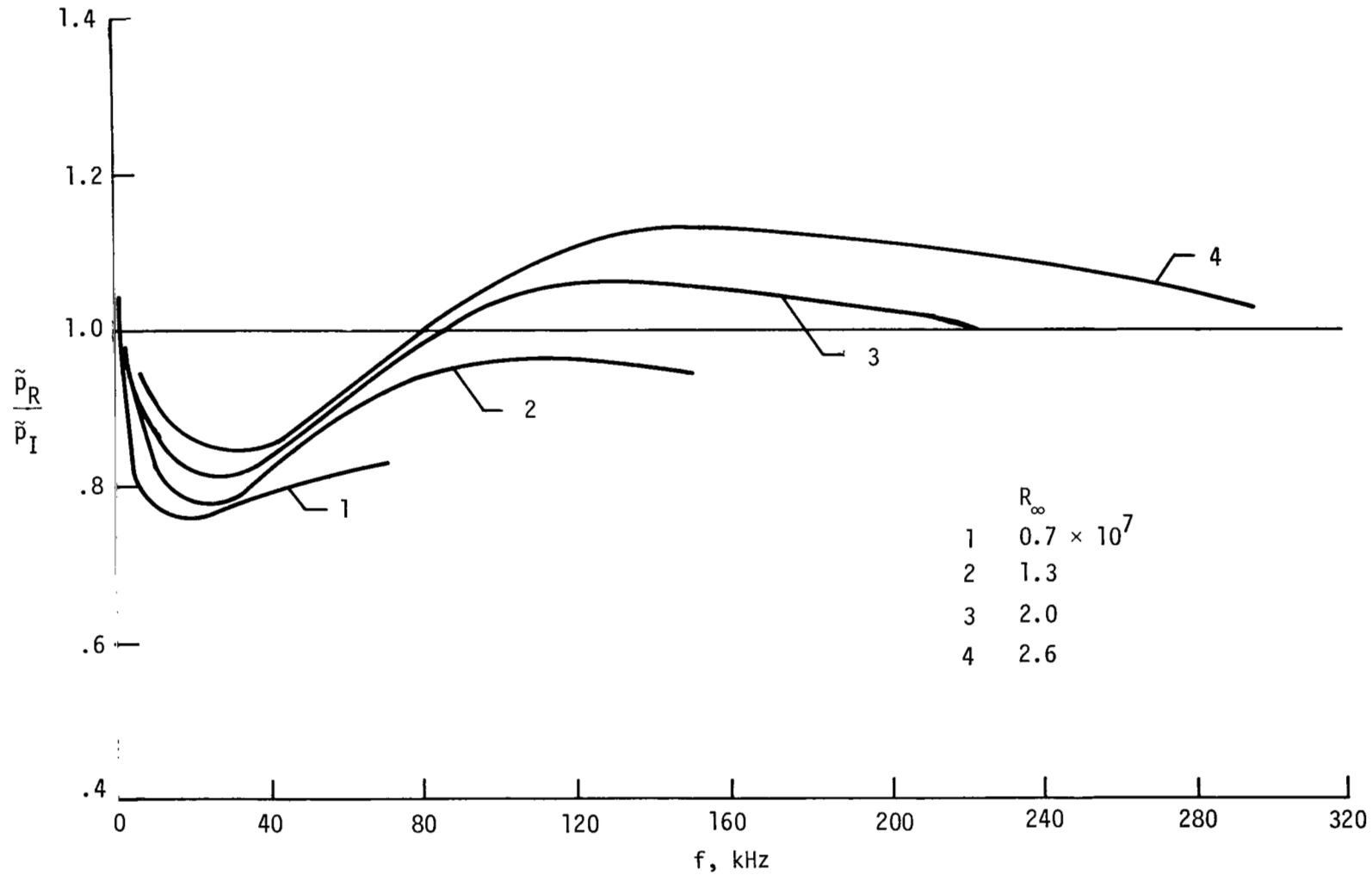

(b) Data, private communication.

Figure 20.- Concluded.

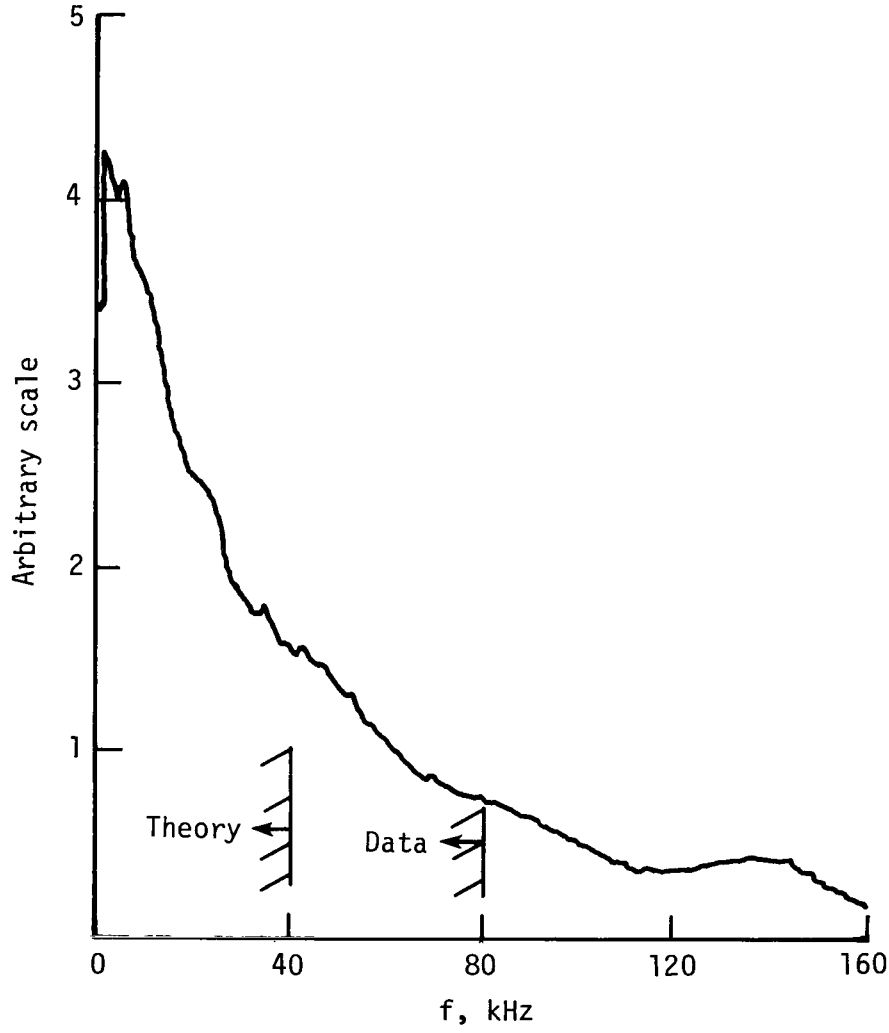

Figure 21.- Frequency spectrum of free-stream noise from fluctuating pitot-pressure transducer in the Langley 20-Inch Mach 6 Tunnel. $R_\infty = 1.6 \times 10^7$.

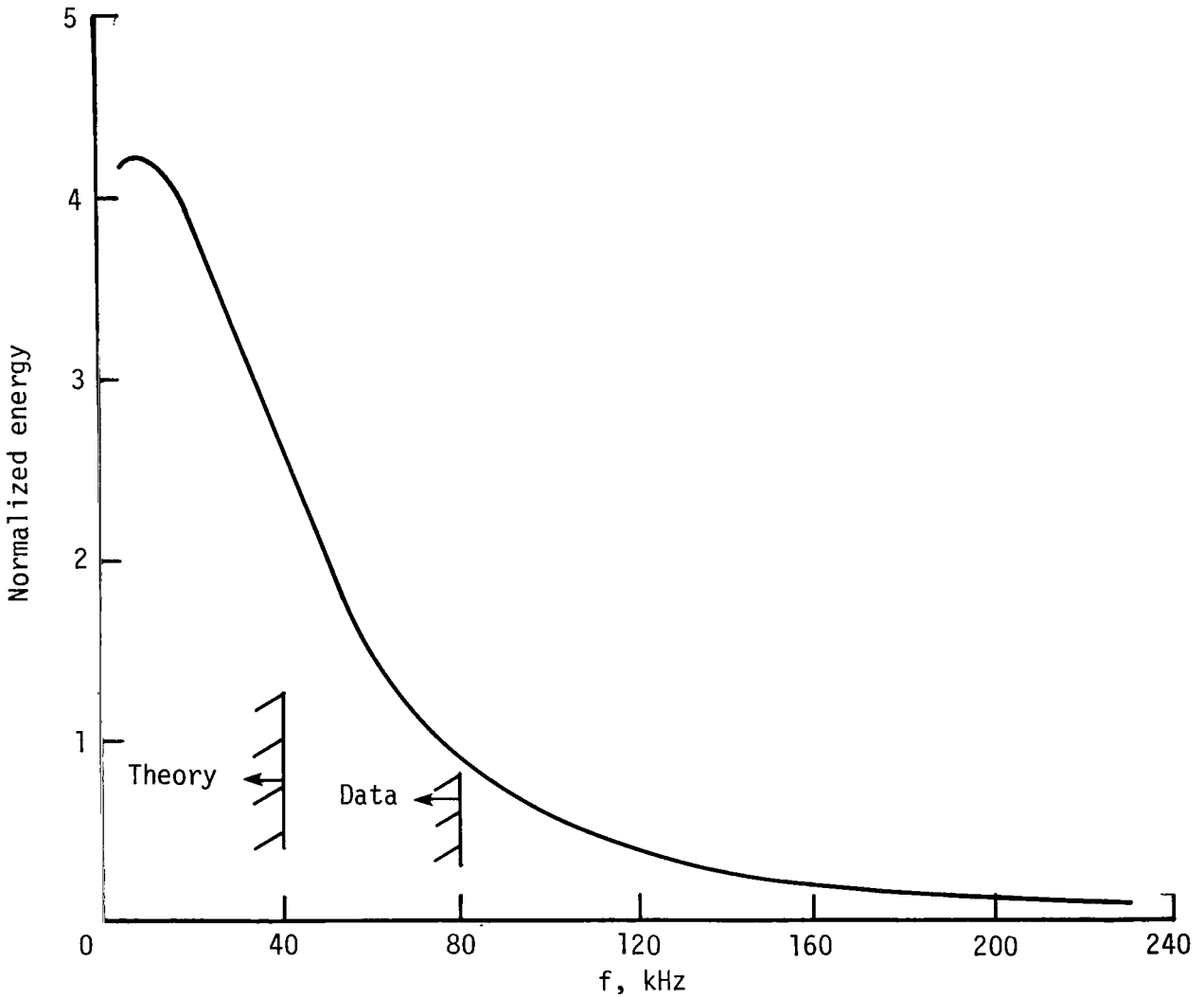

Figure 22.- Frequency spectrum of free-stream noise from hot-wire probe in the JPL 20-inch continuous flow tunnel. $M_\infty = 5.6$; $R_\infty = 3.3 \times 10^6$ (ref. 15).

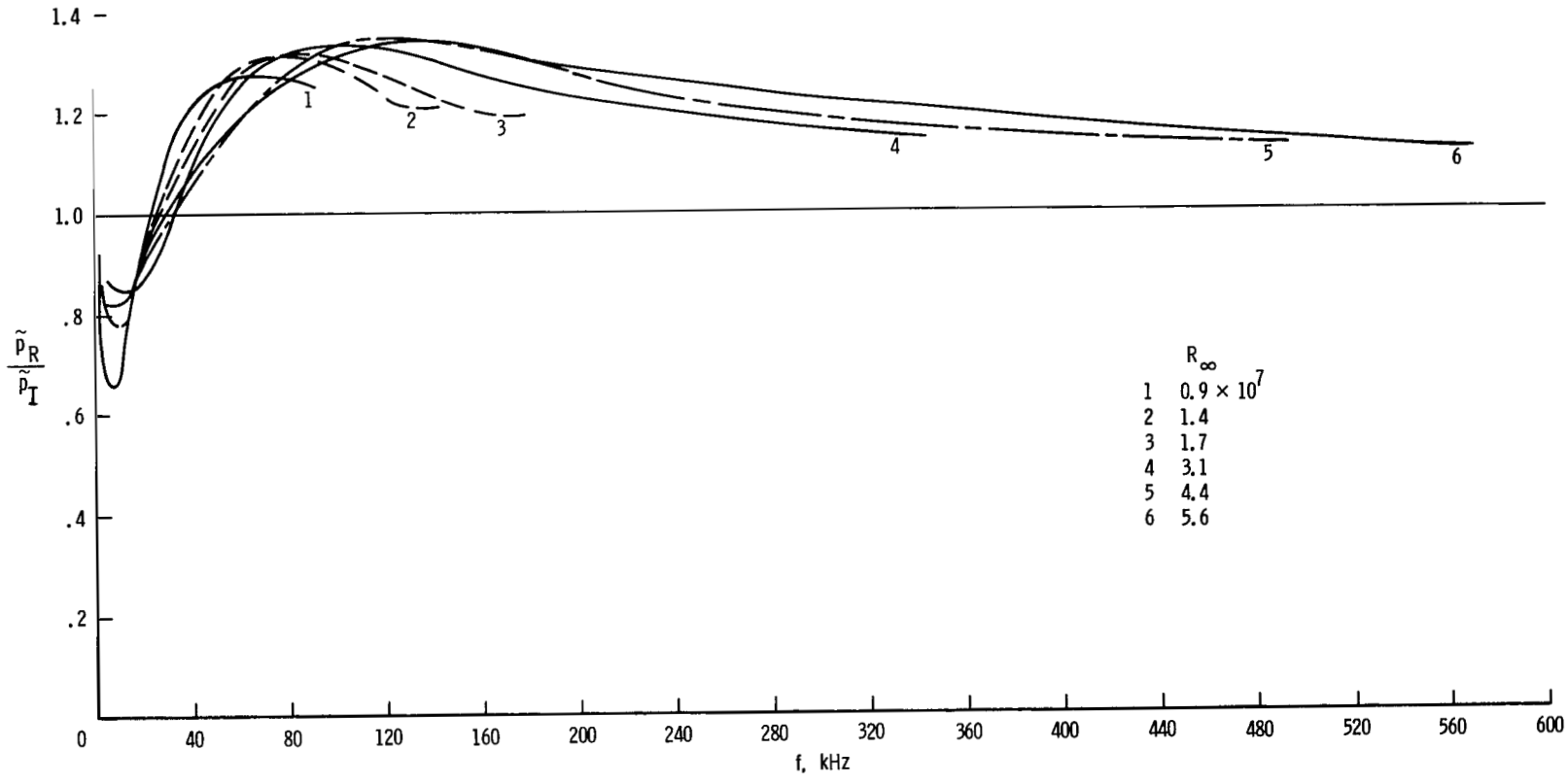

(a) Theory, reference 13 and private communication.

Figure 23.- Application of sound-reflection theory and data for adiabatic flat plate (M = 4.5) to rectangular rod-wall sound shield. M_∞ = 4.9.

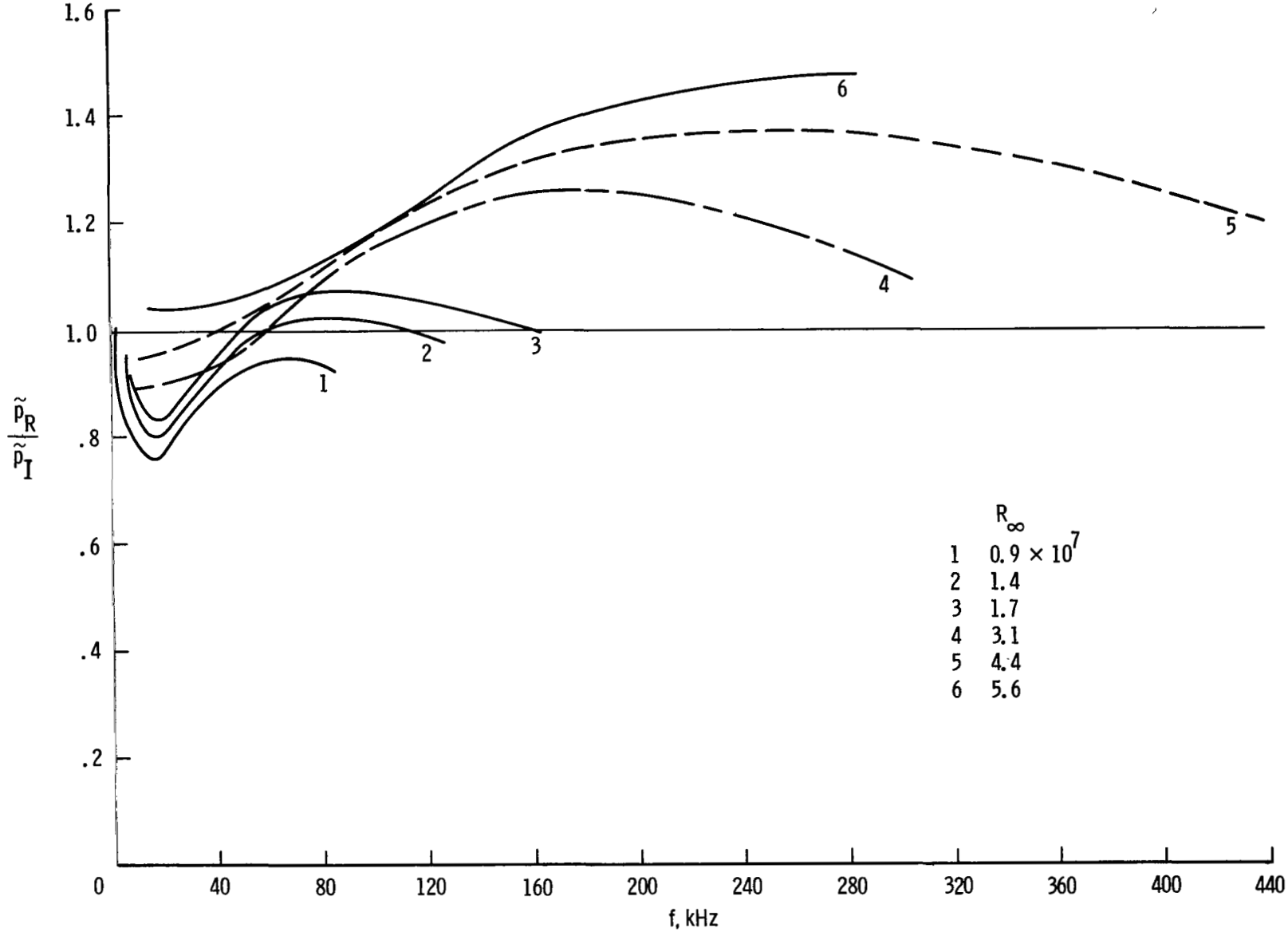

(b) Data, private communication.

Figure 23.- Concluded.

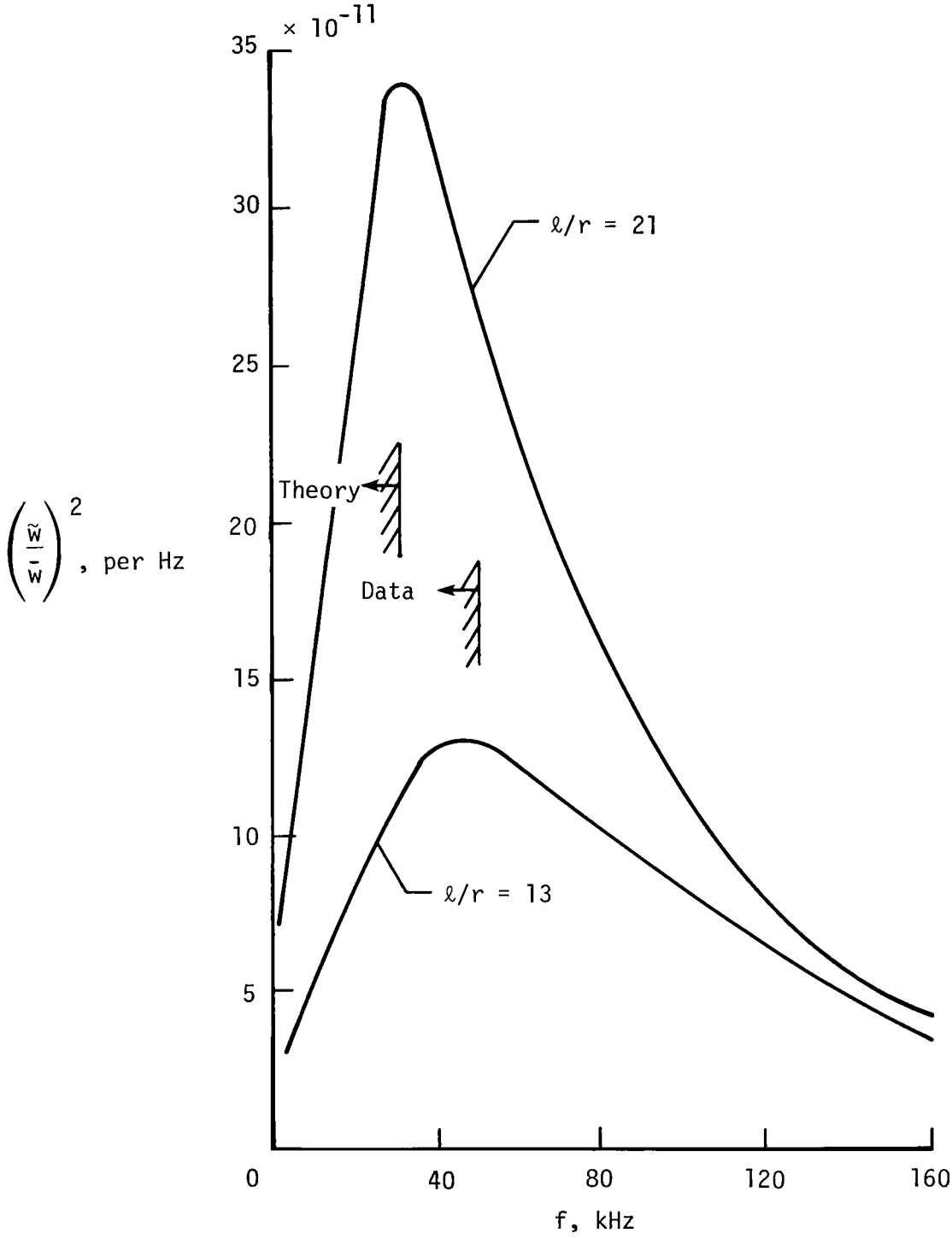

Figure 24.- Normalized hot-wire free-stream noise spectra (ref. 10) in the rapid-expansion nozzle. $R_\infty = 2.65 \times 10^7$.

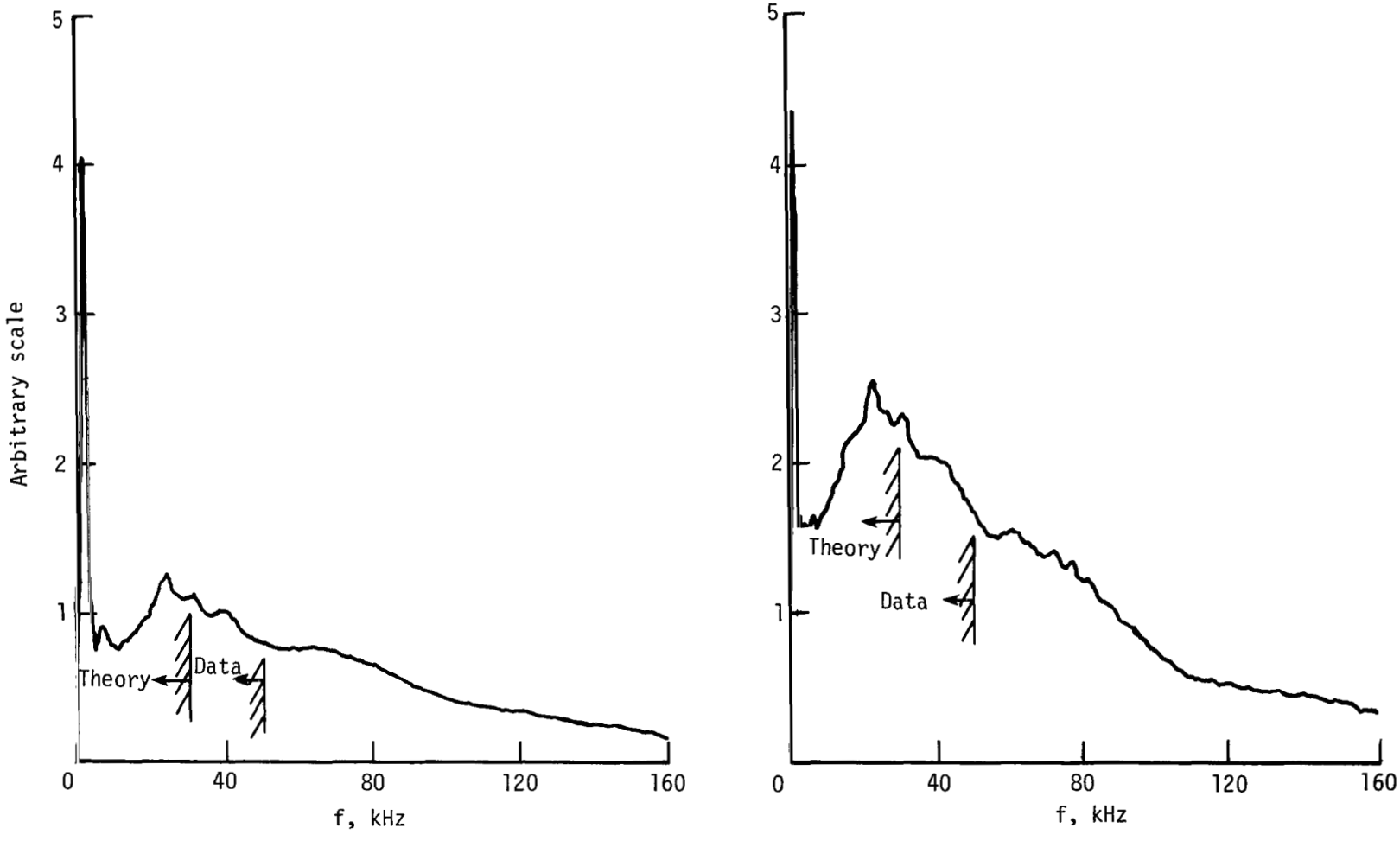

Figure 25.- Free-stream noise spectra from fluctuating pitot probe in the rapid expansion nozzle. $R_\infty = 1.6 \times 10^7$; $M_\infty = 4.9$.

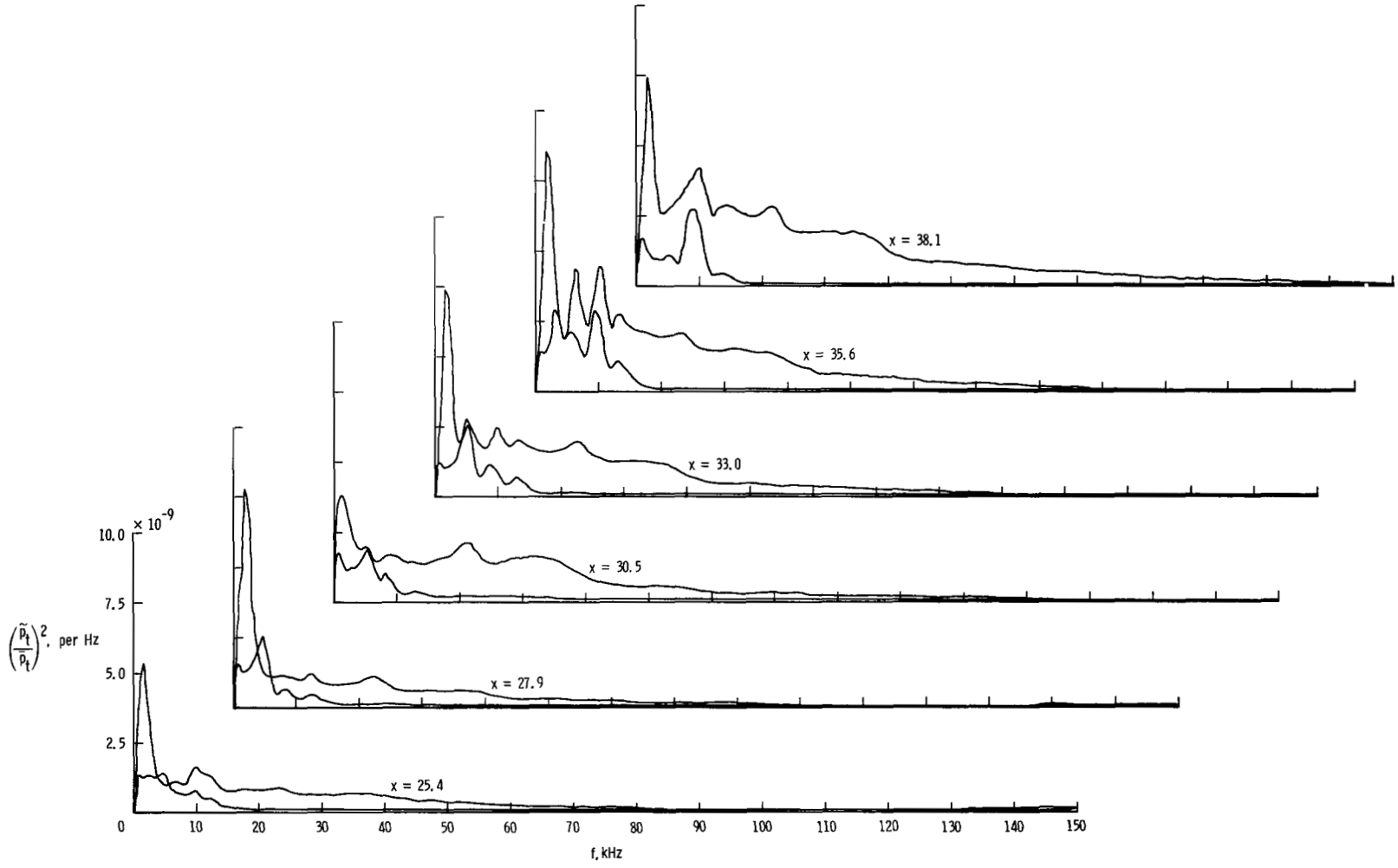

(a) $R_\infty = 1.5 \times 10^7$; probe diameter = 0.64 cm.

Figure 26.- Pitot-probe noise spectra in rod-wall model, on centerline. Lower curve for each station or Reynolds number represents acceleration component as measured by covered transducer. $M_\infty = 4.9$.

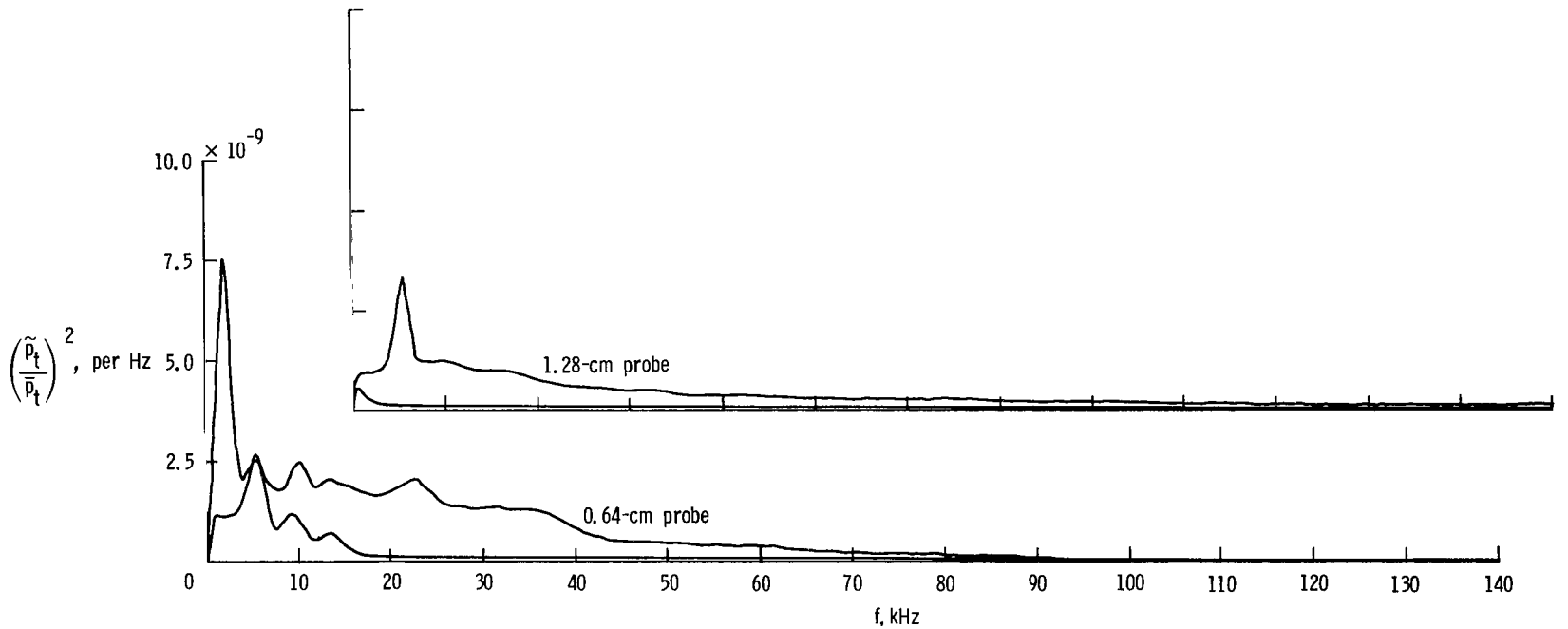

(b) Probe diameters = 0.64 cm and 1.28 cm.
$R_\infty \cong 1.5 \times 10^7$. $x_p = 33.0$.

Figure 26.- Continued.

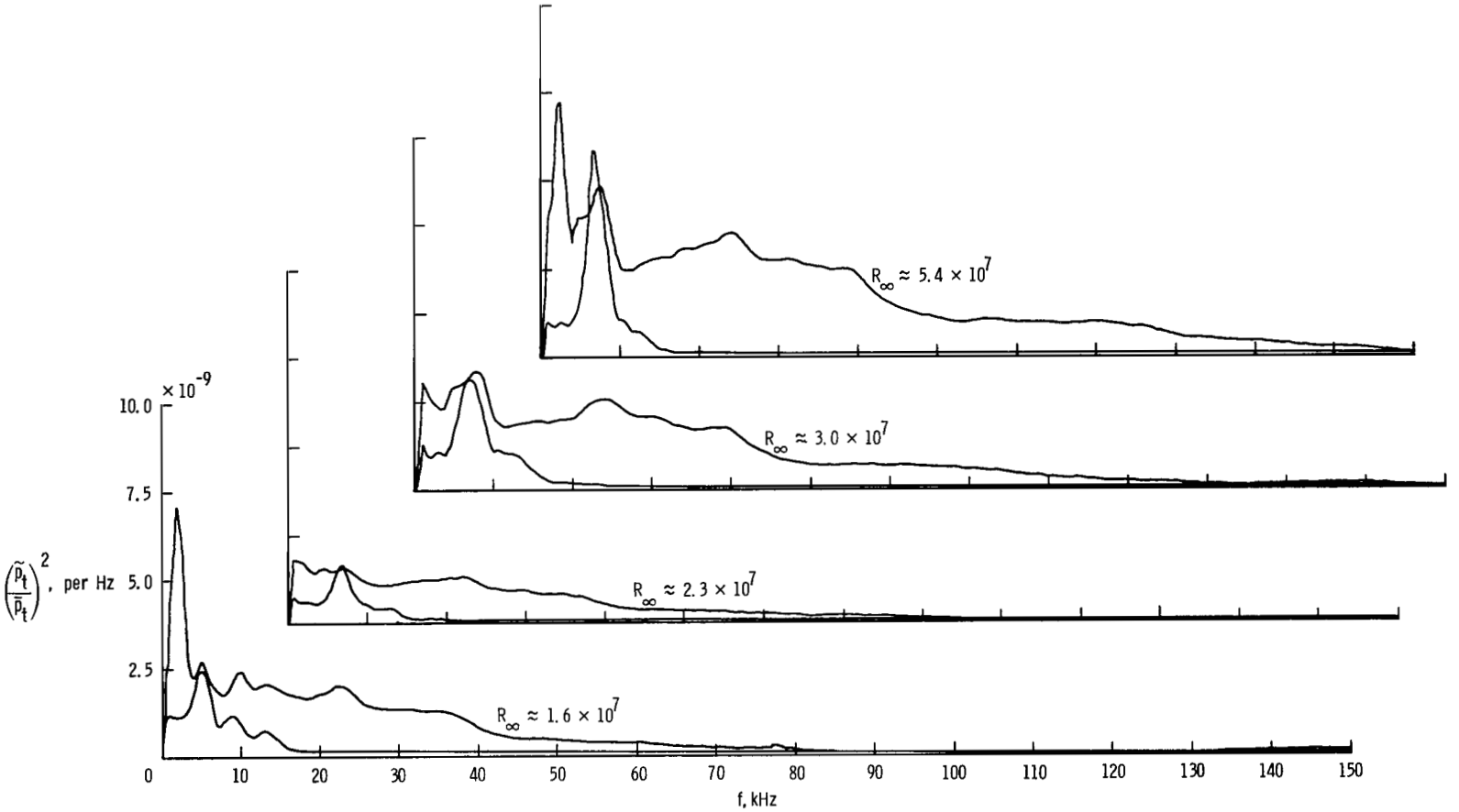

(c) Probe diameter = 0.64 cm; $R_\infty = 1.5 \times 10^7$ to 5.4×10^7; $x_p = 33.0$.

Figure 26.- Concluded.

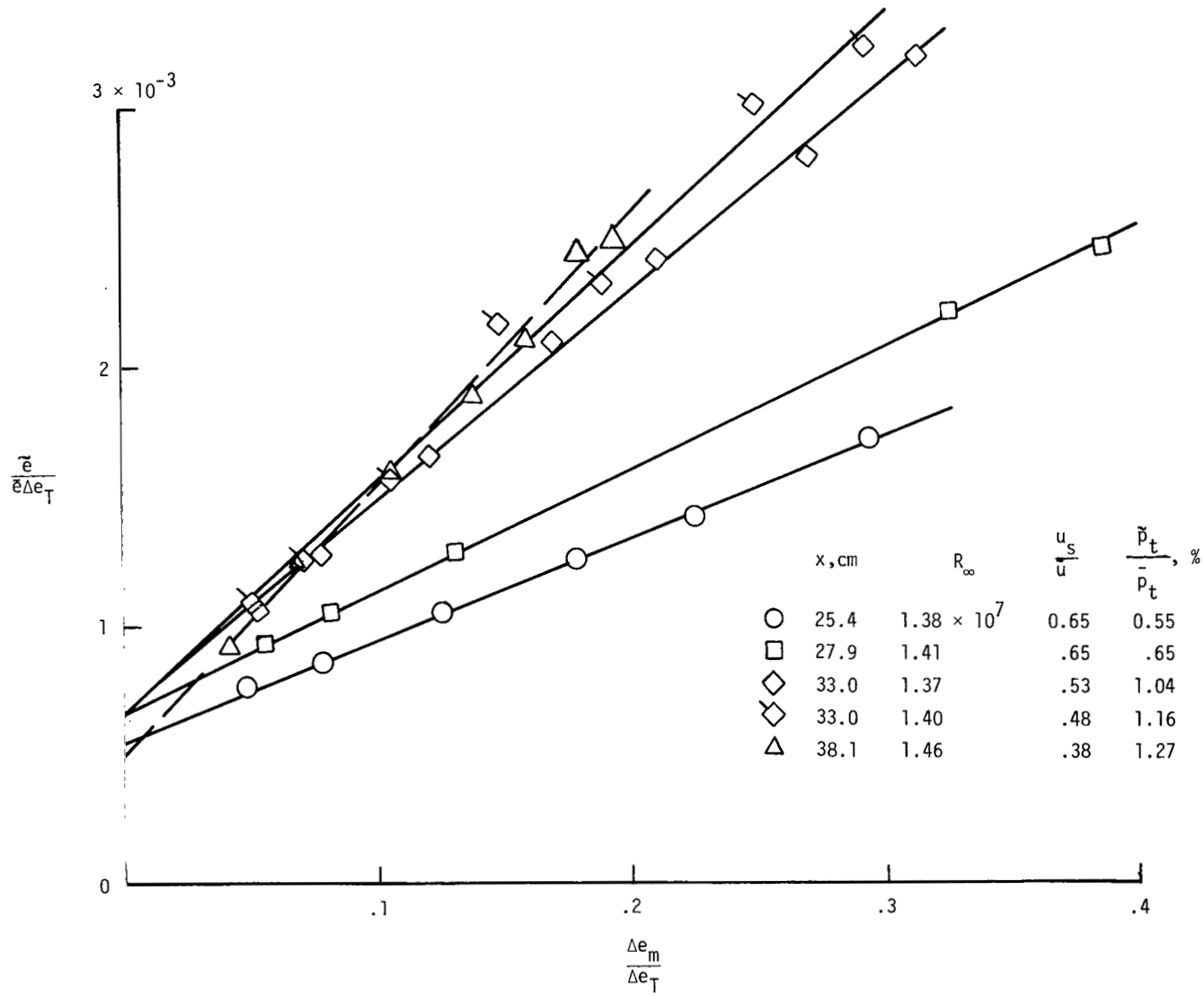

Figure 27.- Hot-wire mode diagrams for Mod V at four stations on the model centerline. $R_\infty \cong 1.4 \times 10^7$.

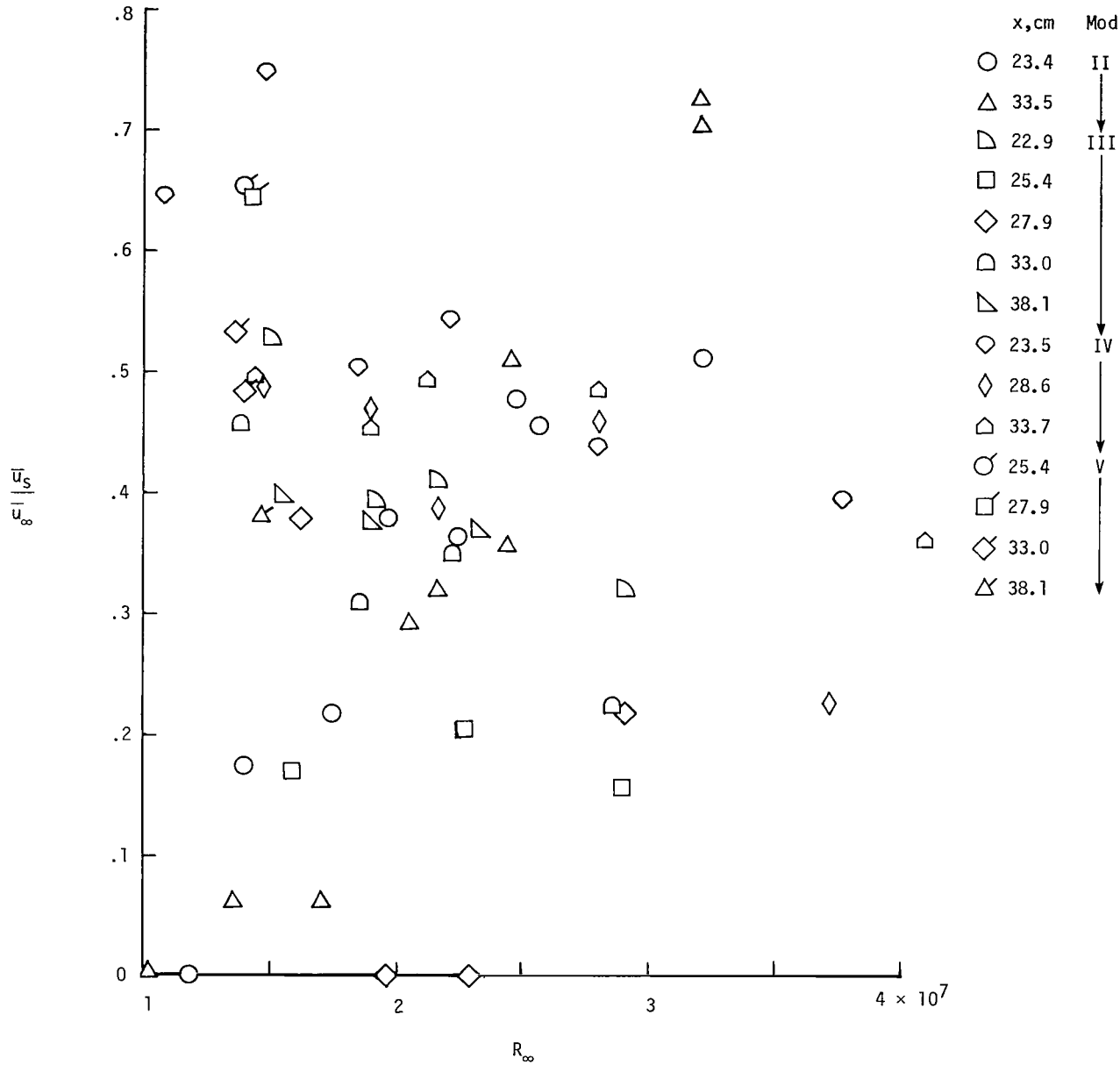

Figure 28.- Source velocity variation with free-stream unit Reynolds number for Mod II through Mod V.

1. Report No.	2. Government Accession No.	3. Recipient's Catalog No.
NASA TP-1672		

4. Title and Subtitle

NOISE REDUCTION IN A MACH 5 WIND TUNNEL WITH A RECTANGULAR ROD-WALL SOUND SHIELD

5. Report Date: June 1980

6. Performing Organization Code

7. Author(s)

Theodore R. Creel, Jr., J. Wayne Keyes, and Ivan E. Beckwith

8. Performing Organization Report No.: L-13451

9. Performing Organization Name and Address

NASA Langley Research Center
Hampton, VA 23665

10. Work Unit No.: 505-31-23-04

11. Contract or Grant No.

12. Sponsoring Agency Name and Address

National Aeronautics and Space Administration
Washington, DC 20546

13. Type of Report and Period Covered: Technical Paper

14. Sponsoring Agency Code

15. Supplementary Notes

16. Abstract

A rod-wall sound shield was tested over a range of Reynolds numbers of 0.5×10^7 to 8.0×10^7 per meter. The model consisted of a rectangular array of longitudinal rods with boundary-layer suction through gaps between the rods. Suitable measurement techniques were used to determine properties of the mean flow and acoustic disturbances in the shield and transition in the rod boundary layers. Measurements indicated that for a Reynolds number of 1.5×10^7 the noise in the shielded region was significantly reduced, but only when the flow is mostly laminar on the rods. Actual nozzle "input" noise measured on the nozzle centerline before reflection at the shield walls was attenuated only slightly even when the rod boundary layers were laminar. At a lower Reynolds number, nozzle input noise at noise levels in the shield were still too high for application to a quiet tunnel. At Reynolds numbers above 2.0×10^7 per meter, measured noise levels were generally higher than nozzle input levels, probably due to transition in the rod boundary layers. The small attenuation of nozzle input noise at intermediate Reynolds numbers for laminar rod layers at the acoustic origins is apparently due to high frequencies of noise.

17. Key Words (Suggested by Author(s))	18. Distribution Statement
Boundary layer Noise reduction Transition Supersonic wind tunnels	Unclassified - Unlimited Subject Category 34

19. Security Classif. (of this report)	20. Security Classif. (of this page)	21. No. of Pages	22. Price*
Unclassified	Unclassified	79	$6.00

N-305

For sale by the National Technical Information Service, Springfield, Virginia 22161

NASA-Langley, 1980